Nonlinear Water Waves with Shear

Thesis by

Anatoly I. Baumstein

In Partial Fulfillment of the Requirements

for the Degree of

Doctor of Philosophy

California Institute of Technology

Pasadena, California

1997

(Submitted May 5, 1997)

Acknowledgements

I would like to thank my advisor, Professor P.G. Saffman, for his support, encouragement, and invaluable guidance during my years at Caltech. I would also like to thank Dr. M.Z. Caponi for suggesting the topic discussed in chapter 4. Mr. D.A. Gallagher stole time from his research to critique the manuscript and made many important comments, which are greatly appreciated. I immensely benefited from many fruitful discussions with Prof. D.I. Meiron, Dr. K. Ardalan, Dr. A. Balk, Mr. D. Hill, Mr. M. Louie, and Mr. P.J. Park. I am grateful to the entire department of Applied Mathematics for providing an outstanding environment for study and research.

This work was supported in part by the Office of Naval Research Grant N00014-92-J-1435.

Abstract

Various aspects of nonlinear inviscid gravity waves in the presence of shear in the air and water are investigated. The shear, which appears due to the presence of wind in the air and current in the water, is modeled by a piecewise linear velocity profile.

The interaction of short and long gravity waves is studied numerically, using spectral methods, and analytically, using perturbation methods. Special attention is paid to the verification of observations and experimental results. It is confirmed that finite amplitude waves propagating in the same direction as the wind or current are more stable with respect to superharmonic infinitesimal perturbations than the waves moving against the wind or current.

Infinitesimal perturbations in the form of side bands are also investigated both numerically and analytically. The nonlinear cubic Schrödinger equation for the wave envelope of a slowly varying wave train is derived. It is shown that depending on the direction of propagation (along or against the shear) of the finite amplitude waves, the effect of the shear on the stability is substantially different. In most cases, however, the shear strength increase first enhances the instability, but later suppresses it.

Three-wave interactions of gravity waves with shear in the water are considered. The interaction equations are derived with the help of two different perturbation approaches. The question of stability is addressed for both resonant and near-resonant interactions. The regions of explosive and "pump-wave" instability are identified for various types of three-wave interactions.

A new type of steady two-dimensional gravity waves with water shear is computed numerically. These waves appear at relatively low amplitudes and lack symmetry with respect to any crest or trough. A boundary integral formulation is used to obtain a one-parameter family of non-symmetric solutions through a symmetry-breaking bifurcation.

Contents

List of Figures

List of Tables

Chapter 1 Introduction

This thesis deals with the following aspects of the influence of winds and currents on the stability and shape of gravity water waves: (1) stability of short wind-generated waves in the presence of finite amplitude waves of permanent form; (2) effect of water current on the stability of finite amplitude waves with respect to perturbations of a wavelength close to that of the basic wave; (3) three-wave interactions and associated instabilities; (4) analysis of the shape of the waves of permanent form in the presence of a current.

A number of approaches can be employed for modeling shear. We will be using a piecewise linear velocity profile ("stick" profile) both in the water and in the air. This profile is simple enough to facilitate investigation of the finite amplitude waves and, at the same time, is sufficient to obtain qualitative agreement with experiments and observations.

In chapter 2 we consider the interaction of short infinitesimal waves with long waves of finite amplitude. It has been known for a long time that the stability properties of water waves in the presence of wind and current change significantly depending on the directions of the wind, water current, and wave propagation. For example, J.R.D. Francis [9] writes: "A number of phenomena are still unexplained, and are very relevant to engineering problems. For example, it has been known by many generations of sailors that waves produced by wind when it opposes a quite small current are greater that those when the same wind is in the same direction as the current. With 'wind against tide' the sea appears rougher, small ships toss about far more and there is more broken water seen. ...Sailors are taciturn folk; and so there are few references to this in the literature, and none at all in scientific work." There is also substantial experimental evidence that a long steep wave, propagating in the direction of the wind, tends to sweep short wind waves, while a wave propagating against the wind tends to enhance the instability associated with the short waves.

This phenomenon was observed in the experiments by Mitsuyasu [6]. We confirm these findings using both numerical and asymptotic approaches. Several background flows are considered: (1) water current in the absence of wind, (2) wind without any shear in the water (corresponds to early stages of the onset of wind), (3) wind combined with the wind-induced shear in the water. In case (2) we compare our results with the findings of Caponi, Saffman, and Yuen [4].

In chapter 3 we consider a related issue of the wave interaction in the case when the wavenumbers of participating waves are very close. This case is reduced to the well-known Benjamin-Feir instability, if the amplitude of the basic wave is sufficiently small and there is no shear. In a recent paper, Q.P. Zhou [22] investigated a smooth (exponential) weak velocity profile and derived the Zakharov integral equation describing slow evolution of the wave field. We use a simpler piecewise linear velocity profile, but do not assume that the shear is weak. Since the difference between the wavenumbers of the finite amplitude and infinitesimal waves is very small, it can be expressed in terms of a small parameter, proportional to the wave amplitude. This allows us to apply the method of two-timing to derive the nonlinear Schrödinger equation for the wave envelope, and investigate the influence of the strength and depth of the shear on the stability of the infinitesimal perturbations. In order to verify our results numerically, as well as study the range of validity of the asymptotic two-timing approach, we use a slightly modified numerical scheme from chapter 2. We also re-derive the main results for the "two-stick" profile, which uses two layers of constant vorticity instead of just one, and demonstrate that differences between the "two-stick" and "one-stick" profiles are not significant. Since the "two-stick" profile can be considered to be a better approximation to some smooth velocity distribution than the simple "one-stick" profile, the fact that the differences are small serves as a justification for using a piecewise linear profile instead of a smooth one.

Chapter 4 is concerned with three-wave interactions. In the case of gravity waves these interactions occur only in the presence of shear in the air or in the water. The case of air shear was studied by Romanova and Shrira [18]. They derived the interaction equations and indicated several regions of explosive instability. A more

general formulation for an arbitrary continuously varying shear profile was developed by Becker and Grimshaw [1]. Their results, although applicable to an arbitrary continuous profile, involve expressions for the interaction coefficients which cannot be easily evaluated for a given background velocity profile. Another approach, presented by Vanneste and Vial [20], employs an expansion in the normal modes of the linearized problem, instead of a small parameter expansion, and requires numerical evaluation of the interaction coefficients. We concentrate on deriving simple expressions for the interaction coefficients in the case of piecewise constant shear in the water and investigating two different types of instability associated with this shear.

In chapter 5 steady asymmetric waves of finite amplitude are investigated. A family of low amplitude asymmetric waves is found to be bifurcating from a solution branch that is associated with the presence of shear. Previously known high amplitude irrotational asymmetric waves, bifurcating from regular waves of period $2\pi/6$ (Zufiria [23]), are also reproduced.

Chapter 2 Superharmonic instability

2.1 Introduction

As pointed out in [5], knowledge of possible short wave instabilities is "... important, for example, for the interpretation of high frequency radar imaging. Some of the primary sensors for remote investigation of the ocean properties are high frequency radars that respond only to wind sensitive short waves, in the wavelength range of 1 to 10 cm." Hence, the interpretation of radar images requires an understanding of the interaction of short wind-generated waves with longer waves and currents.

2.2 Mathematical formulation

As indicated in the introduction, we will study changes in the stability of an infinitesimal wave, riding on top of a finite amplitude wave of permanent form, in the presence of shear in the air and water. The background velocity profile is a continuous piecewise linear function as outlined in fig. 2.1. The velocity profile is characterized by the depths (Δ_W and Δ_A) and the vorticities (Ω_W and Ω_A) of the shear layers in the water and air. For simplicity, the wavelength of the wave of permanent form is taken to be 2π and the short infinitesimal waves are supposed to have the wavelength $2\pi/k_s$, where $k_s = 2, 3, \ldots$. Thus, we can restrict our attention to the interval $0 < x < 2\pi$. The motion in each region is described by the streamfunctions satisfying the following Poisson (or Laplace) equations:

$$\begin{aligned}
\nabla^2\psi_T^A &= 0 \quad \text{for} \quad y_A < y < \infty;\\
\nabla^2\psi_B^A &= -\Omega_A \quad \text{for} \quad y_T < y < y_A;\\
\nabla^2\psi_T^W &= -\Omega_W \quad \text{for} \quad y_B < y < y_T;\\
\nabla^2\psi_B^W &= 0 \quad \text{for} \quad -\infty < y < y_B.
\end{aligned}$$

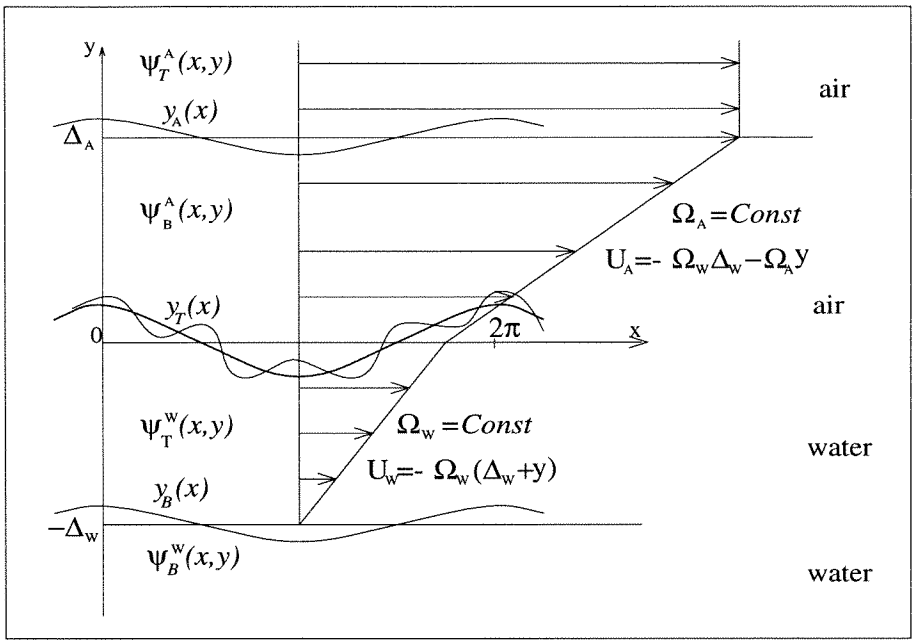

Figure 2.1: Velocity profile. Velocities U_A and U_W are shown as they would have appeared in the absence of waves.

We also require that there be no motion as $y \to -\infty$, and the flow be uniform with the speed V_A ($V_A = -\Omega_A\Delta_A - \Omega_W\Delta_W$) as $y \to +\infty$. It is convenient to change to the system of coordinates moving with the speed c of the finite amplitude wave. Then the general solution to the above equations can be represented in the following form:

$$\psi_T^W = \Psi_1^W + \varepsilon\psi_1^W,$$

$$\Psi_1^W = \sum_{k=-N}^{N} e^{ikx}\left(A_k^W e^{|k|y} + B_k^W e^{-|k|y}\right) - \frac{1}{2}\Omega_W y^2 + (c - \Omega_W\Delta_W)y,$$

$$\psi_1^W = e^{\sigma t}\sum_{k=-N}^{N} e^{ikx}\left(a_k^W e^{|k|y} + b_k^W e^{-|k|y}\right);$$

$$\psi_B^W = \Psi_2^W + \varepsilon\psi_2^W,$$

$$\Psi_2^W = \sum_{k=-N}^{N} e^{ikx} D_k^W e^{|k|y} + cy,$$

$$\psi_2^W = e^{\sigma t} \sum_{k=-N}^{N} e^{ikx} d_k^W e^{|k|y};$$

$$\psi_T^A = \Psi_1^A + \varepsilon \psi_1^A,$$

$$\Psi_1^A = \sum_{k=-N}^{N} e^{ikx} \left(A_k^A e^{|k|y} + B_k^A e^{-|k|y} \right) - \frac{1}{2} \Omega_A y^2 + (c - \Omega_W \Delta_W) y,$$

$$\psi_1^A = e^{\sigma t} \sum_{k=-N}^{N} e^{ikx} \left(a_k^A e^{|k|y} + b_k^A e^{-|k|y} \right);$$

$$\psi_B^A = \Psi_2^A + \varepsilon \psi_2^A,$$

$$\psi_2^A = e^{\sigma t} \sum_{k=-N}^{N} e^{ikx} d_k^A e^{|k|y},$$

$$\Psi_2^A = \sum_{k=-N}^{N} e^{ikx} D_k^A e^{|k|y} + (c - \Omega_W \Delta_W - \Omega_A \Delta_A) y,$$

where ε is a formal small parameter; A_k^W, B_k^W, D_k^W, a_k^W, b_k^W, d_k^W, A_k^A, B_k^A, D_k^A, a_k^A, b_k^A, d_k^A are the unknown coefficients; N is the number of coefficients used; and σ determines the wave speed and the growth rate of the infinitesimal perturbations. The quantities denoted by capital letters (such as Ψ above) refer to the finite amplitude wave, while the quantities denoted by the lower-case letters (ψ) pertain to the infinitesimal perturbations. Note that the nonlinear boundary conditions discussed below can only be satisfied in the limit $N \to \infty$, although we take a finite N for the purposes of numerical simulation.

Similarly, the functions $y_{T,B,A}(x,t)$ describing the shapes of the interfaces can be expressed in terms of Fourier series:

$$H_j(x) = \sum_{k=-N}^{N} H_{jk} e^{ikx} \text{ for } j = 1, \ldots, 3, \text{ where } H_{jk} = H_{j(-k)};$$

$$h_j(x,t) = e^{\sigma t} \sum_{k=-N}^{N} h_{jk} e^{ikx} \text{ for } j = 1, \ldots, 3;$$

$$y_T = H_1 + \varepsilon h_1; \; y_B = H_2 + \varepsilon h_2; \; y_A = H_3 + \varepsilon h_3.$$

Let us derive the boundary conditions necessary to complete the formulation of

the problem:

1. We start with the kinematic condition at the free surface ($y = y_T(x)$):

$$\frac{D}{Dt}(y - y_T) = 0 \Rightarrow \left(v = \frac{\partial y_T}{\partial t} + u\frac{\partial y_T}{\partial x} \right)\Big|_{y=y_T} \Rightarrow$$

$$-\frac{\partial \psi_T^W}{\partial x}\Big|_{y=y_T} = \frac{\partial y_T}{\partial t} + \frac{\partial \psi_T^W}{\partial y}\Big|_{y=y_T}\frac{\partial y_T}{\partial x}.$$

Equating the $O(\varepsilon^0)$ and $O(\varepsilon^1)$ terms, we obtain

$$\frac{\partial \Psi_1^W}{\partial x} + \frac{\partial \Psi_1^W}{\partial y}\frac{\partial H_1}{\partial x} = 0 \text{ or } \Psi_1^W = \text{const};$$

$$\frac{\partial \psi_1^W}{\partial x} + \frac{\partial^2 \Psi_1^W}{\partial x \partial y}h_1 + \frac{\partial h_1}{\partial t} + \left(\frac{\partial \psi_1^W}{\partial y} + h_1\frac{\partial^2 \Psi_1^W}{\partial y^2} \right)\frac{\partial H_1}{\partial x} + \frac{\partial \Psi_1^W}{\partial y}\frac{\partial h_1}{\partial x} = 0$$

on $y = H_1(x)$.

2. Similar conditions can be obtained for Ψ_1^W on $y = H_{2,3}(x)$, Ψ_2^W on $y = H_2(x)$, Ψ_1^A on $y = H_{1,3}(x)$, and Ψ_2^A on $y = H_3(x)$.

3. Next, we use the continuity of the normal stress at the free surface ($y = y_T(x)$). First let us consider all quantities related to the water. Following [19], we let $\tilde{\psi}_T^W = \psi_T^W + \frac{1}{2}\Omega_W y^2$. Then $\nabla^2 \tilde{\psi}_T^W = 0$. Therefore, we can introduce $\phi_T^W = \Phi_1^W + \varepsilon\phi_1^W$ such that

$$\frac{\partial \phi_T^W}{\partial x} = \frac{\partial \tilde{\psi}_T^W}{\partial y}; \quad \frac{\partial \phi_T^W}{\partial y} = -\frac{\partial \tilde{\psi}_T^W}{\partial x}.$$

A modified form of the Bernoulli equation can be used to obtain

$$\frac{\partial \phi_T^W}{\partial t} + \frac{1}{2}\left|\nabla \psi_T^W\right|^2 + \Omega_W \psi_T^W - T\frac{\dfrac{\partial^2 y_T}{\partial x^2}}{\left(1 + \left(\dfrac{\partial y_T}{\partial x}\right)^2\right)^{\frac{3}{2}}} + g y_T$$

$$= \rho\left(\frac{\partial \phi_T^A}{\partial t} + \frac{1}{2}\left|\nabla \psi_T^A\right|^2 + \Omega_A \psi_T^A + g y_T \right) + F(t)$$

for $y = y_T(x)$, where $\rho = \rho_A/\rho_W$ is the ratio of the air density to water density, and T is the surface tension.

A simple calculation shows that

$$\left|\nabla\psi_T^W\right|^2 = \left(\frac{\partial\Psi_1^W}{\partial x}\right)^2 + \left(\frac{\partial\Psi_1^W}{\partial y}\right)^2 + 2\varepsilon\left[\frac{\partial\Psi_1^W}{\partial x}\frac{\partial\psi_1^W}{\partial x} + \frac{\partial\Psi_1^W}{\partial y}\frac{\partial\psi_1^W}{\partial y} + h_1\frac{\partial\Psi_1^W}{\partial x}\frac{\partial^2\Psi_1^W}{\partial x\partial y} + h_1\frac{\partial\Psi_1^W}{\partial y}\frac{\partial^2\Psi_1^W}{\partial y^2}\right],$$

where all the terms on the right-hand side are evaluated at $y = H_1(x)$.

ϕ_T^W can also be easily determined:

$$\Phi_1^W = -i\sum_{k=-N}^{N} e^{ikx}\mathrm{sgn}(k)\left(A_k^W e^{|k|y} - B_k^W e^{-|k|y}\right);$$

$$\phi_1^W = -ie^{\sigma t}\sum_{k=-N}^{N} e^{ikx}\mathrm{sgn}(k)\left(a_k^W e^{|k|y} - b_k^W e^{-|k|y}\right).$$

Note that we omitted some irrelevant terms which drop out after the differentiation with respect to t. All the air related quantities can be treated similarly.

Thus, equating the $O(\varepsilon^0)$ and $O(\varepsilon^1)$ terms (for $y = H_1(x)$), we obtain

$$\left(\frac{\partial\Psi_1^W}{\partial x}\right)^2 + \left(\frac{\partial\Psi_1^W}{\partial y}\right)^2 + \Omega_W\Psi_1^W + gH_1 - T\frac{H_1''}{(1+(H_1')^2)^{3/2}} = \rho\left(\left(\frac{\partial\Psi_1^A}{\partial x}\right)^2 + \left(\frac{\partial\Psi_1^A}{\partial y}\right)^2 + \Omega_A\psi_1^A + gH_1\right) + F(t);$$

$$\frac{\partial\phi_1^W}{\partial t} + \frac{\partial\Psi_1^W}{\partial x}\frac{\partial\psi_1^W}{\partial x} + \frac{\partial\Psi_1^W}{\partial y}\frac{\partial\psi_1^W}{\partial y} + h_1\frac{\partial\Psi_1^W}{\partial x}\frac{\partial^2\Psi_1^W}{\partial x\partial y} + h_1\frac{\partial\Psi_1^W}{\partial y}\frac{\partial^2\Psi_1^W}{\partial y^2} + \Omega_W\psi_1^W + \Omega_W\frac{\partial\Psi_1^W}{\partial y}h_1 + gh_1 - T\left(\frac{h_1''}{(1+(H_1')^2)^{3/2}} - \frac{3H_1''H_1'h_1'}{(1+(H_1')^2)^{5/2}}\right) = \rho\left(\frac{\partial\phi_1^A}{\partial t} + \frac{\partial\Psi_1^A}{\partial x}\frac{\partial\psi_1^A}{\partial x} + \frac{\partial\Psi_1^A}{\partial y}\frac{\partial\psi_1^A}{\partial y} + h_1\frac{\partial\Psi_1^A}{\partial x}\frac{\partial^2\Psi_1^A}{\partial x\partial y}\right.$$

$$+h_1\frac{\partial\Psi_1^A}{\partial y}\frac{\partial^2\Psi_1^A}{\partial y^2}+\Omega_A\psi_1^A+\Omega_A\frac{\partial\Psi_1^A}{\partial y}h_1+gh_1\Bigg).$$

4. Two similar equations can be obtained if we use the continuity of pressure across y_B and y_A.

5. Note that the resulting equations for the short wave are linear with respect to the Fourier coefficients, so that we can let $h_{1k_s}=1$ without any loss of generality.

6. To complete the system, we should add an equation fixing the amplitude h of the long wave:

$$H_1(0)=h/2.$$

In the case $h=0$, the system of equations for the short wave decouples in the sense that it possesses solutions in the form of monochromatic waves. It has been shown in [2] that σ satisfies a quartic equation. A wave is linearly unstable if this equation has roots with positive real part.

For $h\neq 0$, the above equations cannot be solved analytically. We use two approaches to deal with this problem:

1. First, let us neglect all the $o(h^2)$ terms, which is equivalent to linearizing the equation for the long wave. Then the wave speed can be determined from the quartic equation (note that within this approximation the wave speed is independent of h). Secondly, let us use three Fourier coefficients for the short wave, namely those corresponding to k_s and $k_s\pm 1$. Now the problem is simple enough to equate (using a symbolic manipulator, e.g., *Mathematica*) the Fourier coefficients corresponding to e^{ik_sx} and $e^{i(k_s\pm 1)x}$. The resulting generalized eigenvalue problem can be solved to obtain a dispersion relation for σ.

2. Alternatively, we can solve the problem numerically. In this case collocation can be employed to set up two systems of equations: one for the long wave (it has to be solved first) and one for the short wave. The system of

equations for the long wave is nonlinear, while the equations for the short wave take the form of a generalized eigenvalue problem. Both systems can be solved using Newton's method with a good initial guess obtained from the linearized equations. We can then use a path-following technique to continue our solution in h and thus study how the stability changes with amplitude.

While investigating the stability, we distinguish two principal cases: finite amplitude waves propagating in the direction of the shear (these waves will be also referred to as co-flowing) and waves moving against the shear (counter-flowing). There also are two "intermediate" finite amplitude waves, associated with the presence of shear in the air and water. These branches disappear in the limit of zero vorticity, and are not considered here. However, we cannot discard them in our later discussion of the infinitesimal perturbations, since they are the ones responsible for the linear instability.

2.3 Linear stability diagrams

First let us determine which combination of the physical parameters Ω_A, Ω_W, Δ_A, Δ_W, k can lead to the linear instability.

The diagrams presented below (see also [2]) in figs. 2.2–2.3 were obtained by plotting the regions where the linear dispersion relation (in the form of a quartic equation) has roots with positive real part.

In order to reduce the number of independent parameters, it was assumed that $V_W/V_A = 0.057$, which is a typical value measured in experiments. We also assume that the tangential stress of the undisturbed profiles is continuous across the air-water interface, i.e., $\rho_A \nu_A V_A/\Delta_A = \rho_W \nu_W V_W/\Delta_W$, and take $\nu_A/\nu_W = 14.94$. The contour lines on each diagram represent the dimensionless growth rate

$$\gamma = \frac{\mathrm{Re}(\sigma)}{c_0 k},$$

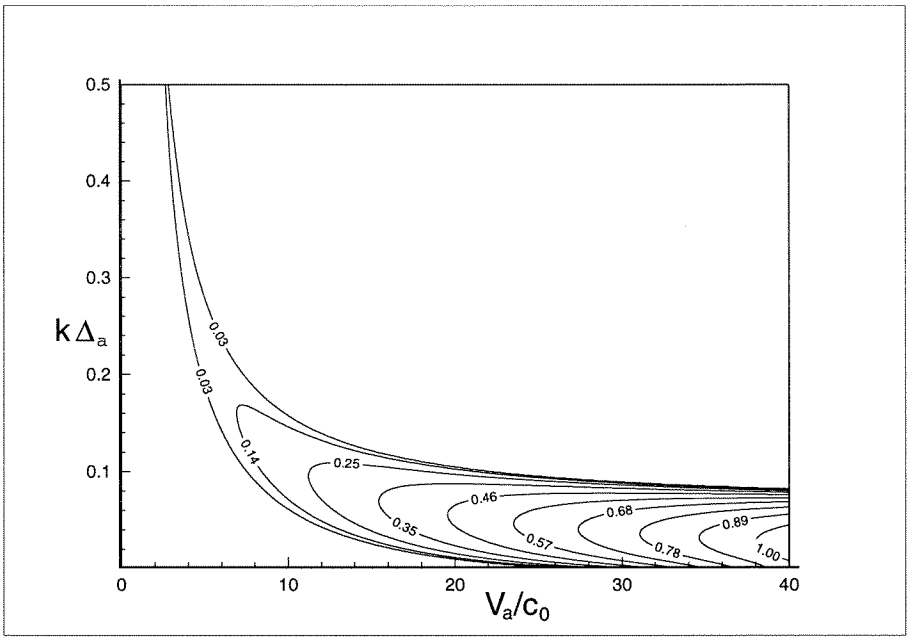

Figure 2.2: Linear stability diagram in the absence of water shear. Contour lines represent the growth rate γ.

where

$$c_0 = \sqrt{\frac{g(1-\rho) + Tk^2}{k(1+\rho)}}.$$

We also set $\rho = 0.00121$, neglect surface tension since it is very small, and normalize time so that $g = 1$.

The last diagram (fig. 2.4) describes the region of instability for the case of water shear only. The presence of the air is completely neglected, i.e., we set $\rho = 0$. The resulting linear dispersion relation takes the form of a cubic (instead of a quartic) equation.

The above stability diagrams will play an important role in our subsequent discussion, where we will consider short infinitesimal perturbations ($k = k_s$) that fall within one of the unstable regions for $h = 0$, superposed on top of a stable finite amplitude wave ($k = k_L$).

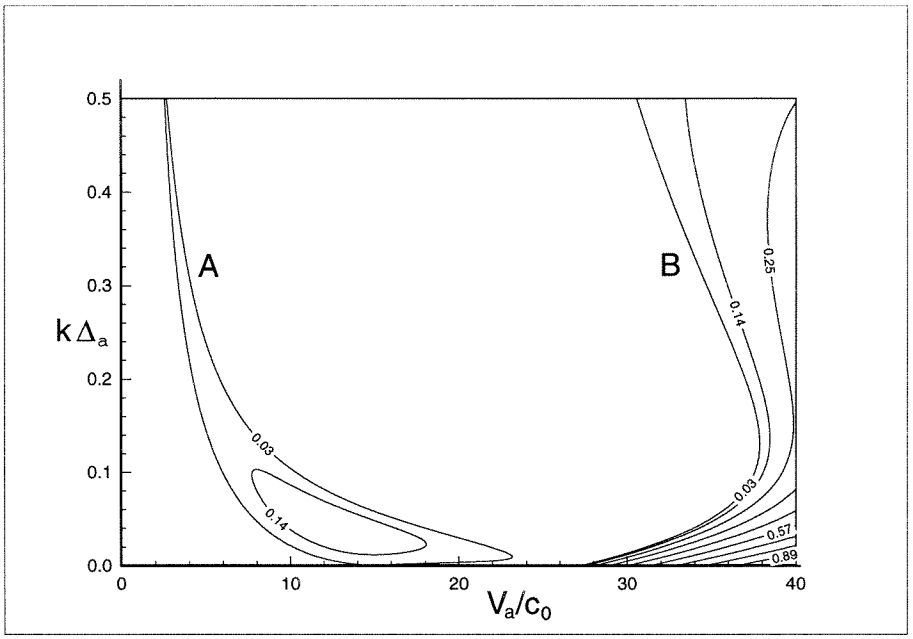

Figure 2.3: Linear stability diagram in the presence of water shear and wind. Contour lines represent the growth rate γ.

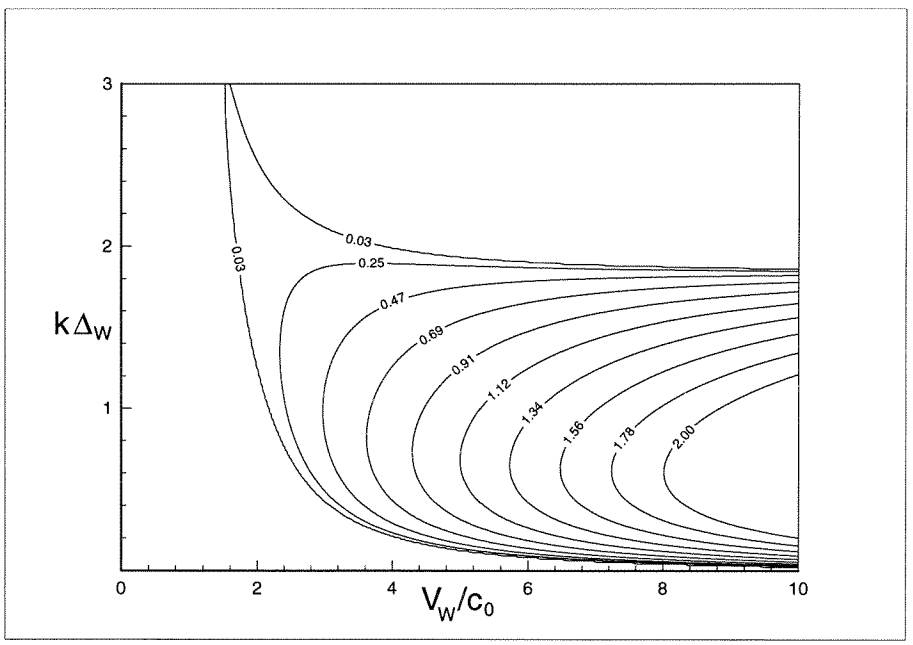

Figure 2.4: Linear stability diagram in the absence of wind. Contour lines represent the growth rate γ.

2.4 Wind without water shear

Numerical calculations in this section were carried out with $N = 30$. Given this resolution it was possible to compute the stability characteristics of the infinitesimal wave for several values of V_A. For each of these values we performed the analysis with three different choices of $k\Delta_A$: near the boundaries of the stability region and approximately in the middle. We also restricted our attention to $V_A/c_0 < 10$, so that the long wave was stable for all amplitudes in question.

2.4.1 Superharmonic perturbations with $k_s = 2$

This case was studied in [4] using a somewhat different approach: the authors derived a joint (coupled) dispersion relation for the long ($k_L = 1$) and short ($k_s = 2$) waves and, unlike the present treatment, avoided splitting the solution process into two steps (solving for the finite amplitude wave and then solving for the infinitesimal wave). It was found that the instability was suppressed when the waves propagated in the direction of the wind, and enhanced otherwise. Our results show that although the enhancement of the instability is not observed, the suppression is much more substantial when the long wave propagates in the direction of the wind. For example, figs. 2.5–2.7 illustrate that the growth rate for the co-flowing wave decreases much faster than the growth rate for the counter-flowing wave. Numerical calculations in this section were compared with the asymptotic approach described in section 2.2. This comparison served two purposes: on the one hand it helped to verify the absence of errors in the numerical approach; on the other hand, it demonstrated the limitations of asymptotics and the importance of using a sufficient number of Fourier coefficients. Note that the lines corresponding to the numerical and asymptotic results for the counter-flowing waves are indistinguishable in figs. 2.6 and 2.7.

The suppression of the instability appears to be due to the excitation of the Fourier mode corresponding to the long wave. In our case, $k_L = 1$, $k_s = 2$, it is the first mode in the expansion of each interface and streamfunction: h_{j1}, a_1^A, b_1^A, and d_1^A. For example, initially $a_1^A = 0$, so that a_2^A is the only nonzero coefficient in the

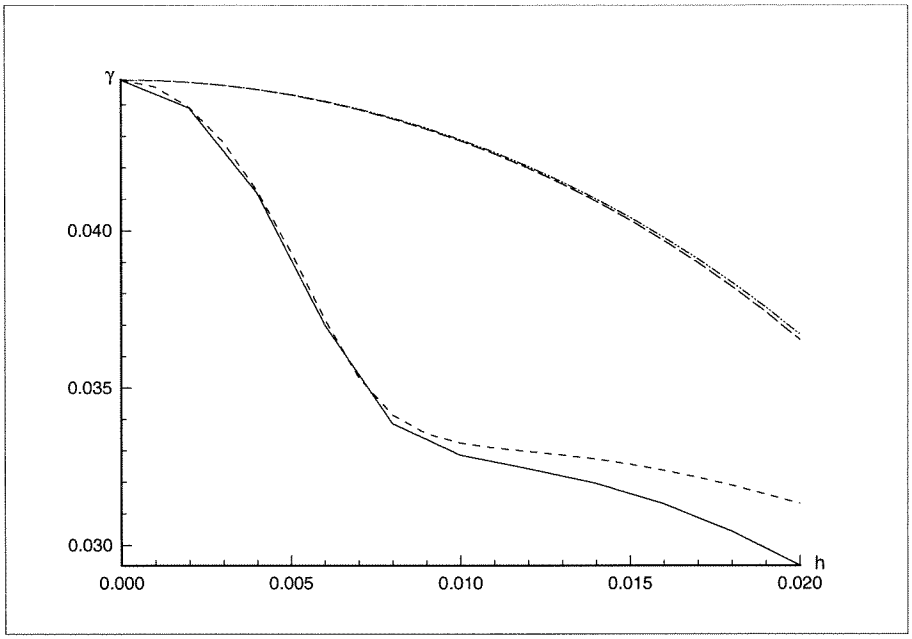

Figure 2.5: γ vs. h for $V_A/c_0 = 5$, $\Delta_A k_s = 0.19$, $k_s = 2$. —, numerics, co-flowing waves; --, asymptotics, co-flowing waves; ——, numerics, counter-flowing waves; —·—, asymptotics, counter-flowing waves.

expansion of ψ_1^A. As the amplitude h of the long wave increases from zero, so does a_1^A. Eventually, a_1^A overtakes a_2^A and becomes dominant. This may result not only in the suppression of the instability, but also in an unusual growth rate behavior, as illustrated in fig. 2.8. We can see that the growth rate for the co-flowing wave has an interim minimum and increases before going to zero. Let us take a closer look at the *imaginary* part of σ (recall that the growth rate is given by the *real* part of σ) in the neighborhood of the dip. Fig. 2.9 shows that the solution branch we have been following (solid line) intersects with a stable(!) branch (dashed line) exactly at the point where the minimum of the growth rate (dotted line) occurs. The nature of this new branch can be clarified by plotting a_1^A/a_2^A. We can see from fig. 2.10 that it corresponds to a wave, which was initially dominated by a_1^A, and not a_2^A as our original wave was. Thus, although the growth rate for the co-flowing wave was initially decreasing faster than the growth rate for the counter-flowing wave, it was prevented from going to zero by the interaction with another wave propagating with

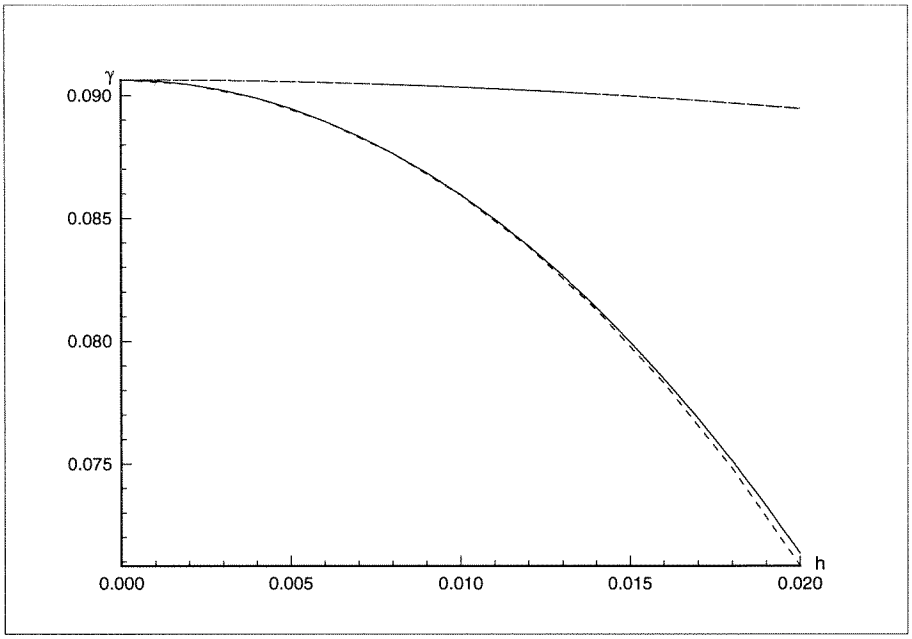

Figure 2.6: γ vs. h for $V_A/c_0 = 5$, $\Delta_A k_s = 0.23$, $k_s = 2$. —, numerics, co-flowing waves; --, asymptotics, co-flowing waves; ——, numerics, counter-flowing waves; —·—, asymptotics, counter-flowing waves.

the same phase speed. On the other hand, fig. 2.9 suggests that the instability can abruptly disappear through a spontaneous bifurcation from the unstable branch (solid line) to the stable branch (dashed line). We will later encounter another example of the same type of behavior (fig. 2.19).

2.4.2 Superharmonic perturbations with $k_s > 2$

As k_s increases from 2, the roles of the waves propagating along and against the wind are gradually exchanged (see figs. 2.11 and 2.12). So for sufficiently large k_s, the waves going against the wind stabilize faster than the waves going in the direction of the wind. Fig. 2.12 indicates that the growth rate for the co-flowing waves can even increase.

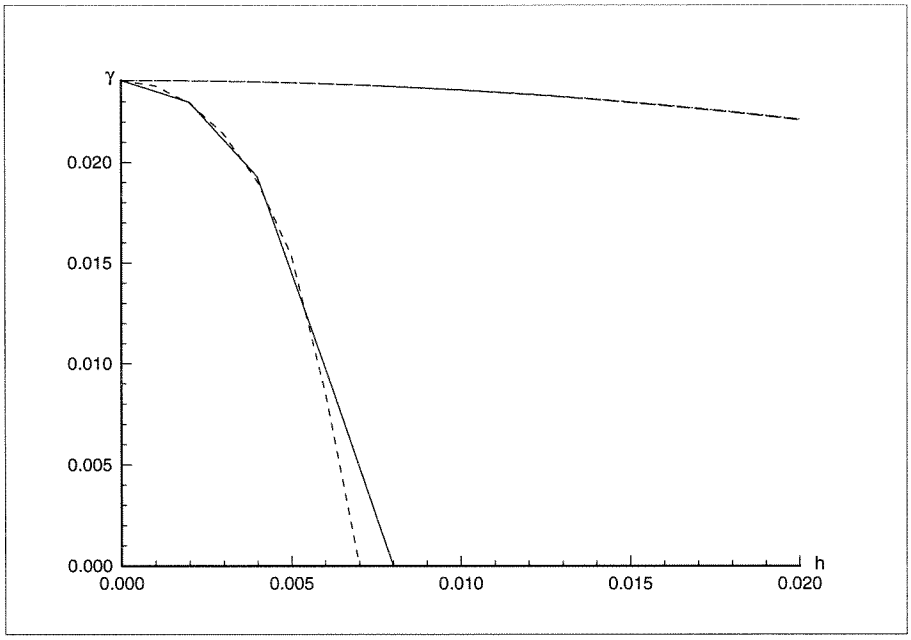

Figure 2.7: γ vs. h for $V_A/c_0 = 5$, $\Delta_A k_s = 0.28$, $k_s = 2$. —, numerics, co-flowing waves; --, asymptotics, co-flowing waves; ——, numerics, counter-flowing waves; —·—, asymptotics, counter-flowing waves.

2.5 Wind and water shear combined

In the experiments conducted by Mitsuyasu [17], the wind speed was kept at 20 m/sec, the wavenumbers of the finite amplitude wave were taken to be $k_L = 1, 2, 4$, the wavenumbers of the short wave varied so that $k_s/k_L = 5, 15, 30$, and the height of the shear layer in the air was $\Delta_A = 0.3$, i.e., $15 < V_A/c_0 < 40$, $1.5 < \Delta_A k_s < 10$. These values clearly indicate that the instabilities in question are associated with the region B in fig. 2.3, i.e., the presence of water shear is essential. If we now consider a few sample values in the upper part of this region, we can see (figs. 2.13–2.15) that for the wavenumbers in question the waves propagating in the direction of the wind stabilize much faster than the waves propagating against the wind.

Unfortunately, the calculations cannot be carried out for small values of k_s for two reasons: (1) the matrices are extremely ill-conditioned for the large values of Δ_A and Δ_W, which are associated with small wavenumbers; (2) the long wave becomes

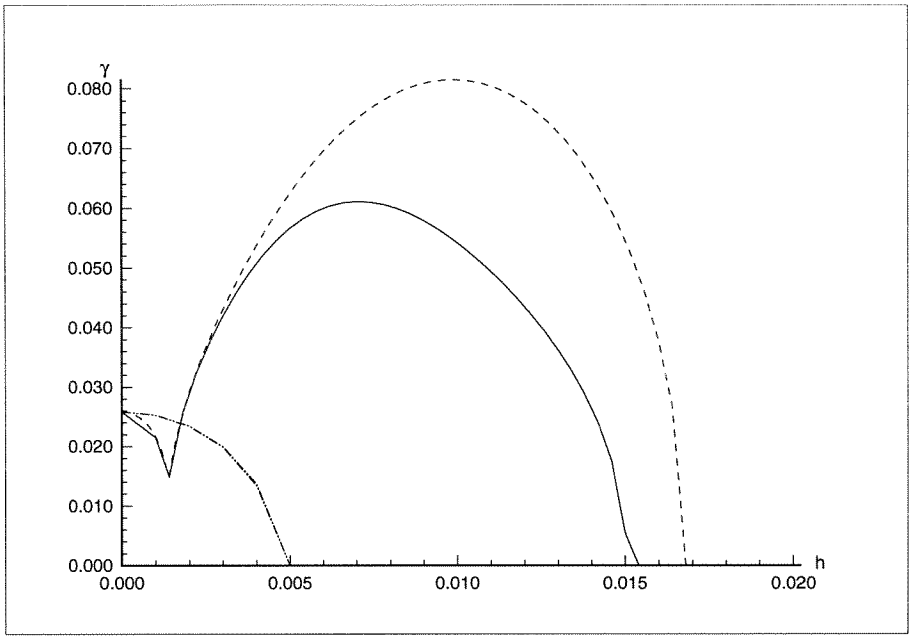

Figure 2.8: γ vs. h for $V_A/c_0 = 8$, $\Delta_A k_s = 0.09$, $k_s = 2$. —, numerics, co-flowing waves; --, asymptotics, co-flowing waves; ——, numerics, counter-flowing waves; —·—, asymptotics, counter-flowing waves.

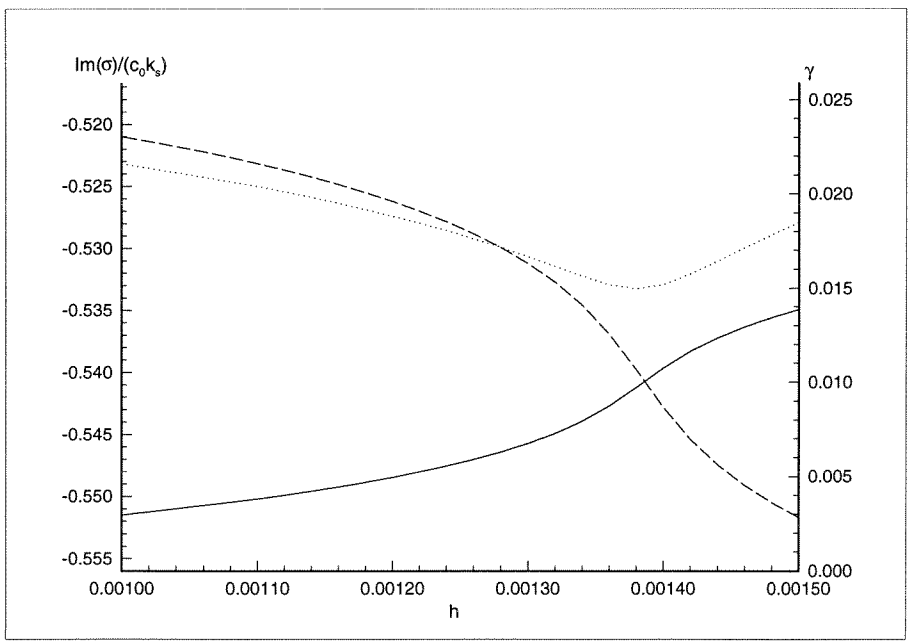

Figure 2.9: Im(σ) and γ vs. h for $V_A/c_0 = 8$, $\Delta_A k_s = 0.09$, $k_s = 2$. —, Im(σ), original branch; ——, Im(σ), new branch; ··, growth rate γ.

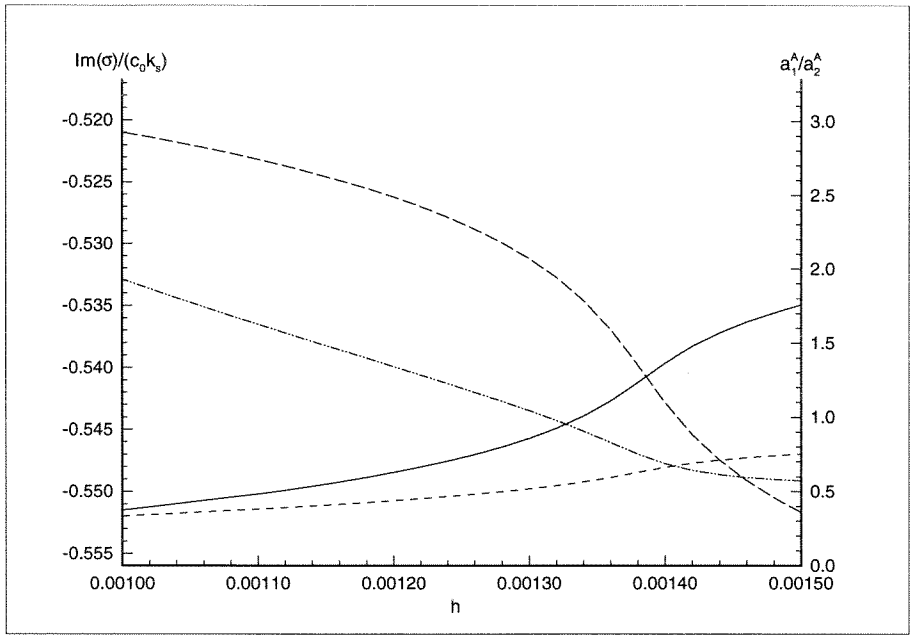

Figure 2.10: $\mathrm{Im}(\sigma)$ and a_1^A/a_2^A vs. h for $V_A/c_0 = 8$, $\Delta_A k_s = 0.09$, $k_s = 2$. —, $\mathrm{Im}(\sigma)$, original branch; ——, $\mathrm{Im}(\sigma)$, new branch; --, a_1^A/a_2^A, original branch; — · ·—, a_1^A/a_2^A, new branch.

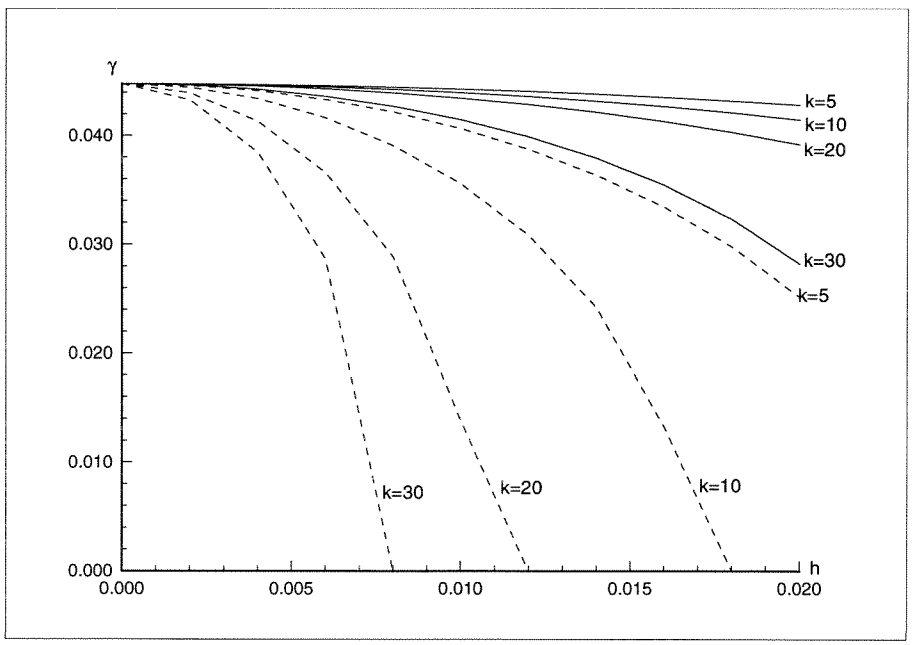

Figure 2.11: γ vs. h for $V_A/c_0 = 5$, $\Delta_A k_s = 0.19$. —, co-flowing waves; --, counter-flowing waves.

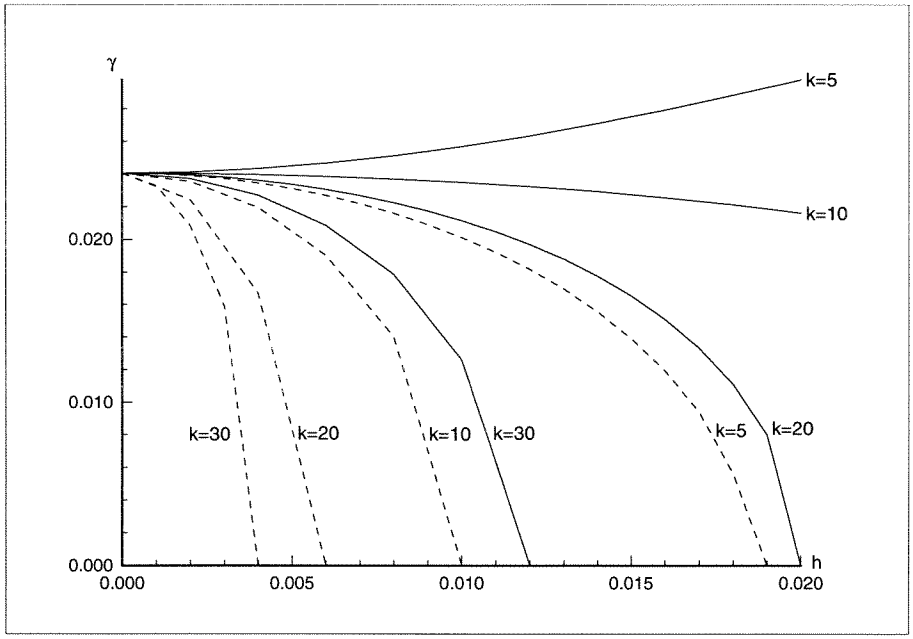

Figure 2.12: γ vs. h for $V_A/c_0 = 5$, $\Delta_A k_s = 0.28$. —, co-flowing waves; --, counter-flowing waves.

unstable for some of those values.

The instabilities associated with the region A in fig. 2.3 are qualitatively the same as those discussed in section 2.4 in the absence of water shear.

2.6 Water current without wind

In the case when the wind is absent, we have to restrict our attention to $V_W/c_0 < 3$, for the reasons similar to those described in section 2.4. It can be seen that the co-flowing waves are generally more stable than the counter-flowing waves. The results are presented in figs. 2.16–2.21. In the spirit of section 2.4 we carried out calculations for two values of the current speed $V_W/c_0 = 1.8$ and 2.0. For each of these speeds we investigated three values of the dimensionless shear depth $\Delta_W k_s$, so that the resulting locations in the stability diagram would be approximately near the lower and upper boundaries, and in the middle of the instability region. One can observe that the trend is for the growth rates to be smaller for shorter waves.

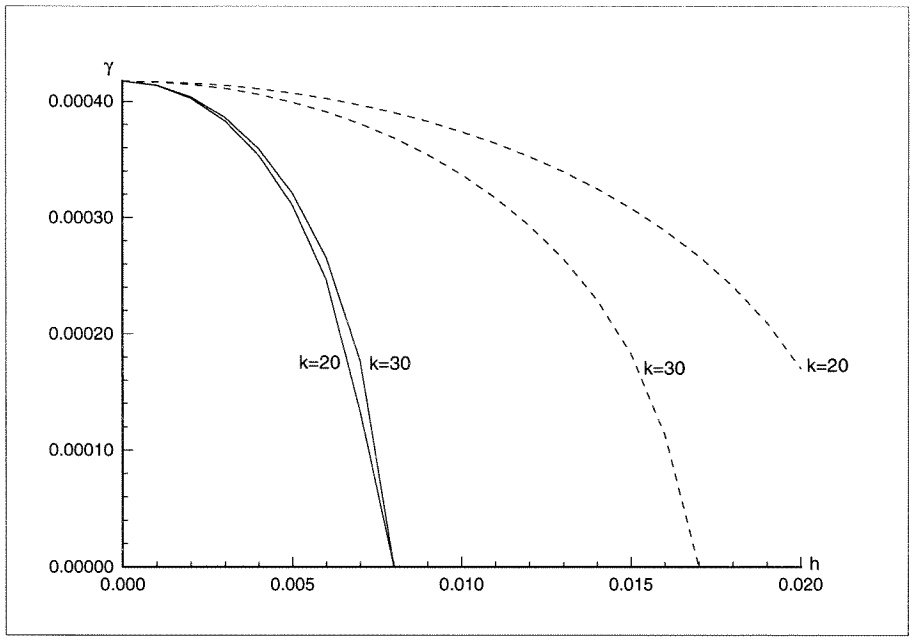

Figure 2.13: γ vs. h for $V_A/c_0 = 15$, $\Delta_A k_s = 1.35$. —, co-flowing waves; --, counter-flowing waves.

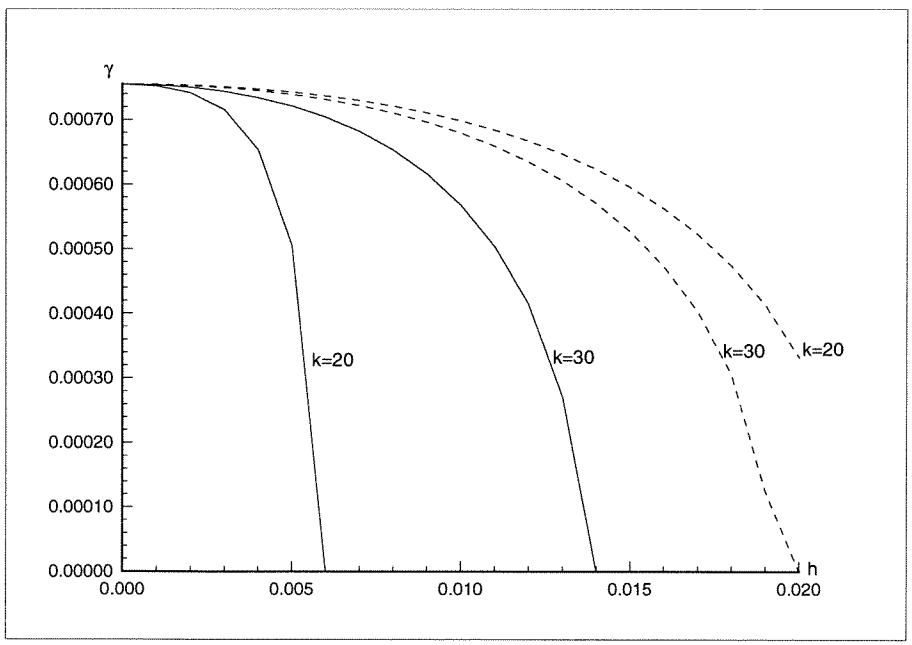

Figure 2.14: γ vs. h for $V_A/c_0 = 21$, $\Delta_A k_s = 1.91$. —, co-flowing waves; --, counter-flowing waves.

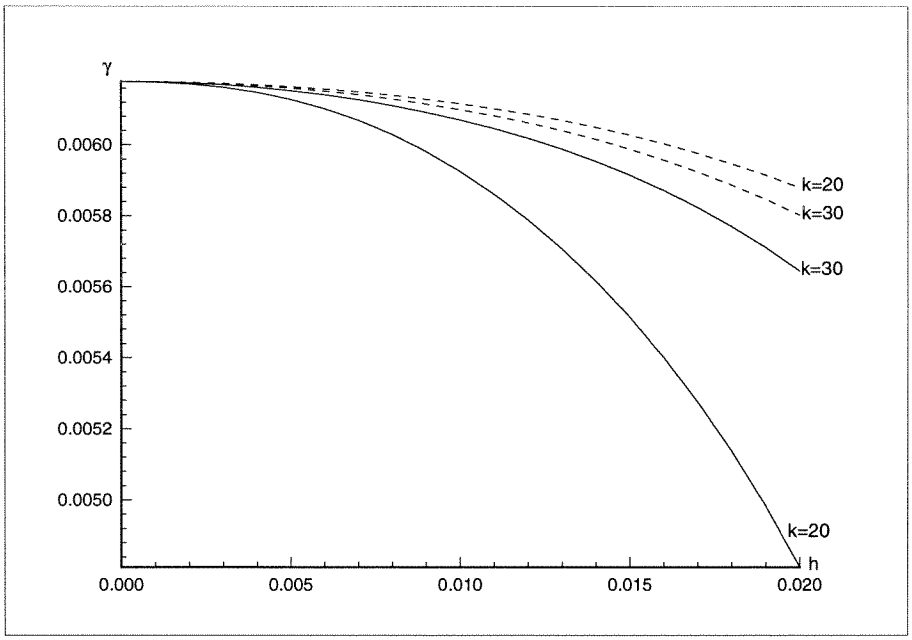

Figure 2.15: γ vs. h for $V_A/c_0 = 23$, $\Delta_A k_s = 1.35$. —, co-flowing waves; --, counter-flowing waves.

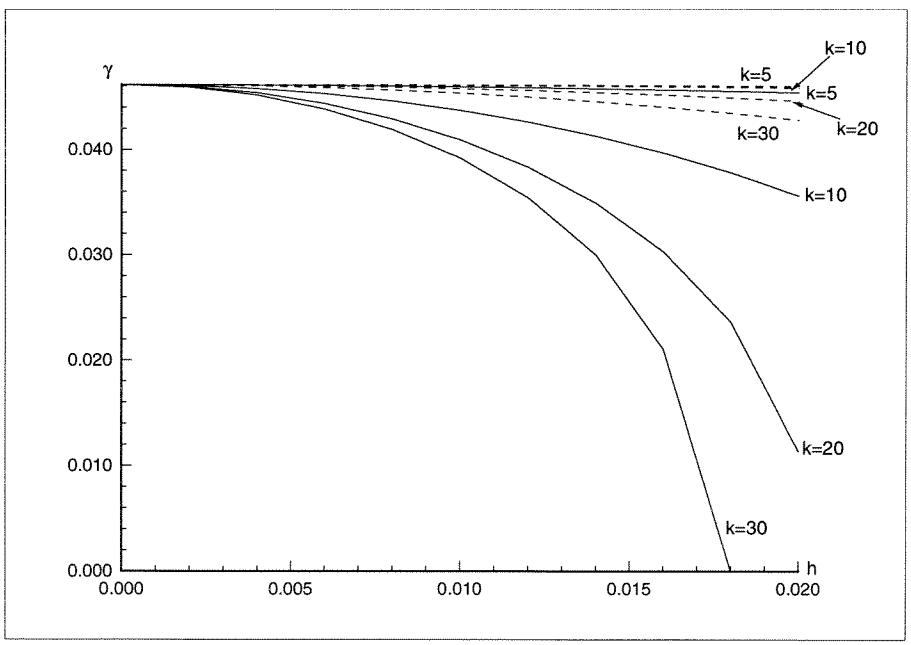

Figure 2.16: γ vs. h for $V_W/c_0 = 1.8$, $\Delta_W k_s = 1.7$. —, co-flowing waves; --, counter-flowing waves.

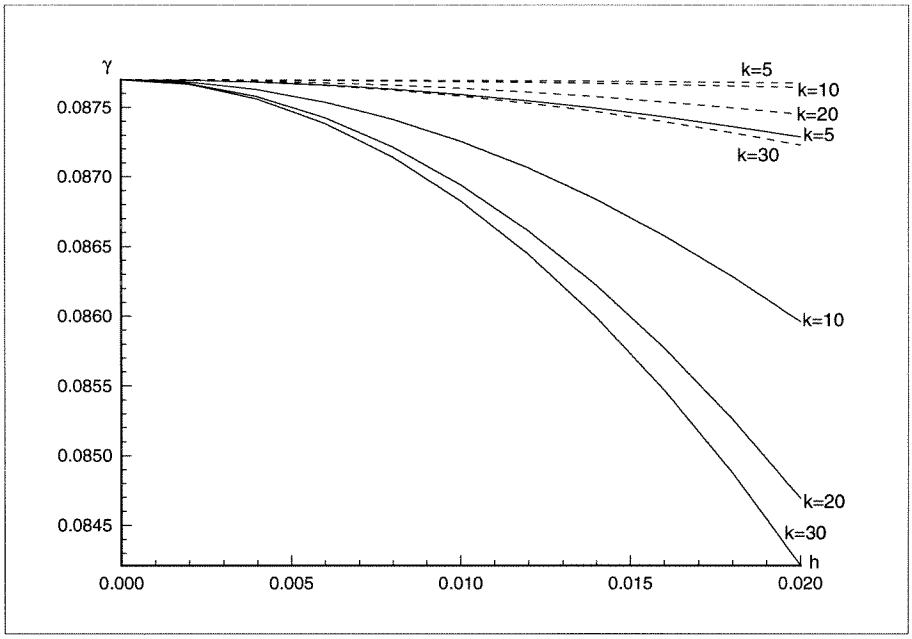

Figure 2.17: γ vs. h for $V_W/c_0 = 1.8$, $\Delta_W k_s = 2.2$. —, co-flowing waves; --, counter-flowing waves.

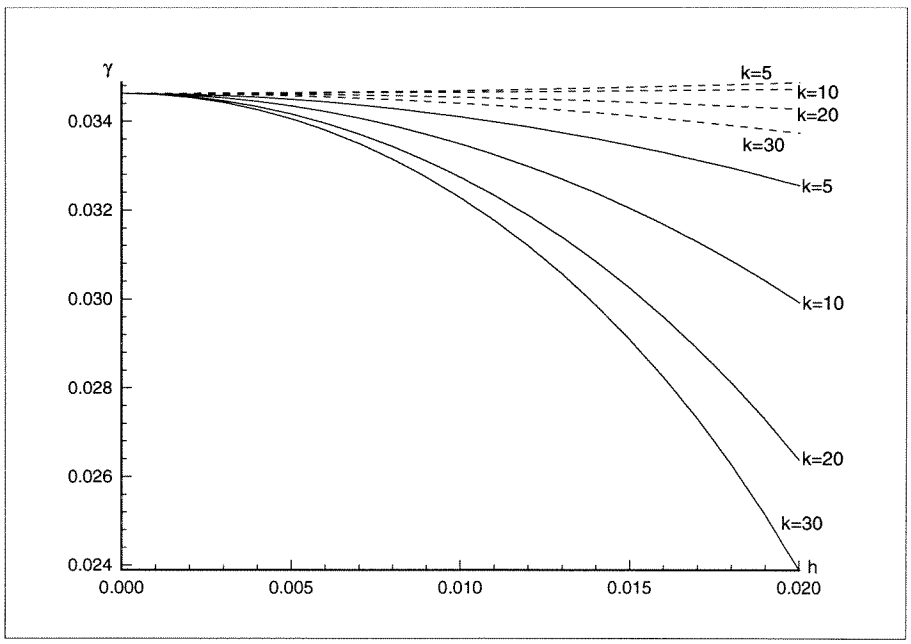

Figure 2.18: γ vs. h for $V_W/c_0 = 1.8$, $\Delta_W k_s = 2.7$. —, co-flowing waves; --, counter-flowing waves.

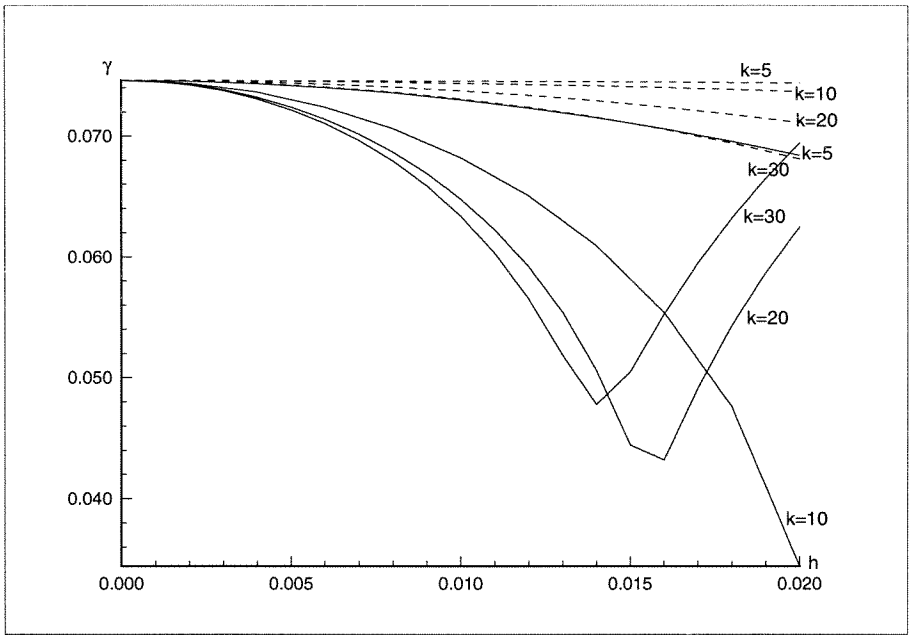

Figure 2.19: γ vs. h for $V_W/c_0 = 2.0$, $\Delta_W k_s = 1.3$. —, co-flowing waves; --, counter-flowing waves.

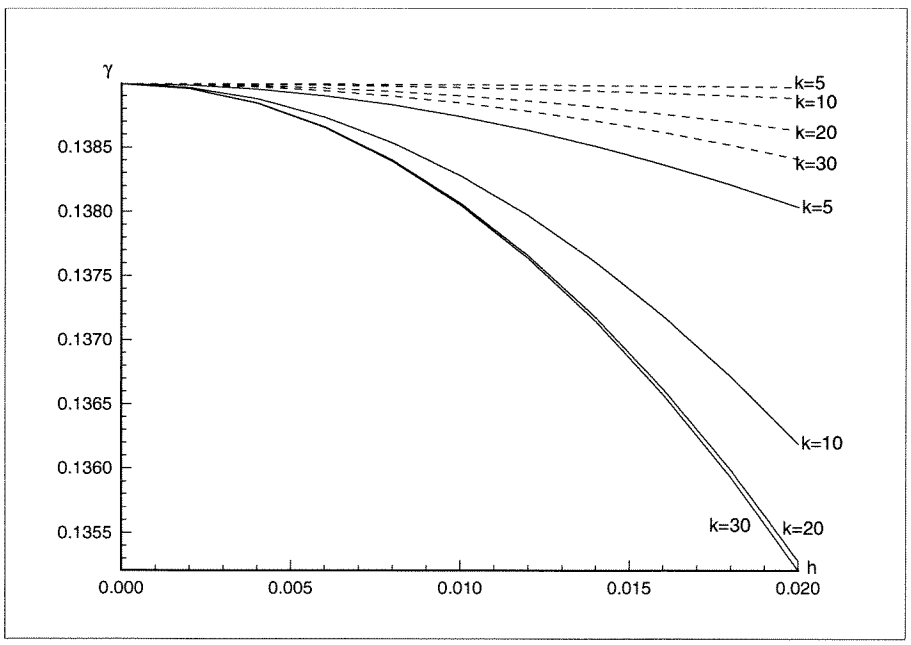

Figure 2.20: γ vs. h for $V_W/c_0 = 2.0$, $\Delta_W k_s = 1.9$. —, co-flowing waves; --, counter-flowing waves.

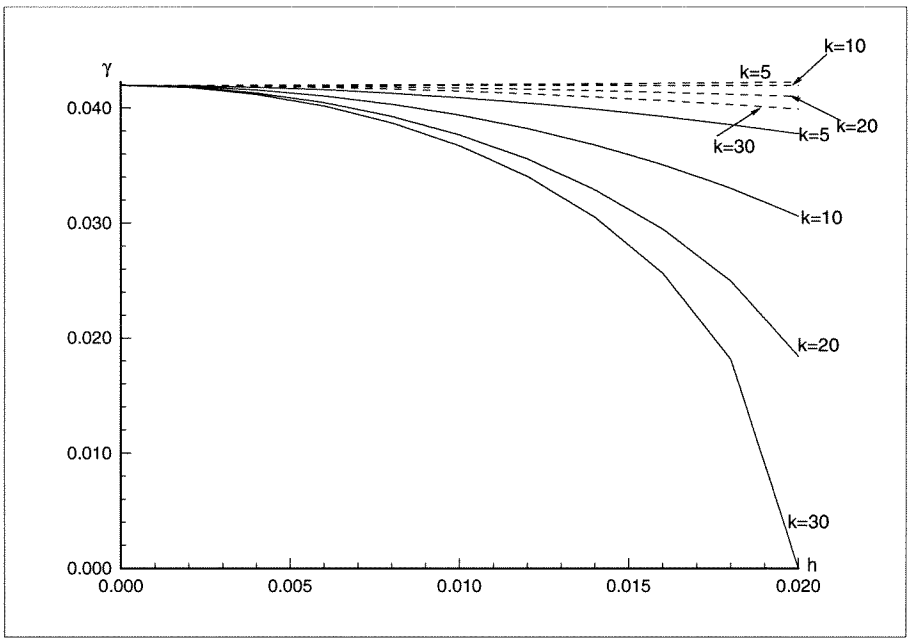

Figure 2.21: γ vs. h for $V_W/c_0 = 2.0$, $\Delta_W k_s = 2.5$. —, co-flowing waves; --, counter-flowing waves.

Chapter 3 Modulation of gravity waves with shear in water

3.1 Introduction

In this chapter our focus is on the case when the amplitude of the basic wave is sufficiently small (in section 3.5 we use a numerical approach to study what happens for large amplitudes) and the wavenumbers of the interacting waves are very close, which would have resulted in the well-known Benjamin-Feir instability, had the waves been irrotational. This instability was studied numerically by Longuet-Higgins [15] and analytically (using the modulation approach) by Hasimoto and Ono [11]. The latter showed that the wave envelope of a slowly varying wave train satisfies the nonlinear cubic Schrödinger equation (NLS). We derive this equation for the waves on a water current varying linearly with depth and study the dependence of the growth rate of infinitesimal perturbations on the strength of the current. We compare the results obtained with those of Li, Hui and Donelan [14] for the special case of the infinitely deep shear. A numerical approach similar to that of Longuet-Higgins [15] and the one used in the previous chapter is also pursued.

It is shown that depending on the direction of the propagation (along or against the shear flow) of the finite amplitude waves, the effect of the shear on the stability of infinitesimal perturbations is substantially different. In most cases, however, the shear strength increase first enhances the instability, but later suppresses it.

3.2 Equations and boundary conditions

In this and all subsequent chapters, we neglect the presence of the air for the sake of simplicity. We therefore drop the superscripts A and W, since all the quantities are

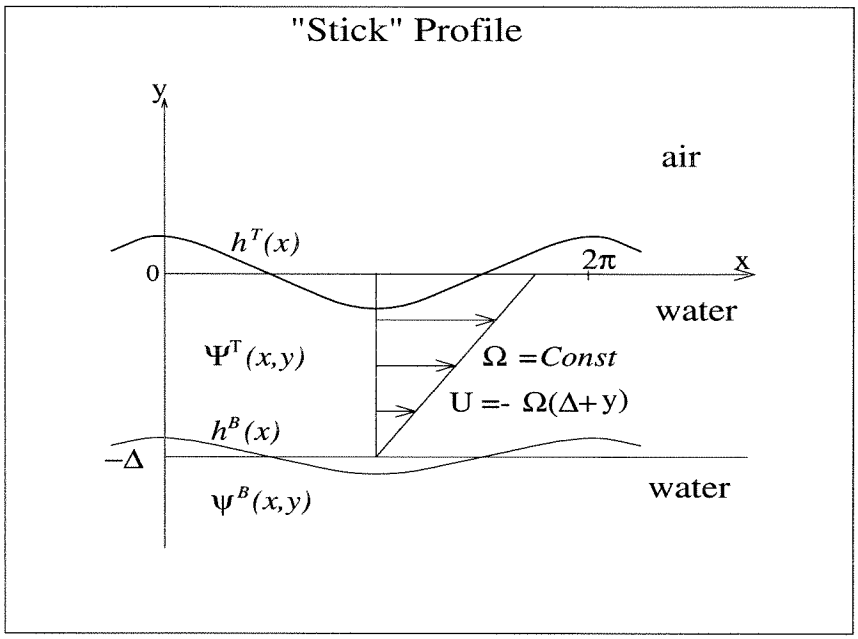

Figure 3.1: Velocity profile for water shear. Velocity U is shown as it would have appeared in the absence of waves.

related to the water (refer to fig. 3.1 for the new notation).

The superscript "T" is used for all quantities pertaining to the region with vorticity (also to be referred to as the upper region), while the superscript "B" is reserved for the quantities from the irrotational region (lower region).

The shapes of the free surface and the interface between the upper and the lower regions are given by $h^{T,B} = h^{T,B}(x,t)$, and the flow is described by two streamfunctions $\Psi^T = \Psi^T(x,y,t)$ and $\psi^B = \psi^B(x,y,t)$, which satisfy

$$\nabla^2\Psi^T = -\Omega \text{ for } h^B < y < h^T; \tag{3.1}$$

$$\nabla^2\psi^B = 0 \text{ for } -\infty < y < h^B. \tag{3.2}$$

Ψ^T can be written in the form

$$\Psi^T(x,y,t) = -\frac{1}{2}\Omega y^2 - \Omega\Delta y + \psi^T(x,y,t), \tag{3.3}$$

where ψ^T is harmonic and therefore has a conjugate function ϕ^T such that

$$\frac{\partial \phi^T}{\partial x} = \frac{\partial \psi^T}{\partial y}; \ \frac{\partial \phi^T}{\partial y} = -\frac{\partial \psi^T}{\partial x}. \tag{3.4}$$

Similarly, there exists $\phi^B = \phi^B(x, y, t)$ such that

$$\frac{\partial \phi^B}{\partial x} = \frac{\partial \psi^B}{\partial y}; \ \frac{\partial \phi^B}{\partial y} = -\frac{\partial \psi^B}{\partial x}. \tag{3.5}$$

To complete the formulation of the problem, we use the boundary conditions from chapter 2. Using our new notation, we can rewrite them as follows:

1. We assume that the velocities are zero at infinite depth (this condition will be modified in section 3.5 in order to account for a change of coordinates):

$$\frac{\partial \phi^B}{\partial y} \to 0, \ \frac{\partial \phi^B}{\partial x} \to 0 \text{ as } y \to -\infty. \tag{3.6}$$

2. The kinematic condition on $y = h^T(x, t)$ gives us:

$$\frac{D}{Dt}(y - h^T) = 0$$

or

$$\frac{\partial \phi^T}{\partial y} = \frac{\partial h^T}{\partial t} + \left(\frac{\partial \phi^T}{\partial x} - \Omega(h^T + \Delta)\right)\frac{\partial h^T}{\partial x}. \tag{3.7}$$

3. Similarly,

$$\frac{\partial \phi^B}{\partial y} = \frac{\partial h^B}{\partial t} + \frac{\partial \phi^B}{\partial x}\frac{\partial h^B}{\partial x} \tag{3.8}$$

on $y = h^B(x, t)$.

4. We require that the pressure across the free surface be continuous:

$$\begin{aligned} \frac{\partial \phi^T}{\partial t} + \frac{1}{2}\left[\left(\frac{\partial \phi^T}{\partial x} - \Omega(h^T + \Delta)\right)^2 + \left(\frac{\partial \phi^T}{\partial y}\right)^2\right] & \\ +\Omega\left(\psi^T - \frac{1}{2}\Omega(h^T)^2 - \Omega\Delta h^T\right) + gh^T &= F(t) \end{aligned} \tag{3.9}$$

on $y = h^T(x,t)$.

5. Likewise, we can use the continuity of pressure across the lower interface:

$$\begin{aligned}&\frac{\partial\phi^T}{\partial t} + \frac{1}{2}\left[\left(\frac{\partial\phi^T}{\partial x} - \Omega(h^B+\Delta)\right)^2 + \left(\frac{\partial\phi^T}{\partial y}\right)^2\right]\\ &+\Omega\left(\psi^T - \frac{1}{2}\Omega(h^B)^2 - \Omega\Delta h^B\right)\\ &\quad = \frac{\partial\phi^B}{\partial t} + \frac{1}{2}\left[\left(\frac{\partial\phi^B}{\partial x}\right)^2 + \left(\frac{\partial\phi^B}{\partial y}\right)^2\right]\end{aligned} \tag{3.10}$$

on $y = h^B(x,t)$.

6. Finally, the continuity of normal velocity across the lower interface yields:

$$\frac{\partial h^B}{\partial x}\left(\frac{\partial\phi^T}{\partial x} - \Omega(h^B+\Delta)\right) - \frac{\partial\phi^T}{\partial y} = \frac{\partial h^B}{\partial x}\frac{\partial\phi^B}{\partial x} - \frac{\partial\phi^B}{\partial y} \tag{3.11}$$

on $y = h^B(x,t)$.

The last two conditions are equivalent to requiring that the velocity be continuous at the interface, i.e.,

$$\frac{\partial\phi^T}{\partial x} - \Omega(h^B+\Delta) = \frac{\partial\phi^B}{\partial x}, \tag{3.12}$$

$$\frac{\partial\phi^T}{\partial y} = \frac{\partial\phi^B}{\partial y} \tag{3.13}$$

on $y = h^B(x,t)$.

It is easy to prove that the continuity of pressure and normal velocity indeed implies the continuity of tangential velocity, and hence the continuity of velocity itself. First observe that on $y = h^B(x,t)$:

$$\begin{aligned}&\frac{d}{dx}\left[\frac{\partial\phi^T}{\partial t} + \Omega\left(\psi^T - \frac{1}{2}\Omega(h^B)^2 - \Omega\Delta h^B\right) - \frac{\partial\phi^B}{\partial t}\right]\\ &\quad = \frac{\partial}{\partial t}\left[\frac{\partial\phi^T}{\partial x} - \frac{\partial\phi^B}{\partial x} + \frac{\partial\phi^T}{\partial y}\frac{\partial h^B}{\partial x} - \frac{\partial\phi^B}{\partial y}\frac{\partial h^B}{\partial x}\right]\\ &+\Omega\left(\frac{\partial\psi^T}{\partial x} + \frac{\partial\psi^T}{\partial y}\frac{\partial h^B}{\partial x} - \Omega(h^B+\Delta)\frac{\partial h^B}{\partial x}\right)\end{aligned}$$

(use a condition similar to (3.7) to simplify the expression in parenthesis)

$$= \frac{\partial}{\partial t}\left[\frac{\partial \phi^T}{\partial x} - \frac{\partial \phi^B}{\partial x} + \frac{\partial \phi^T}{\partial y}\frac{\partial h^B}{\partial x} - \frac{\partial \phi^B}{\partial y}\frac{\partial h^B}{\partial x}\right] - \Omega\frac{\partial h^B}{\partial t}$$

$$= \frac{\partial}{\partial t}\left[\frac{\partial \phi^T}{\partial x} - \Omega(h^B + \Delta) + \frac{\partial \phi^T}{\partial y}\frac{\partial h^B}{\partial x}\right] - \frac{\partial}{\partial t}\left[\frac{\partial \phi^B}{\partial x} + \frac{\partial \phi^B}{\partial y}\frac{\partial h^B}{\partial x}\right] = \frac{\partial v_\tau^T}{\partial t} - \frac{\partial v_\tau^B}{\partial t},$$

where v_τ^T and v_τ^B are the tangential velocities above and below the interface respectively. Therefore, the continuity of pressure and normal velocity (equations (3.10) and (3.11)) imply that

$$\frac{\partial v_\tau^T}{\partial t} + \frac{1}{2}\frac{d(v_\tau^T)^2}{dx} = \frac{\partial v_\tau^B}{\partial t} + \frac{1}{2}\frac{d(v_\tau^B)^2}{dx}. \tag{3.14}$$

Suppose that the velocities are small, i.e.,

$$v_\tau^{T,B} = \sum_{l=1}^{\infty} \varepsilon^l (v_\tau^{T,B})^{(l)},$$

where ε is a small parameter to be defined in section 3.3. In addition, let us assume that $(v_\tau^{T,B})^{(l)} \sim e^{i(kx-\omega t)}$, which is exactly the form that we are going to use later on. Then $\frac{\partial}{\partial t}(v_\tau^{T,B})^{(l)} = -i\omega(v_\tau^{T,B})^{(l)}$ and it follows from (3.14) that $(v_\tau^T)^{(l)} = (v_\tau^B)^{(l)}$. Thus, the tangential and normal velocities, and hence the horizontal and vertical velocities, are continuous at the interface.

We will find later on that the use of the continuity of horizontal and vertical velocities, instead of the pressure and normal velocity, simplifies algebraic manipulations.

3.3 Derivation of Schrödinger equation

In order to derive an equation for h^T, we apply the method of multiple scales to the equations (3.1) and (3.2), as well as to the boundary conditions (3.6)–(3.9), (3.12), and (3.13). Let ε denote a formal small parameter (it will be later related to the amplitude of the wave of permanent form). Following [11], we introduce "slow" variables:

$$\xi = \varepsilon(x - c_g t), \ \tau = \varepsilon^2 t, \tag{3.15}$$

where $c_g = \frac{d\omega}{dk}$ is the group velocity and ω is the frequency of the finite amplitude wave obtained from the linear dispersion relation. The velocity potentials ϕ^T and ϕ^B, as well as the interfaces h^T and h^B, can be represented in the following form:

$$\phi^T = \sum_{n=-\infty}^{\infty} \phi_n^T E^n, \; h^T = \sum_{n=-\infty}^{\infty} h_n^T E^n; \tag{3.16}$$

$$\phi^B = \sum_{n=-\infty}^{\infty} \phi_n^B E^n, \; h^B = \sum_{n=-\infty}^{\infty} h_n^B E^n; \tag{3.17}$$

where

$$E = e^{i(kx-\omega t)}, \; \phi_{-n}^{T,B} = \left(\phi_n^{T,B}\right)^*, \; h_{-n}^{T,B} = \left(h_n^{T,B}\right)^*,$$

$$\phi_n^{T,B} = \sum_{j=|n|}^{\infty} \varepsilon^j \phi_{n,j}^{T,B}(\xi, y, \tau),$$

$$h_n^{T,B} = \sum_{j=|n|}^{\infty} \varepsilon^j h_{n,j}^{T,B}(\xi, \tau).$$

Note that

$$\frac{\partial}{\partial x} \to \frac{\partial}{\partial x} + \varepsilon \frac{\partial}{\partial \xi}; \; \frac{\partial}{\partial t} \to \frac{\partial}{\partial t} - \varepsilon c_g \frac{\partial}{\partial \xi} + \varepsilon^2 \frac{\partial}{\partial \tau}.$$

We substitute the above expansions (3.16) and (3.17) in the equations (3.1) and (3.2) respectively, and equate powers of E. In order to simplify the notation, we drop the superscripts T and B in all subsequent relations which are true for both.

$$\varepsilon^2 \frac{\partial^2 \phi_n}{\partial \xi^2} + 2nik\varepsilon \frac{\partial \phi_n}{\partial \xi} - n^2 k^2 \phi_n + \frac{\partial^2 \phi_n}{\partial y^2} = 0 \text{ for } n = 0, .., \infty,$$

or

$$\sum_{j=|n|}^{\infty} \left(\varepsilon^2 \frac{\partial^2 \phi_{n,j}}{\partial \xi^2} + 2nik\varepsilon \frac{\partial \phi_{n,j}}{\partial \xi} - n^2 k^2 \phi_{n,j} + \frac{\partial^2 \phi_{n,j}}{\partial y^2} \right) \varepsilon^j = 0 \text{ for } n = 0, .., \infty.$$

Denote

$$L_n(\cdot) \equiv (\frac{\partial^2}{\partial y^2} - n^2 k^2)(\cdot).$$

First consider $n = 1$. Then equating the $O(\varepsilon^1)$ terms, we obtain

$$L_1\phi_{1,1} = 0.$$

Hence, $\phi_{1,1} = e^{\pm ky}$. Similarly, for $n = 2$: $\phi_{2,2} = e^{\pm 2ky}$. For ϕ^B we should also use the boundary condition (3.6). So,

$$\phi^T_{1,1} = A^T_1 e^{ky} + A^T_2 e^{-ky},$$

$$\phi^B_{1,1} = A^B_1 e^{ky},$$

$$\phi^T_{2,2} = B^T_1 e^{2ky} + B^T_2 e^{-2ky},$$

$$\phi^B_{2,2} = B^B_1 e^{2ky}.$$

Now consider $n = 1$ once more and equate the $O(\varepsilon^2)$ terms:

$$L_1\phi_{1,2} + 2ik\frac{\partial\phi_{1,1}}{\partial\xi} = 0.$$

This equation yields

$$\phi^T_{1,2} = -i\frac{\partial A^T_1}{\partial\xi}ye^{ky} + i\frac{\partial A^T_2}{\partial\xi}ye^{-ky} + C^T_1 e^{ky} + C^T_2 e^{-ky},$$

$$\phi^B_{1,2} = -i\frac{\partial A^B_1}{\partial\xi}ye^{ky} + C^B_1 e^{ky}.$$

Finally, equating the $O(\varepsilon^3)$ terms for $n = 1$ gives

$$L_1\phi_{1,3} + 2ik\frac{\partial\phi_{1,2}}{\partial\xi} + \frac{\partial^2\phi_{1,1}}{\partial\xi^2} = 0.$$

Therefore,

$$\begin{aligned}\phi^T_{1,3} \;=\; & -i\frac{\partial C^T_1}{\partial\xi}ye^{ky} + i\frac{\partial C^T_2}{\partial\xi}ye^{-ky} - \frac{1}{2}\frac{\partial^2 A^T_1}{\partial\xi^2}y^2e^{ky} - \frac{1}{2}\frac{\partial^2 A^T_2}{\partial\xi^2}y^2e^{-ky} \\ & + D^T_1 e^{ky} + D^T_2 e^{-ky},\end{aligned}$$

$$\phi^B_{1,3} = -i\frac{\partial C^B_1}{\partial \xi} y e^{ky} - \frac{1}{2}\frac{\partial^2 A^B_1}{\partial \xi^2} y^2 e^{ky} + D^B_1 e^{ky}.$$

Note that since the fluid is of infinite depth, the mean level of the free surface can be set to zero, i.e.,

$$h_{0,j} = 0,\ \phi_{0,j} = 0 \text{ for } j = 0, 1, \ldots,$$

with the exception of $h^B_{0,0} = -\Delta$.

The expansion coefficients of the streamfunction can be determined from (3.4) and (3.5) as follows:

$$\psi^{T,B}_{1,1} = ik \int \phi^{T,B}_{1,1} dy,$$

$$\psi^{T,B}_{1,2} = ik \int \left(\phi^{T,B}_{1,2} + \frac{\partial \phi^{T,B}_{1,1}}{\partial \xi} \right) dy,$$

$$\psi^{T,B}_{1,3} = ik \int \left(\phi^{T,B}_{1,3} + \frac{\partial \phi^{T,B}_{1,2}}{\partial \xi} \right) dy,$$

$$\psi^{T,B}_{2,2} = 2ik \int \phi^{T,B}_{2,2} dy.$$

The most difficult step of the derivation is the substitution of the expansions into the boundary conditions. We retain the terms which are bigger than $o(\varepsilon^4)$, then equate the coefficients corresponding to $E^1\varepsilon^1, E^1\varepsilon^2, E^1\varepsilon^3, E^2\varepsilon^2$. The resulting system of twenty equations (see appendix A) has a solution provided that two compatibility conditions hold.

One of these conditions is the linear dispersion relation. It has been shown in [3] that ω satisfies a cubic equation. A wave is linearly unstable if this equation has roots with nonzero imaginary part. This linear instability has to be distinguished from the instability studied in the present work and associated with nonlinearity. We restrict our attention to the smallest and the largest roots of the cubic dispersion relation, since the third ("middle") root disappears in the limit $\Omega \to 0$.

The other compatibility condition turns out to be the nonlinear Schrödinger equation (NLS):

$$i\frac{\partial h^T_{1,1}}{\partial \tau} + \mu\frac{\partial^2 h^T_{1,1}}{\partial \xi^2} + q\left|h^T_{1,1}\right|^2 h^T_{1,1} = 0,$$

where μ and q depend on Ω and Δ. This dependence is investigated in detail below, but explicit formulas for μ and q are very difficult to obtain, even with the use of a symbolic calculator (such as *Mathematica*). Instead, we compute μ and q for specific values of Ω and Δ.

The only exception is the case $\Delta \to \infty$, when explicit expressions for μ and q can be obtained:

$$\mu = -\frac{\omega_d}{k^2}\frac{(1-\Omega_d)^2}{(2-\Omega_d)^3},$$

$$q = \frac{1}{2}\omega_d k^2(\Omega_d^3 - 6\Omega_d^2 + 6\Omega_d - 4),$$

where

$$\omega_d = \omega - \Omega\Delta k,\ \Omega_d = \frac{\Omega}{\omega_d}.$$

The dispersion relation becomes

$$\omega_d = \omega - \Omega\Delta k = (\Omega \pm \sqrt{\Omega^2 + 4gk})/2.$$

These expressions were previously obtained in [14] with the formula for q being somewhat different:

$$\begin{aligned} q &= -4\omega_d k^2 \frac{-\frac{1}{8}\Omega_d^4 + \frac{5}{4}\Omega_d - 2\Omega_d + 1}{2-\Omega_d} \\ &\equiv \frac{1}{2}\omega_d k^2(-\Omega_d^3 + 2\Omega_d^2 + 6\Omega_d - 4), \end{aligned} \tag{3.18}$$

where we made appropriate changes to the original notation of [14] to allow a comparison with our results.

It is known that the NLS has the following solution representing a nonlinear plane wave:

$$h_{1,1}^T = h_0 e^{i(\kappa\xi - \alpha\tau)},$$

where $h_0 = \text{const}$, $\alpha = \mu\kappa^2 - q|h_0|^2$. Then

$$h^T = \varepsilon h_{1,1}^T e^{i(kx-\omega t)} + O(\varepsilon^2) = \varepsilon h_0 e^{i(\kappa\xi-\alpha\tau)} e^{i(kx-\omega t)} + O(\varepsilon^2).$$

At this point it is suitable to let $\varepsilon = 1$ and assume instead that the quantities multiplied by ε (namely h_0 and κ) are small themselves. Recall that $\xi = \varepsilon(x - c_g t)$ and $\tau = \varepsilon^2 t$. Then

$$h^T = h_0 e^{i\left((k+\kappa)x - (\omega + c_g\kappa + \mu\kappa^2 - q|h_0|^2)t\right)} + O(h_0^2).$$

This expression can be viewed as a solution with a slightly modified wavenumber and an appropriately modified dispersion law. Therefore,

$$\mu = \omega''(k)/2,$$

allowing us to verify the correctness of μ analytically using the linear dispersion relation (see fig 3.2).

The other coefficient q will be verified numerically, since it is related to the non-linear correction to the dispersion law.

The solution corresponding to the finite amplitude wave with the wavenumber k is recovered if we set $\kappa = 0$:

$$h_{1,1}^T = h_0 e^{i\alpha\tau}.$$

3.4 Stability analysis

We can now carry out standard stability analysis using the NLS (see [11]). Let us perturb $h_{1,1}^T$:

$$h_{1,1}^T = (h_0 + \widehat{\varepsilon}\widehat{h})e^{i(\alpha\tau + \widehat{\varepsilon}\widehat{\theta})}, \tag{3.19}$$

where $\widehat{h}$ and $\widehat{\theta}$ are proportional to $e^{i(\widehat{k}\xi - \widehat{\omega}\tau)}$; $\widehat{\varepsilon}$ is a formal small parameter (corresponding to ε in the numerical approach described in section 3.5); $\widehat{k}$ and $\widehat{\omega}$ are the wavenumber and frequency of the perturbation respectively. Upon substituting into the NLS, we obtain the following dispersion relation for the perturbations:

$$\widehat{\omega} = \mu\widehat{k}^2\sqrt{1 - 2\frac{qh_0^2}{\mu\widehat{k}^2}}. \tag{3.20}$$

This formula is valid for sufficiently small values of h_0 and $\widehat{k}$. The region of validity is further restricted by the fact that in the case of the co-flowing waves, the asymptotic series for h^T (and all other quantities) becomes disordered if the shear strength $\Omega\Delta$ is too large, e.g., we get $h^T_{2,2} \sim 1000(h^T_{1,1})^2$. However, $h^T_{2,2}/(h^T_{1,1})^2$ is bounded as a function of Δ, so that the case of the infinitely deep shear can still be investigated for sufficiently small amplitudes $h^T_{1,1}$. In the case of the counter-flowing waves, $h^T_{2,2}/(h^T_{1,1})^2$ remains less than 1, but the finite amplitude waves become linearly unstable themselves for large values of $\Omega\Delta$, so that the present approach is no longer applicable.

Obviously, the instability occurs when $\widehat{\omega}$ becomes imaginary. This happens for $h_0 > \widehat{k}\sqrt{\frac{\mu}{2q}}$. Therefore, $q\mu > 0$ is a necessary condition for the instability. We will see later that q always has the same sign as Ω; hence, it is the sign of μ that plays the pivotal role.

Let $h = 2h_0/\widehat{k}$ denote the "normalized" amplitude (note that the dimension of h is L^2) and $\gamma = \widehat{\omega}/\widehat{k}^2$ denote the "normalized" growth rate (actually the growth rate is given by $\mathrm{Im}[\gamma]$). Then we can rewrite (3.20) in the form

$$\gamma = \mu\sqrt{1 - \frac{1}{2}\frac{qh^2}{\mu}}. \tag{3.21}$$

From now on we also assume that $g = 1$. Note that apart from normalizing the amplitude h, the growth rate γ, and the acceleration due to gravity g, we preserve the original dimensions of all other quantities.

We start with the co-flowing waves: $\Omega \geq 0$, $\omega < 0$.

For $\Omega = 0$ we have $q = 2$ and $\mu = \frac{1}{8}$ (if we take $k = 1$, $\omega = -1$). Therefore, a wave becomes unstable for $h = \sqrt{2}/4$.

In the generic case of $\Omega \neq 0$ and $\Delta < \infty$, the behavior of μ is presented in fig. 3.2 (we will only consider the case $k = 1$ in order to facilitate comparison with numerical results). As μ goes to zero, so does the critical amplitude h at which the wave becomes unstable (see fig. 3.3). When μ becomes negative, the instability abruptly disappears. This effect is observed for $\Delta < \Delta_{cr}$ ($\Delta_{cr} \approx 0.62$). For $\Delta > \Delta_{cr}$, μ is always positive.

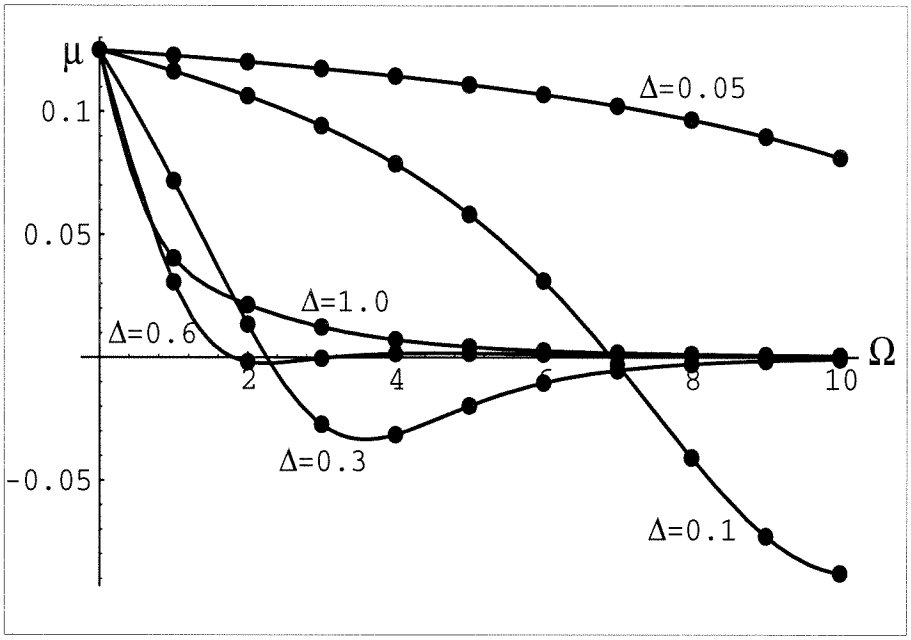

Figure 3.2: NLS coefficient μ vs. vorticity Ω for various values of the shear depth Δ, as given by asymptotics (dots) and $\omega''(k)/2$ (solid line); $k = 1$. Co-flowing waves.

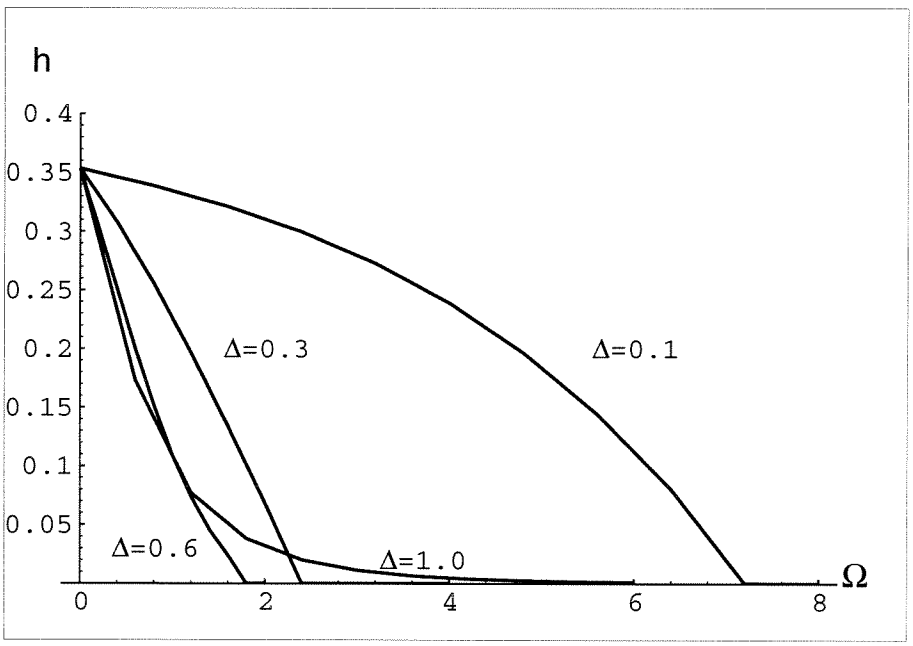

Figure 3.3: Critical amplitude h vs. vorticity Ω for various values of the shear depth Δ; $k = 1$. Co-flowing waves.

Unlike μ, q does not change its sign and therefore has little effect on the stability. This is illustrated in fig. 3.7, which has been placed in section 3.5 (along with some other figures mentioned in the present section) to allow comparison with numerical results.

From (3.21) we obtain the growth rate γ as a function of Ω (for various Δ and h, $k = 1$). We can see from fig. 3.19 (solid line) that for $\Delta = 0.1 < \Delta_{cr}$, the instability is first enhanced, but later suppressed, by the addition of shear. Such behavior is related to the fact that μ becomes negative, so that the instability is no longer possible. In the case of $\Delta = 1.0 > \Delta_{cr}$ (fig. 3.20, solid line) the instability is simply enhanced. This is due to the fact that μ remains positive for all Ω.

In the case of the counter-flowing waves ($\Omega > 0$, $\omega > 0$) the basic wave is unstable for $\Omega\Delta$ large enough, so that the asymptotics becomes invalid. We therefore restrict our attention to small values of Ω. Again, we study the case $k = 1$.

The crucial property is that unlike the case of the waves propagating in the direction of the shear, μ does not change its sign and $\mu q > 0$, so that the instability is always possible. The behavior of μ and q is presented in figs. 3.4 and 3.5.

The critical amplitude h is an increasing function of Ω, as illustrated in fig. 3.6. Hence, we expect an initially unstable perturbation to stabilize for sufficiently large Ω. However, since μ is increasing in magnitude, the growth rate can initially increase. The larger the amplitude of the basic wave, the bigger is the region where the growth rate is increasing. It is sufficient to illustrate this behavior for just one value of Δ, say $\Delta = 1.0$ (solid line in fig. 3.22).

3.5 Numerical simulation

Our next objective is to compute the growth rate numerically and compare the results with those obtained in section 3.4 using the asymptotic approach. We expect the two methods to agree for small amplitudes, with the numerical treatment providing an insight into what happens when the amplitude of the wave of permanent form becomes large.

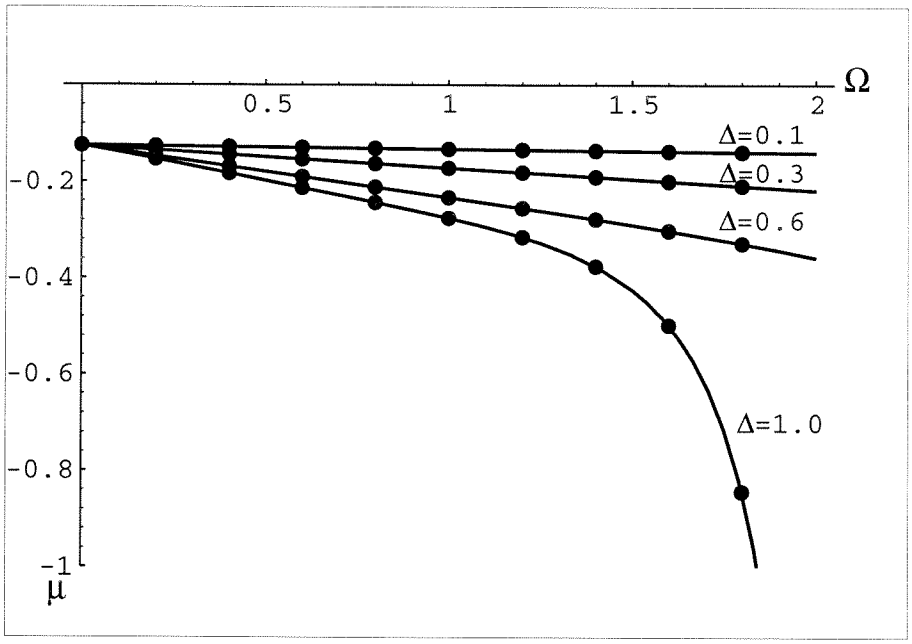

Figure 3.4: NLS coefficient μ vs. vorticity Ω for various values of the shear depth Δ, as given by asymptotics (dots) and $\omega''(k)/2$ (solid line); k=1. Counter-flowing waves.

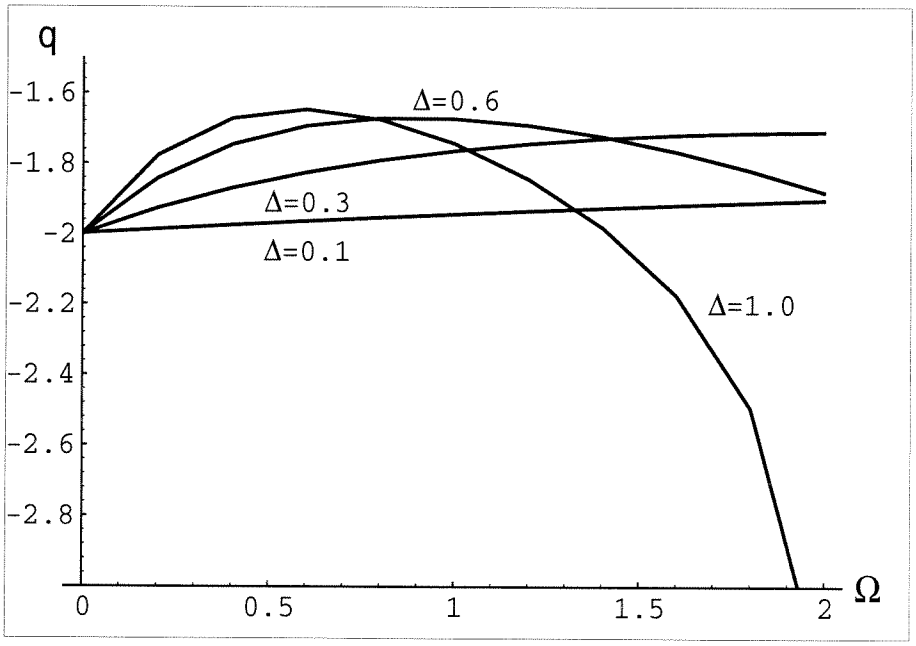

Figure 3.5: NLS coefficient q vs. vorticity Ω for various values of the shear depth Δ; k=1. Counter-flowing waves.

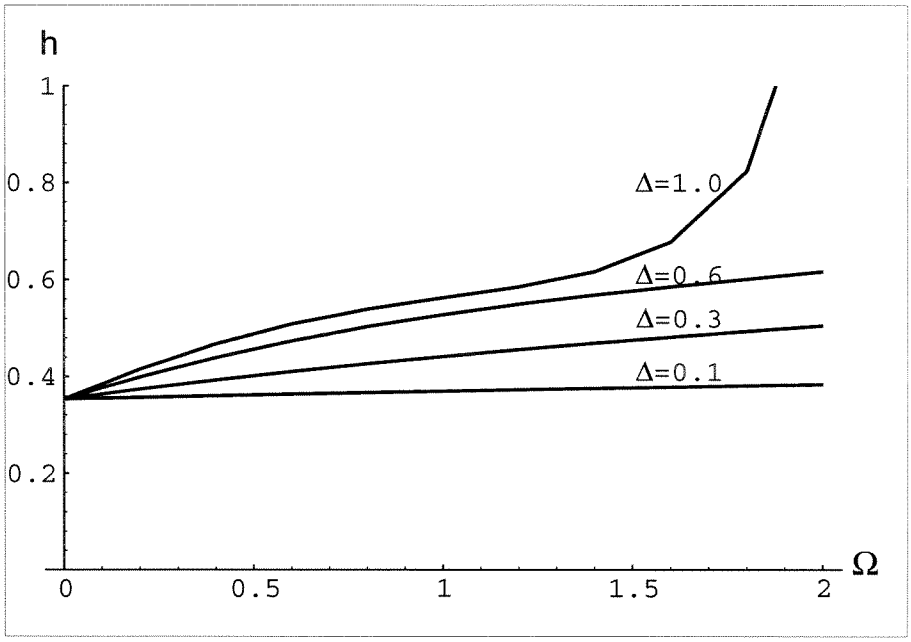

Figure 3.6: Critical amplitude h vs. vorticity Ω for various values of the shear depth Δ; $k = 1$. Counter-flowing waves.

3.5.1 Numerical method

It is quite easy to modify the numerical algorithm from the previous chapter for the present case. In order to ensure a "bug-free" computation, the following two approaches were implemented.

First of all, one has to note that the above modulation approach corresponds to the (four-wave) interaction of the waves with the wavenumbers that are very close. In fact, the wavenumbers must differ by $\widehat{k}$: $k \pm \widehat{k}$. For the purposes of the numerical simulation, we take $\widehat{k} = 1/m$. We now make an observation that the equations are invariant under the transformation

$$\Delta' = \Delta/m, \ \Omega' = \Omega\sqrt{m},$$

with all other dimensional variables being rescaled appropriately. The only nonzero Fourier coefficients in this new wave are those whose subscripts are divisible by m. Thus, a practical procedure for investigating the stability of a wave with $k = 1$ to the

perturbations with $k = (m \pm 1)/m$ is as follows:

1. Calculate the basic wave of finite height with the wavenumber $k = 1$.
2. Rescale the above solution, so that $k = m$.
3. Calculate the infinitesimal wave with $k = m \pm 1$, riding on top of the finite amplitude wave. Note that for this wave the only nonzero Fourier modes are those corresponding to $m \pm 1 + lm$, where l is an integer.
4. Rescale the results back.

Alternatively, we can slightly generalize the algorithm from chapter 2, using the following representation of the streamfunctions and shapes of the interfaces:

$$\psi_1 = e^{\sigma t}\left[\sum_{k=-N}^{N} e^{i(k\pm\widehat{k})x}\left(a_k e^{|k\pm\widehat{k}|y} + b_k e^{-|k\pm\widehat{k}|y}\right)\right],$$

$$h_j(x) = e^{\sigma t}\left(\sum_{k=-N}^{N} h_{jk} e^{i(k\pm\widehat{k})x}\right) \text{ for } j = 1, 2.$$

Both of these approaches were implemented and produced identical results. The first approach requires fewer changes to our previously used algorithm, while the second approach provides more flexibility as far as the choices for $\widehat{k}$ are concerned.

3.5.2 Comparison of numerical and asymptotic approaches

It has to be noted that the numerical and asymptotic approaches have different ranges of validity. For example, the Jacobian in Newton's method is ill-conditioned for small $\widehat{k}$, since in the limit $\widehat{k} \to 0$ the infinitesimal and finite amplitude waves have the same wavenumber, so that the system of equations for the Fourier coefficients of the infinitesimal wave becomes degenerate. Therefore, the numerical simulation proves to be difficult, while the asymptotic expansion gives the best approximation. On the other hand, the asymptotic expansion is not valid for large h_0, where the numerical approach still gives reliable results. As mentioned in section 3.4, the asymptotic approach fails for large values of $\Omega\Delta$, while the numerical approach fails for large

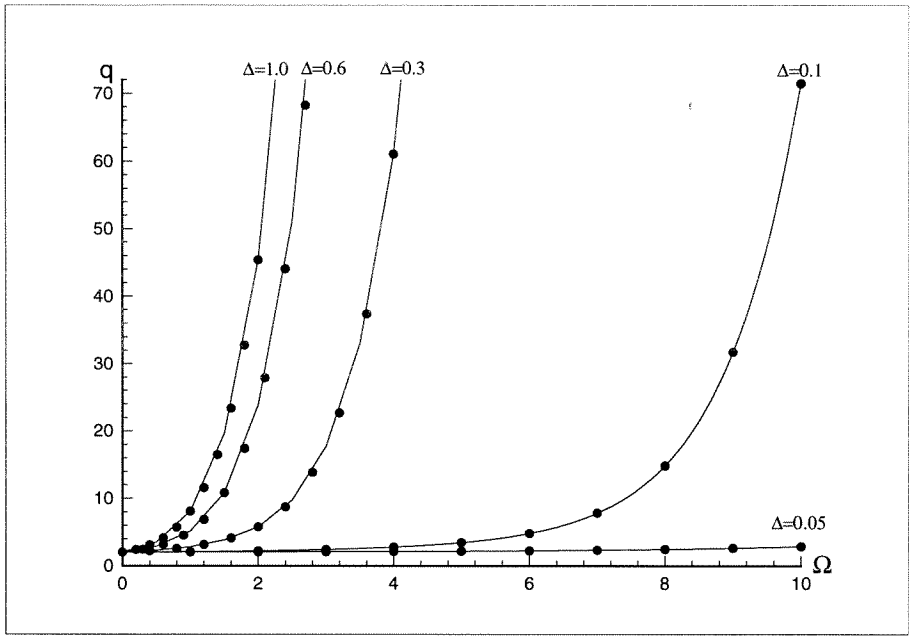

Figure 3.7: NLS coefficient q vs. vorticity Ω for various values of the shear depth Δ for the co-flowing waves, as given by numerics (dots) and asymptotics (solid line). $k = 1$. Co-flowing waves.

Δ (roughly for $\Delta > 1$), since the values of $e^{\pm k\Delta}$ can no longer be represented with sufficient accuracy for higher harmonics.

Now let us verify the correctness of the values of the NLS coefficient q, using the fact that $\omega_{exact} = \omega_{linear} - qh_0^2 + O(h_0^4)$. Therefore, for small amplitudes we should have $\omega_{numerical} \approx \omega_{linear} - qh_0^2$, which allows us to check the correctness of q by computing the dispersion law of the finite amplitude wave. It can be seen from fig. 3.7 that the values of q obtained with the help of the computations agree with those given by the asymptotic approximation.

The numerical results for the dependence of the growth rate on the vorticity Ω are presented in fig. 3.8. In order to explain the disagreement between the numerical and asymptotic solutions, let us perform the computation with only two Fourier coefficients for the finite amplitude wave, which would be similar to the asymptotic approach assumption (3.19). We can see that the picture changes dramatically when we go from $N = 2$ (fig. 3.9) to $N = 3$ (fig. 3.10). Further increase of N results

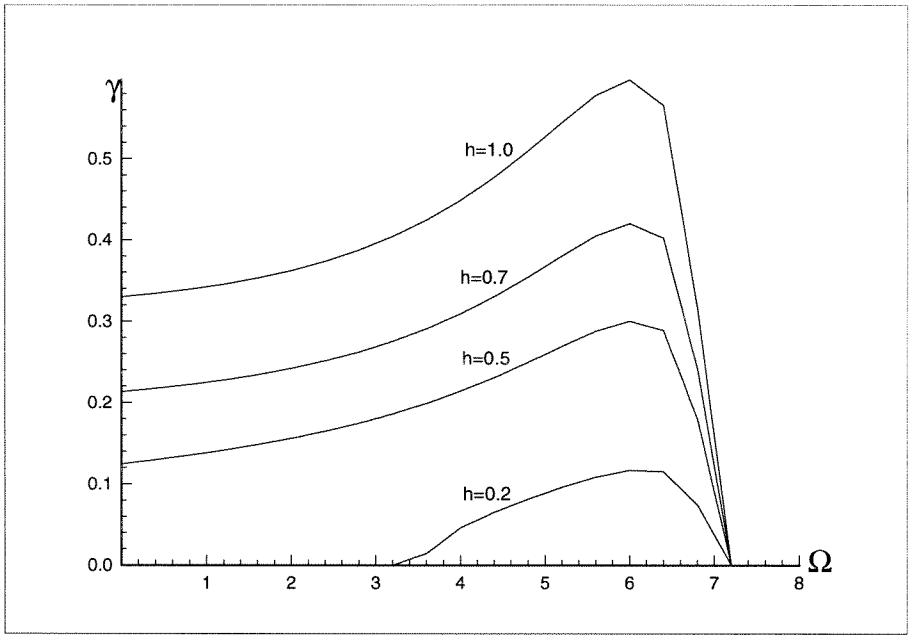

Figure 3.8: Growth rate γ vs. vorticity Ω for various amplitudes h, as given by numerics. $\Delta = 0.1$, $N = 50$. Co-flowing waves.

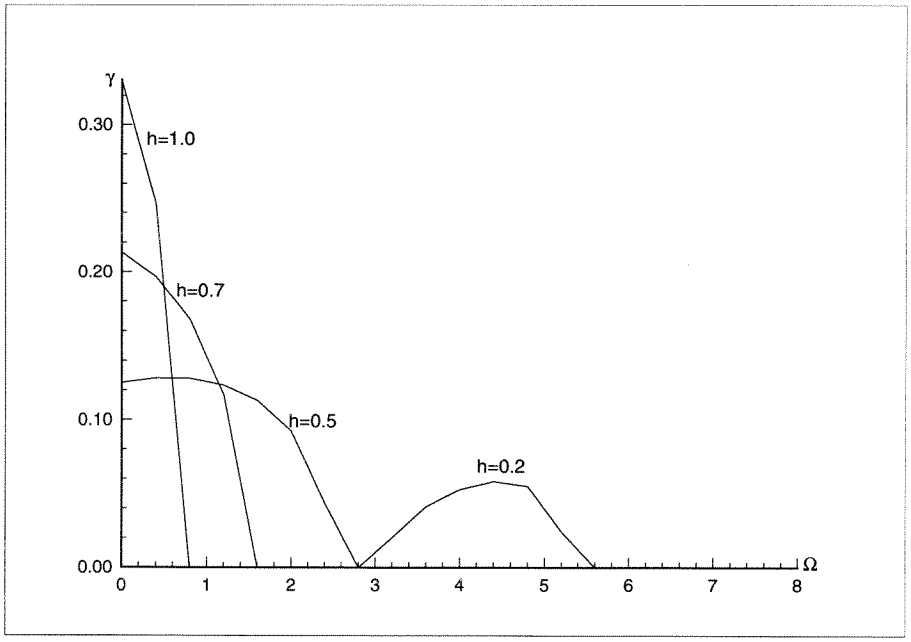

Figure 3.9: Growth rate γ vs. vorticity Ω for various amplitudes h, as given by numerics. $\Delta = 0.1$, $N = 2$. Co-flowing waves.

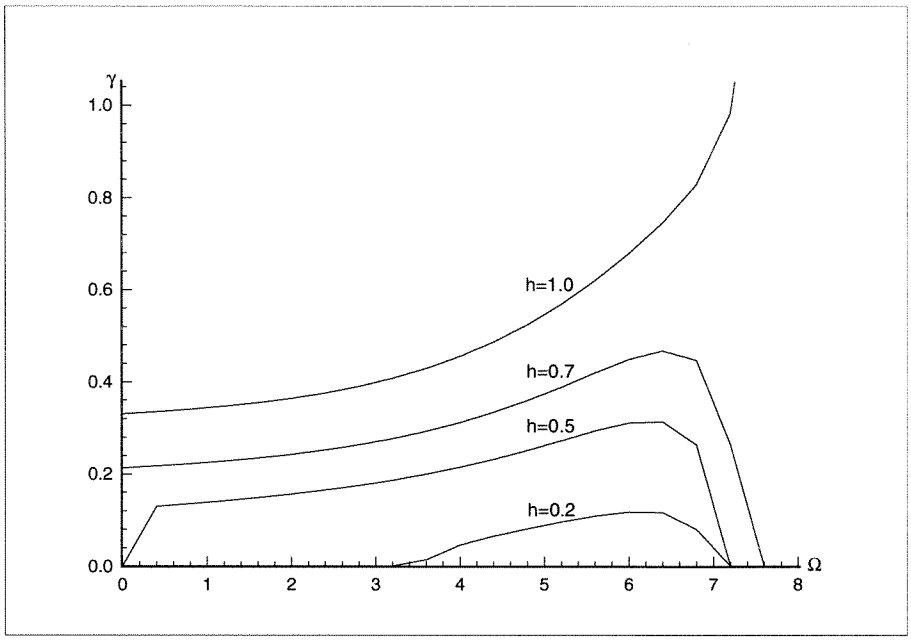

Figure 3.10: Growth rate γ vs. vorticity Ω for various amplitudes h, as given by numerics. $\Delta = 0.1$, $N = 3$. Co-flowing waves.

in rapid convergence to the situation presented in fig. 3.8. Note that the *maximum* growth rates presented in fig. 3.9 ($N = 2$), especially in the case $h = 0.2$, are in better agreement with the asymptotic results.

Now let us determine how well the predictions for the growth rate obtained from the asymptotic theory agree with the numerical calculations for large amplitudes. We set $\Omega = 1$, $\Delta = 0.1$ and carry out the computation for $\widehat{k} = 0.01$ and $\widehat{k} = 0.02$. It can be seen from figs. 3.11 and 3.12 that the agreement is very good for small amplitudes, especially for the smaller of the two values of $\widehat{k}$. As expected, the asymptotic approach fails to predict the decrease of the growth rate for large amplitudes. This behavior is in agreement with [15].

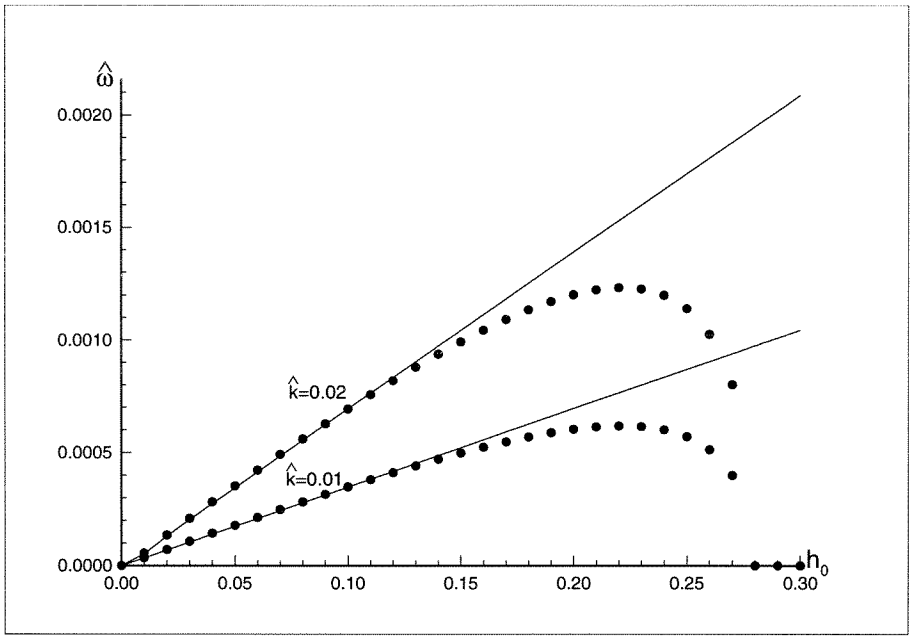

Figure 3.11: Growth rate $\hat{\omega}$ vs. amplitude h_0 for $\Omega = 1$, $\Delta = 0.1$, as given by numerics (dots) and asymptotics (solid line). Co-flowing waves.

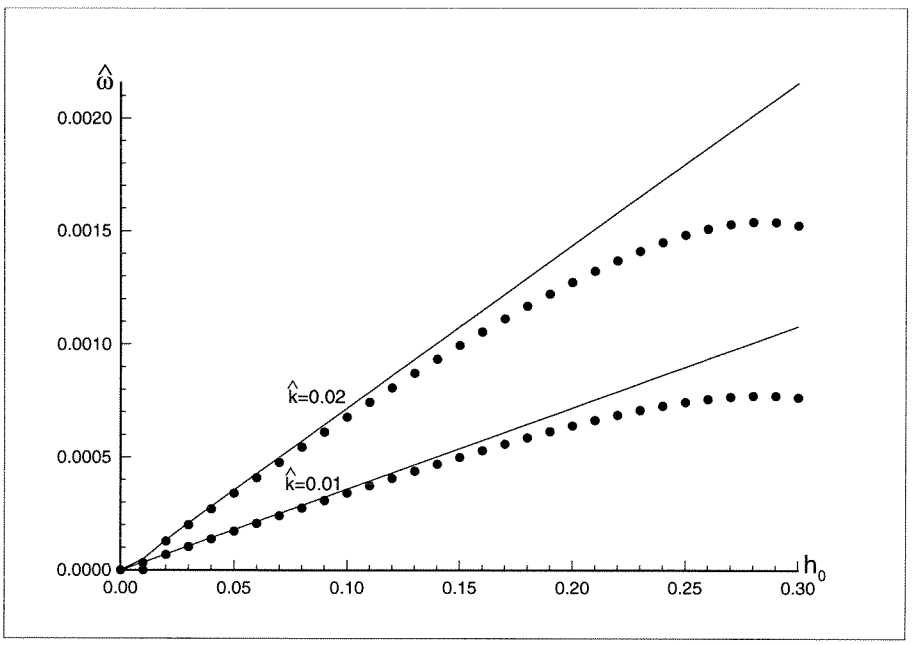

Figure 3.12: Growth rate $\hat{\omega}$ vs. amplitude h_0 for $\Omega = 1$, $\Delta = 0.1$, as given by numerics (dots) and asymptotics (solid line). Counter-flowing waves.

3.6 "Two-stick" profile

Our next task is to obtain a better approximation to a continuous velocity profile. We take an exponential profile of the form

$$U_e = U_0 e^{y/\delta}, \ -\infty < y < 0$$

to be our "model" continuous velocity distribution. First suppose that we use the "one-stick" profile considered above. Since we are trying to model the effect of wind, it is reasonable to require that the velocities at the free surface be equal, i.e.,

$$U_0 = \Omega\Delta.$$

Additionally, we require that total mass fluxes due to the shear flow be the same:

$$\int_{-\infty}^{0} U_e(y)dy = U_0\delta = \frac{1}{2}\Omega\Delta^2,$$

which leads to

$$\Delta = 2\delta.$$

Let us now use a "two-stick" profile of the form

$$U = \begin{cases} \Omega_1(y+\Delta_1) + \Omega_2\Delta_2 & , \quad -\Delta_1 < y < 0 \\ \Omega_2(y+\Delta_1+\Delta_2) & , \quad -(\Delta_1+\Delta_2) < y < -\Delta_1 \\ 0 & , \quad -\infty < y < -(\Delta_1+\Delta_2). \end{cases}$$

In order to determine $\Omega_{1,2}$ and $\Delta_{1,2}$, we assume that

1. the velocities at the free surface are the same:

$$U_0 = \Omega_1\Delta_1 + \Omega_2\Delta_2; \tag{3.22}$$

2. the vorticities at the free surface are the same (this is equivalent to re-

quiring that the derivatives of the velocity profiles be the same at the free surface):

$$U_0/\delta = \Omega_1; \tag{3.23}$$

3. the mass fluxes are the same:

$$U_0\delta = \frac{1}{2}\Omega_1\Delta_1^2 + \frac{1}{2}\Omega_2\Delta_2^2 + \Omega_2\Delta_1\Delta_2. \tag{3.24}$$

Combining (3.23) and (3.24), we obtain

$$U_0^2 = \frac{1}{2}\Omega_1^2 + \frac{1}{2}\Omega_1\Omega_2\Delta_2^2 + \Omega_1\Omega_2\Delta_1\Delta_2.$$

Condition (3.22) yields (after some algebra)

$$\frac{1}{2}\Omega_1^2\Delta_1^2 + \Omega_1\Omega_2\Delta_1\Delta_2 + \Omega_2^2\Delta_2^2 - \frac{1}{2}\Omega_1\Omega_2\Delta_2^2 = 0.$$

Denote $a = \Omega_2/\Omega_1$, $b = \Delta_2/\Delta_1$. Then the last equation becomes

$$\frac{1}{2} + ab + a^2b^2 - \frac{1}{2}ab^2 = 0.$$

We can treat this as a quadratic equation with respect to a (or b). Then

$$a = \frac{b - 2 \pm \sqrt{b^2 - 4b - 4}}{4b}.$$

Real positive solutions exist if and only if

$$b \geq 2(1 + \sqrt{2}).$$

If we choose $b = 2(1+\sqrt{2})$ then there is a unique solution for a: $a = \frac{1}{2}(1 - \frac{\sqrt{2}}{2})$. Thus, the quantities for the "one-stick" and "two-stick" profiles are related by

$$\Delta_1 = \frac{\Delta}{2+\sqrt{2}}, \quad \Delta_2 = \frac{2(1+\sqrt{2})}{2+\sqrt{2}}\Delta,$$

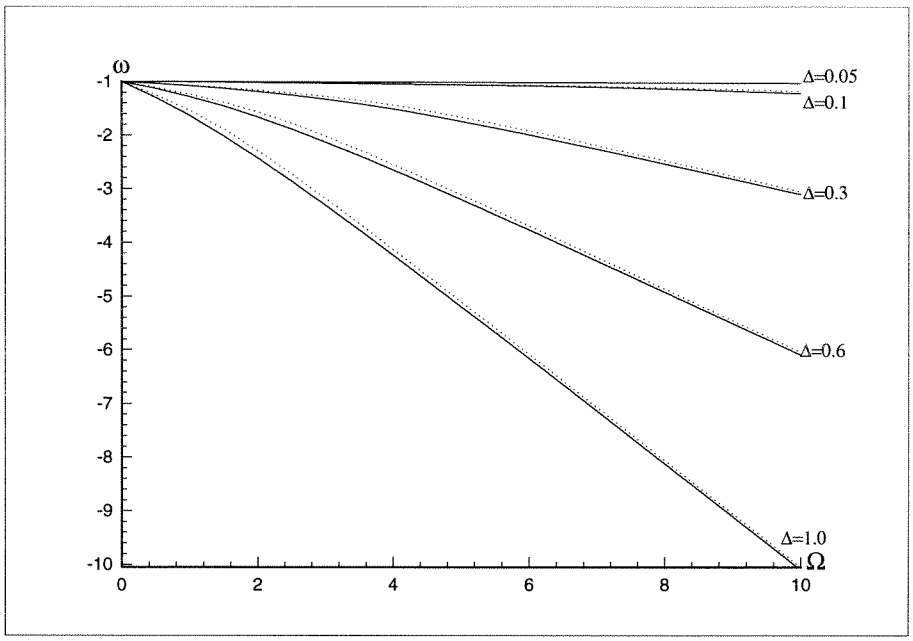

Figure 3.13: Dispersion law ω vs. vorticity Ω for various values of the shear depth Δ. Dotted line, "two-stick" profile; solid line, "one-stick" profile. Co-flowing waves.

$$\Omega_1 = 2\Omega, \ \Omega_2 = \frac{1}{2}(2 - \sqrt{2})\Omega.$$

Given this choice of the coefficients relating the "one-stick" and "two-stick" quantities, let us investigate the agreement between the resulting dispersion relations, the coefficients of the Schrödinger equation and the growth rates. (The derivation of the NLS in the "two-stick" case is virtually identical to the "one-stick" case, although algebraically even more cumbersome.)

First note that in the case of the "two-stick" profile, the dispersion relation takes the form of a quartic, while for the "one-stick" profile it was a cubic. So it is legitimate to compare only the two "extreme" (i.e., the largest and the smallest) roots. As explained earlier in sections 3.3 and 3.4, these roots correspond to the waves propagating along and against the direction of the shear current. We can see from figs. 3.13 and 3.14 that for the co-flowing waves the agreement is very good, while for the counter-flowing waves there are noticeable differences, especially when the strength of the shear is large.

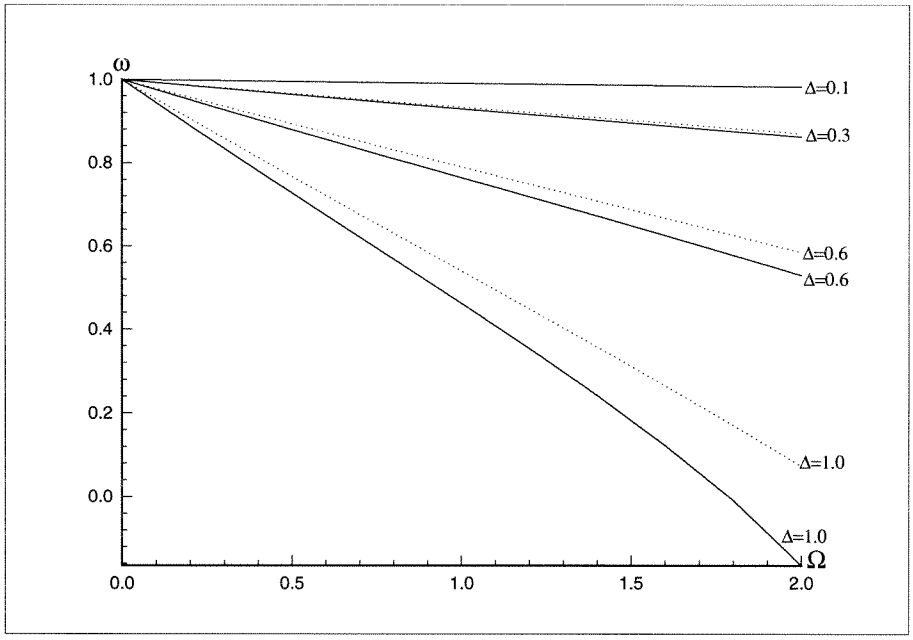

Figure 3.14: Dispersion law ω vs. vorticity Ω for various values of the shear depth Δ. Dotted line, "two-stick" profile; solid line, "one-stick" profile. Counter-flowing waves.

Now we are going to compare the values of μ and q for the two profiles (figs. 3.15–3.18). Again, in the case of the waves propagating along the shear (figs. 3.15 and 3.16), the agreement is very good, even for large values of $\Omega\Delta$. For the counter-flowing waves (figs. 3.17 and 3.18) the two profiles produce somewhat different results starting with $\Delta \approx 0.5$.

Finally, we compare the growth rates for the two profiles (figs. 3.20–3.22). It can be seen that, although there are significant quantitative differences, qualitatively both profiles yield identical results. Overall, this gives us hope that the results obtained with the help of the "stick" profiles provide a good approximation to the exponential profile behavior.

3.7 Conclusion

We have studied the effect of shear on the stability of infinitesimal perturbations (in the form of side bands) superposed on a finite amplitude gravity wave. It has

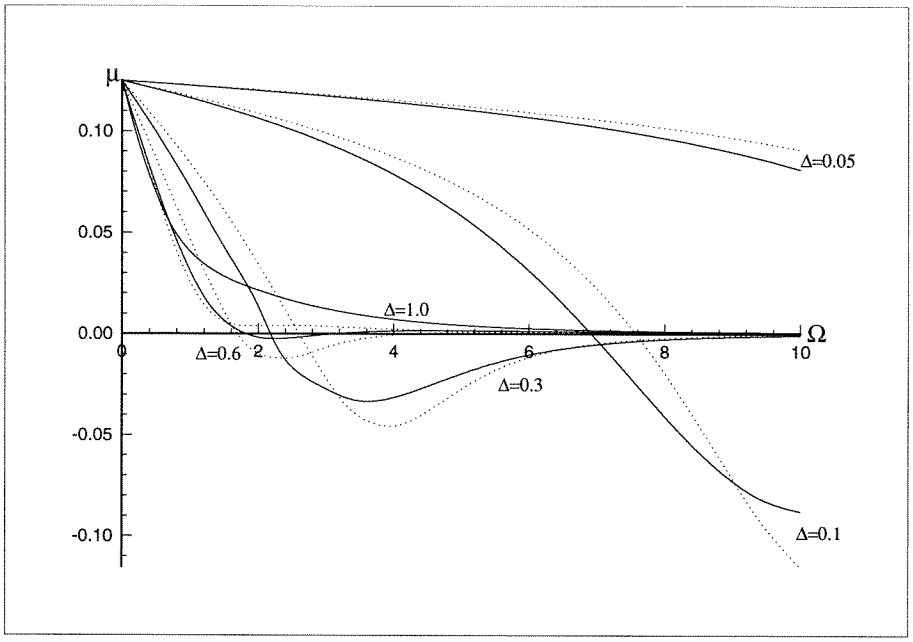

Figure 3.15: NLS coefficient μ vs. vorticity Ω for various values of the shear depth Δ. Dotted line, "two-stick" profile; solid line, "one-stick" profile. Co-flowing waves.

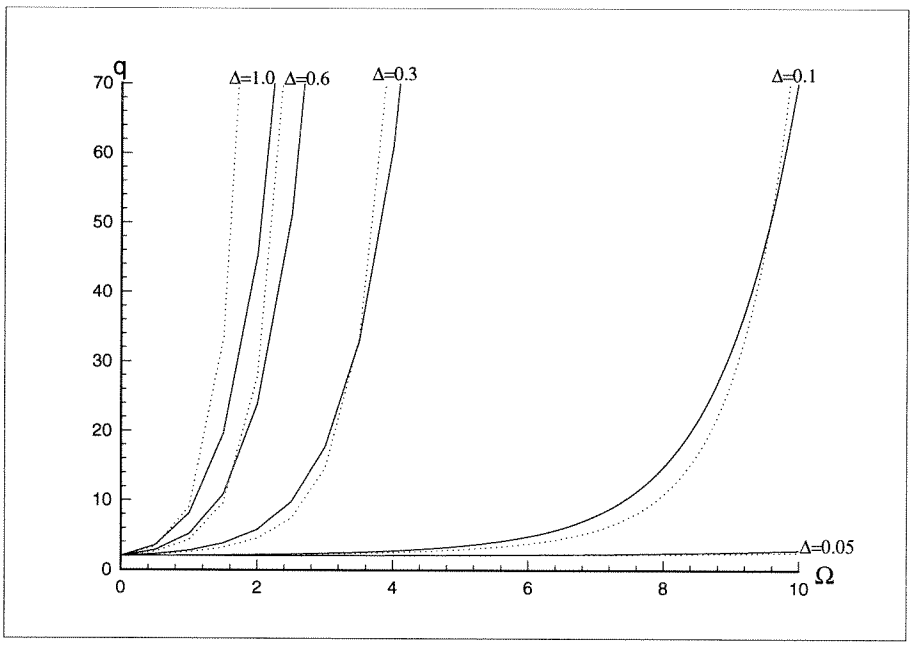

Figure 3.16: NLS coefficient q vs. vorticity Ω for various values of the shear depth Δ. Dotted line, "two-stick" profile; solid line, "one-stick" profile. Co-flowing waves.

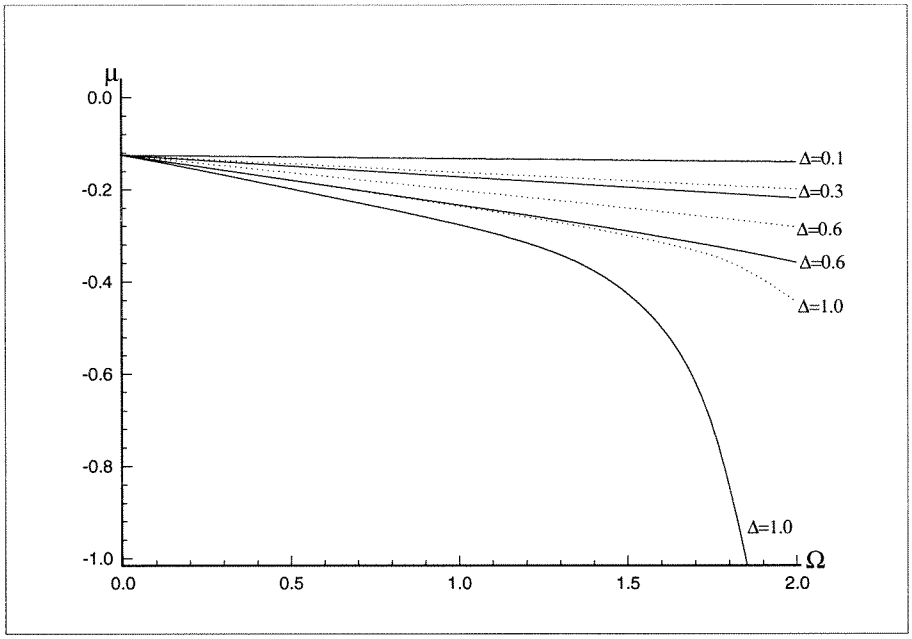

Figure 3.17: NLS coefficient μ vs. vorticity Ω for various values of the shear depth Δ. Dotted line, "two-stick" profile; solid line, "one-stick" profile. Counter-flowing waves.

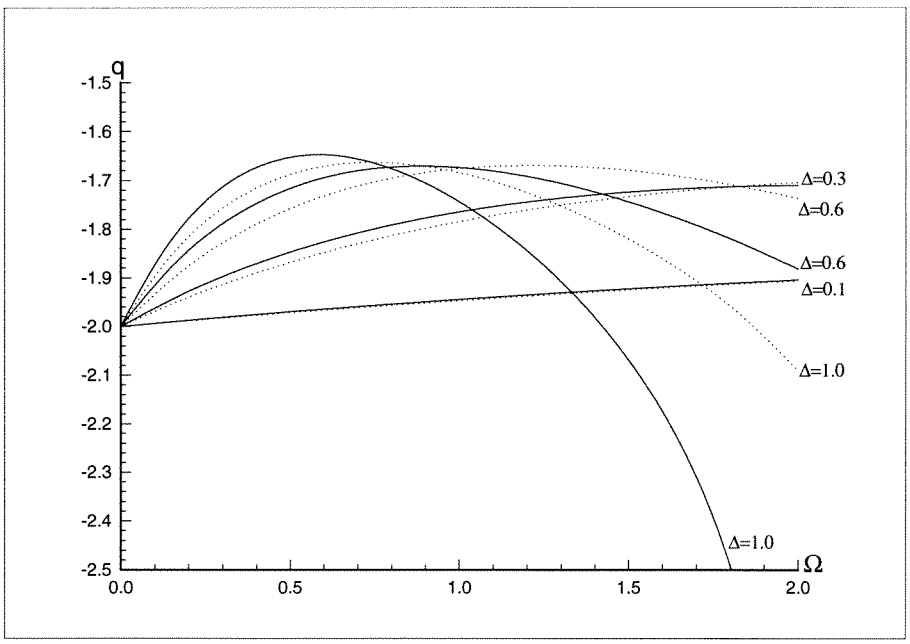

Figure 3.18: NLS coefficient q vs. vorticity Ω for various values of the shear depth Δ. Dotted line, "two-stick" profile; solid line, "one-stick" profile. Counter-flowing waves.

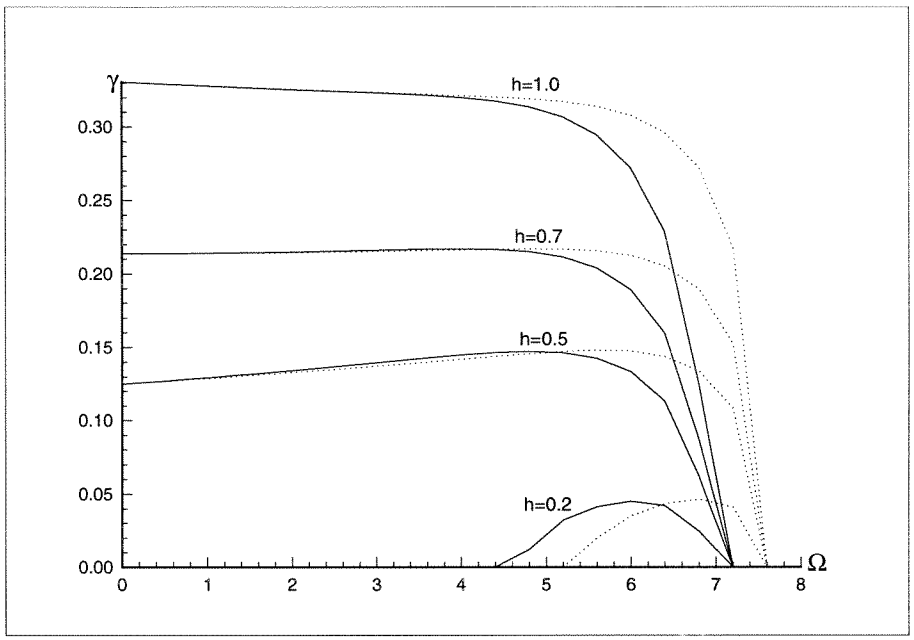

Figure 3.19: Growth rate γ vs. vorticity Ω for various amplitudes h. Shear depth $\Delta = 0.1$. Dotted line, "two-stick" profile; solid line, "one-stick" profile. Co-flowing waves.

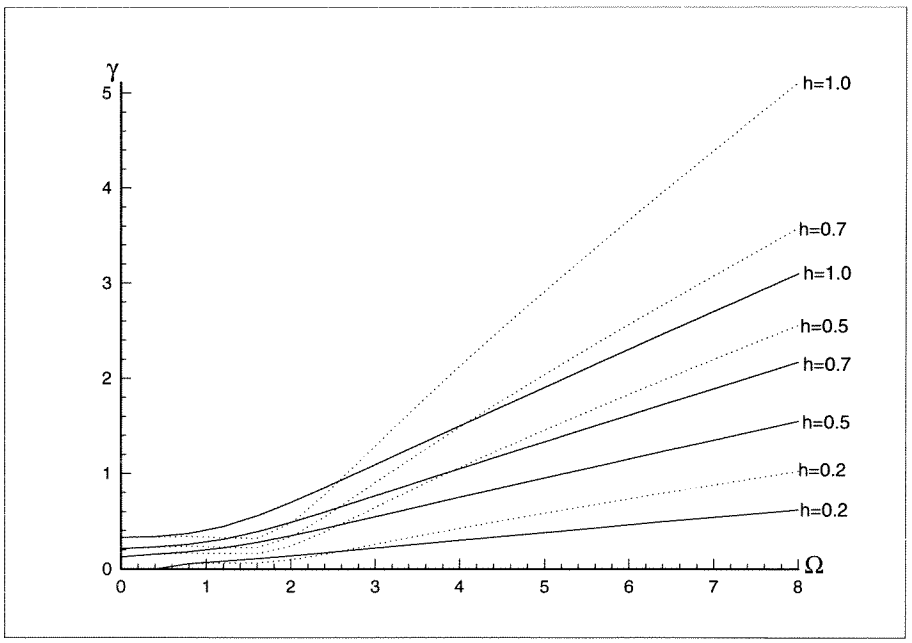

Figure 3.20: Growth rate γ vs. vorticity Ω for various amplitudes h. Shear depth $\Delta = 1.0$. Dotted line, "two-stick" profile; solid line, "one-stick" profile. Co-flowing waves.

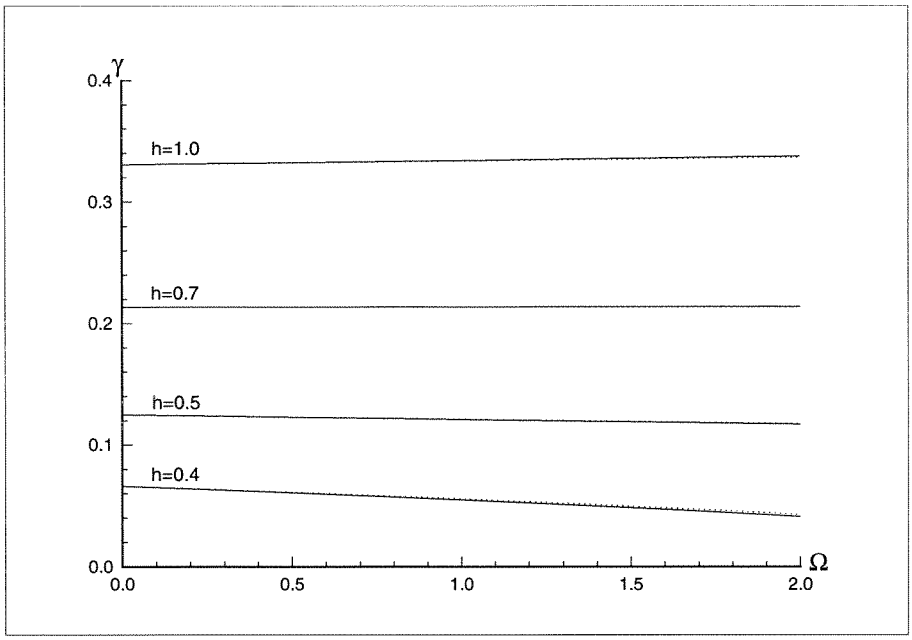

Figure 3.21: Growth rate γ vs. vorticity Ω for various amplitudes h. Shear depth $\Delta = 0.1$. Dotted line, "two-stick" profile; solid line, "one-stick" profile. Counter-flowing waves.

been demonstrated that for the co-flowing waves the addition of shear can lead to the complete suppression of instability. The value of Ω for which the growth rate becomes zero is independent of the wave amplitude provided that the shear depth is less than a certain critical value Δ_{cr}. Otherwise, the instability is enhanced by the addition of shear.

For the counter-flowing waves the picture is less clear, as the finite amplitude waves become linearly unstable themselves if the shear strength is sufficiently large. However, as long as the finite amplitude wave remains linearly stable, the growth rate of the infinitesimal perturbations goes to zero as the shear strength increases. Depending on the amplitude of the wave, the growth rate can initially increase before going to zero. The value of Ω at which the instability disappears is also strongly dependent on the wave amplitude.

Thus, the co- and counter-flowing waves present two substantially different cases as far as the instability is concerned.

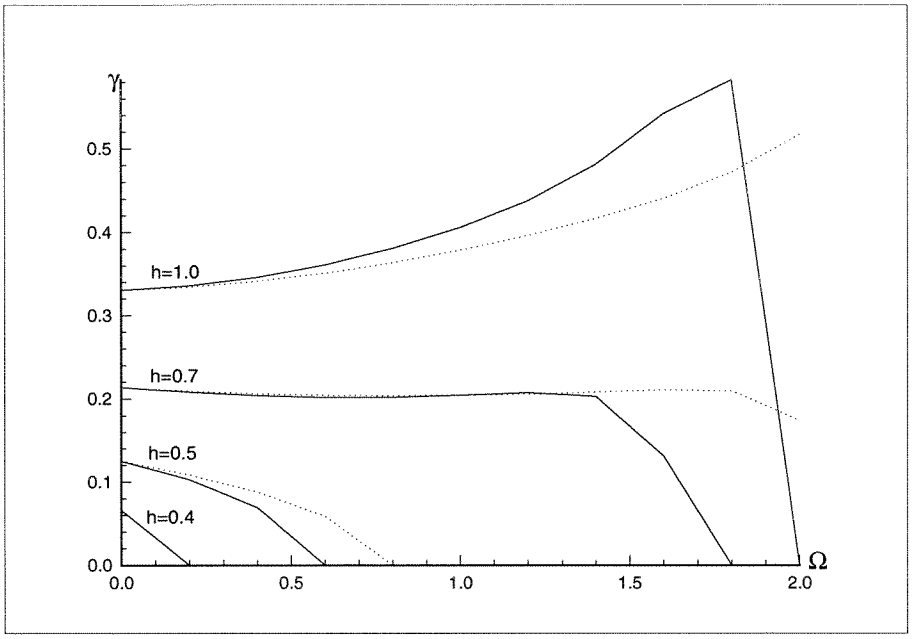

Figure 3.22: Growth rate γ vs. vorticity Ω for various amplitudes h. Shear depth $\Delta = 1.0$. Dotted line, "two-stick" profile; solid line, "one-stick" profile. Counter-flowing waves.

It has been also shown that a refined shear model ("two-stick" profile) produces qualitatively identical and quantitatively similar results.

Further investigation is necessary to determine the nature of the disagreement between the numerical and asymptotic approaches. Of course, a study directly utilizing some continuous vorticity distribution is also desirable.

Chapter 4 Three-wave interactions

4.1 Introduction

In the previous two chapters we considered various aspects of the stability of gravity waves, related to four-wave interactions. These interactions can occur with or without shear in the water. In this chapter we investigate three-wave interactions of gravity waves, which are possible only in the presence of shear. We derive a system of equations describing three-wave interactions and determine when they can cause instability. Two types of instability are considered: "explosive" instability (non-exponential blow-up in finite time) and "pump-wave" instability (the usual exponential growth).

Due to the algebraic complexity of the derivation, we are going to use two independent methods. Each method has its own advantages and the agreement between them guarantees that the result is correct.

4.2 Derivation of the interaction equations

Let k_1, k_2, and k_3 denote the wavenumbers of the interacting waves. We represent each of the velocity potentials $\phi^{T,B}$, as well as the interfaces $h^{T,B}$, as a sum of six waves with the wavenumbers $\pm k_1$, $\pm k_2$, $\pm k_3$ and frequencies $\pm\omega_1$, $\pm\omega_2$, $\pm\omega_3$, satisfying the resonance conditions:

$$k_3 = k_1 + k_2;\ \omega_3 = \omega_1 + \omega_2.$$

Neglecting all higher harmonics and all the $o(\varepsilon^2)$ terms, which play no role in the derivation of the interaction equations, we can write

$$\phi^T = \sum_{n=-3}^{3} (\varepsilon\phi^T_{1,n} + \varepsilon^2\phi^T_{2,n})E_n,\ h^T = \sum_{n=-3}^{3} (\varepsilon h^T_{1,n} + \varepsilon^2 h^T_{2,n})E_n, \tag{4.1}$$

$$\phi^B = \sum_{n=-3}^{3} (\varepsilon\phi^B_{1,n} + \varepsilon^2\phi^B_{2,n})E_n,\ h^B = \sum_{n=-3}^{3} (\varepsilon h^B_{1,n} + \varepsilon^2 h^B_{2,n})E_n, \tag{4.2}$$

where

$$E_n = e^{i(k_n x - \omega_n t)},\ \phi^{T,B}_{j,-n} = \left(\phi^{T,B}_{j,n}\right)^*,\ h^{T,B}_{j,-n} = \left(h^{T,B}_{j,n}\right)^*,\ k_{-n} = -k_n,\ \omega_{-n} = -\omega_n.$$

It is implied that the summation is carried out over all $n \in \{-3, 3\}$, excluding zero.

At this point we apply the method of multiple scales. The appropriate "slow" variables are

$$\xi = \varepsilon x,\ \tau = \varepsilon t. \tag{4.3}$$

Let the coefficients $\phi^{T,B}_{j,n}$ and $h^{T,B}_{j,n}$ be dependent on the slow variables:

$$\phi^{T,B}_{j,n} = \phi^{T,B}_{j,n}(\xi, y, \tau);\ h^{T,B}_{j,n} = h^{T,B}_{j,n}(\xi, \tau).$$

Note that

$$\frac{\partial}{\partial x} \to \frac{\partial}{\partial x} + \varepsilon\frac{\partial}{\partial \xi};\ \frac{\partial}{\partial t} \to \frac{\partial}{\partial t} + \varepsilon\frac{\partial}{\partial \tau}.$$

Similarly to the derivation in section 3.3, the most difficult step is the substitution of the expansions into the boundary conditions. We retain the terms which are bigger than $o(\varepsilon^3)$, then equate the coefficients corresponding to $E^1_n\varepsilon^1, E^1_n\varepsilon^2$, $n = 1, 2, 3$. The resulting system of thirty equations has a solution provided that two compatibility conditions hold. One of these conditions is the same linear dispersion relation in the form of a cubic equation that we encountered in the previous chapters:

$$\begin{aligned} D(k_n, \omega_n) \equiv\ & -(\omega_n + \Omega\Delta k_n)^2 \frac{2k\omega_n + \Omega|k_n|(1 + e^{-2\Delta|k_n|})}{|k_n|(2k_n\omega_n + \Omega|k_n|(1 - e^{-2\Delta|k_n|}))} \\ & + \Omega(\omega_n + \Omega\Delta k_n) + g \qquad = 0. \end{aligned} \tag{4.4}$$

Note that the dispersion relation (4.4) can take many different forms. However, it is the form above that is used in the interaction equations. This particular form comes from the Bernoulli equation and ensures that the pressure is proportional to $D(k, \omega)$,

i.e.,

$$p = \sum_{k=-3}^{3} D(k_n, \omega_n) h_{1,n}^T.$$

The other conditions take the form of a system of three nonlinear partial differential equations:

$$P_1(\frac{\partial}{\partial \tau} - c_g \frac{\partial}{\partial \xi}) h_{1,1}^T = iH \left(h_{1,2}^T\right)^* h_{1,3}^T, \tag{4.5}$$

$$P_2(\frac{\partial}{\partial \tau} - c_g \frac{\partial}{\partial \xi}) h_{1,2}^T = iH \left(h_{1,1}^T\right)^* h_{1,3}^T, \tag{4.6}$$

$$P_3(\frac{\partial}{\partial \tau} - c_g \frac{\partial}{\partial \xi}) h_{1,3}^T = iH h_{1,1}^T h_{1,2}^T, \tag{4.7}$$

where $P_n = P(k_n) = \frac{\partial}{\partial \omega_n} D(k_n, \omega_n)$; H is a real-valued interaction coefficient, which depends on k_n and ω_n, and should be the same for all three equations. In our computations, the latter fact provided a very useful and reliable check on the correctness of our derivation. From now on we assume that our initial conditions are such that $\frac{\partial(\cdot)}{\partial \xi} = 0$, i.e., there is no slow-space modulation.

Although the method we just used is very simple and can be easily employed in conjunction with a symbolic manipulator, thus simplifying the task of solving thirty simultaneous equations and allowing us to minimize the effort by using the techniques from the previous chapter, it does not provide compact expressions for either the interaction coefficient H or the coefficients P_n.

The following approach (Lake and Yuen [21]) provides a better way of obtaining expressions for the coefficients, as well as help us check the correctness of the derivation once more. The disadvantage is that it is more difficult to use a symbolic manipulator, so that a generalization for the case of four (and more) interacting waves is not readily available.

We start by rewriting the boundary conditions. Let $\mathring{\phi}(x,t) = \phi(x, h(x,t), t)$ denote the value of the velocity potential at an interface, or more precisely:

$$\mathring{\phi}^T(x,t) = \phi^T(x, h^T(x,t), t);$$

$$\mathring{\phi}^I(x,t) = \phi^T(x, h^B(x,t), t);$$

$$\mathring{\phi}^B(x,t) = \phi^B(x, h^B(x,t), t).$$

We also need the value of the streamfunction at the free surface:

$$\mathring{\psi}^T(x,t) = \psi^T(x, h^T(x,t), t).$$

Then

$$\frac{\partial\phi}{\partial t} = \frac{\partial\mathring{\phi}}{\partial t} - \frac{\partial\phi}{\partial y}\frac{\partial h}{\partial t};\ \frac{\partial\phi}{\partial x} = \frac{\partial\mathring{\phi}}{\partial x} - \frac{\partial\phi}{\partial y}\frac{\partial h}{\partial x}.$$

Substituting these expressions into (3.7) and (3.8), we obtain

$$\frac{\partial h^T}{\partial t} + \frac{\partial\mathring{\phi}^T}{\partial x}\frac{\partial h^T}{\partial x} - \frac{\partial\phi^T}{\partial y} - \Omega\frac{\partial h^T}{\partial x}(h^T + \Delta) = 0 \tag{4.8}$$

on $y = h^T(x,t)$, and

$$\frac{\partial h^B}{\partial t} + \frac{\partial\mathring{\phi}^I}{\partial x}\frac{\partial h^B}{\partial x} - \frac{\partial\phi^T}{\partial y} - \Omega\frac{\partial h^B}{\partial x}(h^B + \Delta) = 0 \tag{4.9}$$

on $y = h^B(x,t)$, where we neglected third-order terms.

A similar transformation of (3.9) yields

$$\frac{\partial\mathring{\phi}^T}{\partial t} + \frac{1}{2}\left(\frac{\partial\mathring{\phi}^T}{\partial x}\right)^2 - \frac{1}{2}\left(\frac{\partial\phi^T}{\partial y}\right)^2 - \Omega\frac{\partial\mathring{\phi}^T}{\partial x}(h^T + \Delta) + \Omega\mathring{\psi}^T + gh^T = F(t) \tag{4.10}$$

on $y = h^T(x,t)$.

Finally, we use conditions (3.12) and (3.13), which take the following form:

$$\frac{\partial\mathring{\phi}^I}{\partial x} - \Omega(h^B + \Delta) = \frac{\partial\mathring{\phi}^B}{\partial x} \tag{4.11}$$

and

$$\frac{\partial\phi^T}{\partial y} = \frac{\partial\phi^B}{\partial y} \tag{4.12}$$

on $y = h^B(x,t)$.

Now introduce Fourier transforms:

$$h^T(x,t) = \frac{1}{\sqrt{2\pi}} \int_{-\infty}^{\infty} \widehat{h^T}(\kappa,t) e^{i\kappa x} d\kappa, \;\; h^B(x,t) = -\Delta + \frac{1}{\sqrt{2\pi}} \int_{-\infty}^{\infty} \widehat{h^B}(\kappa,t) e^{i\kappa x} d\kappa; \quad (4.13)$$

$$\phi^T(x,y,t) = \frac{1}{\sqrt{2\pi}} \int_{-\infty}^{\infty} (\alpha(\kappa,t) e^{|\kappa| y} + \beta(\kappa,t) e^{-|\kappa| y}) e^{i\kappa x} d\kappa,$$

$$\phi^B(x,y,t) = \frac{1}{\sqrt{2\pi}} \int_{-\infty}^{\infty} \gamma(\kappa,t) e^{|\kappa| y} e^{i\kappa x} d\kappa.$$

Note that the velocity potentials automatically satisfy Laplace's equation. It is easy to relate this integral representation of the potentials and the interfaces to the series representation (4.1)-(4.2) that we used in the beginning of the chapter. For example, for the free surface we can let

$$\widehat{h^T}(\kappa,t) = \sqrt{2\pi} \sum_{n=-3}^{3} (\varepsilon h_{1,n}^T + \varepsilon^2 h_{2,n}^T) e^{-i\omega_n t} \delta(\kappa - k_n). \quad (4.14)$$

Then

$$h^T(x,t) = \sum_{n=-3}^{3} (\varepsilon h_{1,n}^T + \varepsilon^2 h_{2,n}^T) E_n,$$

i.e., we recover our series representation.

The values of the velocity potential at the interfaces can be expressed in terms of the Fourier transform as follows:

$$\mathring{\phi}^T(x,t) = \frac{1}{\sqrt{2\pi}} \int_{-\infty}^{\infty} (\alpha(\kappa,t) e^{|\kappa| h^T(x,t)} + \beta(\kappa,t) e^{-|\kappa| h^T(x,t)}) d\kappa,$$

$$\mathring{\phi}^I(x,t) = \frac{1}{\sqrt{2\pi}} \int_{-\infty}^{\infty} (\alpha(\kappa,t) e^{|\kappa| h^B(x,t)} + \beta(\kappa,t) e^{-|\kappa| h^B(x,t)}) e^{i\kappa x} d\kappa,$$

$$\mathring{\phi}^B(x,t) = \frac{1}{\sqrt{2\pi}} \int_{-\infty}^{\infty} \gamma(\kappa,t) e^{|\kappa| h^B(x,t)} d\kappa.$$

Assuming that the amplitudes are small (more precisely, $\left|\kappa h^{T,B}(x,t)\right|$ should be small), we can expand the exponentials above in Taylor series. Truncating the series

after the first two terms and using (4.13), we obtain

$$\mathring{\phi}^T(x,t) = \frac{1}{\sqrt{2\pi}} \int_{-\infty}^{\infty} (\alpha(\kappa_1,t) + \beta(\kappa_1,t)) e^{i\kappa_1 x} d\kappa_1 \tag{4.15}$$
$$+\frac{1}{2\pi} \int_{-\infty}^{\infty}\int_{-\infty}^{\infty} |\kappa_1|(\alpha(\kappa_1,t) - \beta(\kappa_1,t))\widehat{h^T}(\kappa_2,t) e^{i(\kappa_1+\kappa_2)x} d_{12},$$

$$\mathring{\phi}^I(x,t) = \frac{1}{\sqrt{2\pi}} \int_{-\infty}^{\infty} (\alpha(\kappa_1,t)e^{-|\kappa_1|\Delta} + \beta(\kappa_1,t)e^{|\kappa_1|\Delta}) e^{i\kappa_1 x} d\kappa_1 \tag{4.16}$$
$$+\frac{1}{2\pi} \int_{-\infty}^{\infty}\int_{-\infty}^{\infty} |\kappa_1|(\alpha(\kappa_1,t)e^{-|\kappa_1|\Delta} - \beta(\kappa_1,t)e^{-|\kappa_1|\Delta})\widehat{h^B}(\kappa_2,t) e^{i(\kappa_1+\kappa_2)x} d_{12},$$

$$\mathring{\phi}^B(x,t) = \frac{1}{\sqrt{2\pi}} \int_{-\infty}^{\infty} \gamma(\kappa_1,t)e^{-|\kappa_1|\Delta} e^{i\kappa_1 x} d\kappa_1 \tag{4.17}$$
$$+\frac{1}{2\pi} \int_{-\infty}^{\infty}\int_{-\infty}^{\infty} |\kappa_1|\gamma(\kappa_1,t)e^{-|\kappa_1|\Delta}\widehat{h^B}(\kappa_2,t) e^{i(\kappa_1+\kappa_2)x} d_{12},$$

where $d_{12} \equiv d\kappa_1 d\kappa_2$.

Applying the Fourier transform to both sides of (4.15)-(4.17) and using

$$\delta(\kappa) = \frac{1}{2\pi} \int_{-\infty}^{\infty} e^{i\kappa x} dx,$$

we get

$$\widehat{\mathring{\phi}^T}(\kappa,t) = \alpha(\kappa,t) + \beta(\kappa,t) \tag{4.18}$$
$$+\frac{1}{\sqrt{2\pi}} \int_{-\infty}^{\infty}\int_{-\infty}^{\infty} |\kappa_1|(\alpha(\kappa_1,t) - \beta(\kappa_1,t))\widehat{h^T}(\kappa_2,t)\delta_{123} d_{12},$$

$$\widehat{\mathring{\phi}^I}(\kappa,t) = \alpha(\kappa,t)e^{-|\kappa|\Delta} + \beta(\kappa,t)e^{|\kappa|\Delta} \tag{4.19}$$
$$+\frac{1}{\sqrt{2\pi}} \int_{-\infty}^{\infty}\int_{-\infty}^{\infty} |\kappa_1|(\alpha(\kappa_1,t)e^{-|\kappa|\Delta} - \beta(\kappa_1,t)e^{|\kappa|\Delta})\widehat{h^B}(\kappa_2,t)\delta_{123} d_{12},$$

$$\widehat{\mathring{\phi}^B}(\kappa,t) = \gamma(\kappa,t)e^{-|\kappa|\Delta} \tag{4.20}$$
$$+\frac{1}{\sqrt{2\pi}} \int_{-\infty}^{\infty}\int_{-\infty}^{\infty} |\kappa_1|\gamma(\kappa_1,t)e^{-|\kappa|\Delta}\widehat{h^B}(\kappa_2,t)\delta_{123} d_{12},$$

where $\delta_{123} \equiv \delta(\kappa_1 + \kappa_2 - \kappa)$.

Inverting relationships (4.18)–(4.20), we can find $\alpha(\kappa,t)$, $\beta(\kappa,t)$, and $\gamma(\kappa,t)$ in terms of $\widehat{\mathring{\phi}^T}(\kappa,t)$, $\widehat{\mathring{\phi}^I}$, and $\widehat{\mathring{\phi}^B}$:

$$\alpha(\kappa,t) = \frac{\widehat{\mathring{\phi}^T}(\kappa,t)e^{|\kappa|\Delta} - \widehat{\mathring{\phi}^I}(\kappa,t)}{2\sinh(|\kappa|\Delta)} \tag{4.21}$$
$$-\frac{1}{\sqrt{2\pi}}\int_{-\infty}^{\infty}\int_{-\infty}^{\infty}\frac{|\kappa_1|\delta_{123}}{2\sinh(|\kappa|\Delta)\sinh(|\kappa_1|\Delta)}\left[e^{|\kappa|\Delta}\left(\widehat{\mathring{\phi}^T}(\kappa_1,t)\cosh(|\kappa_1|\Delta) - \widehat{\mathring{\phi}^I}(\kappa_1,t)\right)\right.$$
$$\left.\times\widehat{h^T}(\kappa_2,t) - \left(\widehat{\mathring{\phi}^T}(\kappa_1,t) - \widehat{\mathring{\phi}^I}(\kappa_1,t)\cosh(|\kappa_1|\Delta)\right)\widehat{h^B}(\kappa_2,t)\right]d_{12},$$

$$\beta(\kappa,t) = -\frac{\widehat{\mathring{\phi}^T}(\kappa,t)e^{-|\kappa|\Delta} - \widehat{\mathring{\phi}^I}(\kappa,t)}{2\sinh(|\kappa|\Delta)} + \frac{1}{\sqrt{2\pi}}\int_{-\infty}^{\infty}\int_{-\infty}^{\infty}\frac{|\kappa_1|\delta_{123}}{2\sinh(|\kappa|\Delta)\sinh(|\kappa_1|\Delta)} \tag{4.22}$$
$$\times\left[e^{-|\kappa|\Delta}\left(\widehat{\mathring{\phi}^T}(\kappa_1,t)\cosh(|\kappa_1|\Delta) - \widehat{\mathring{\phi}^I}(\kappa_1,t)\right)\widehat{h^T}(\kappa_2,t)\right.$$
$$\left.-\left(\widehat{\mathring{\phi}^T}(\kappa_1,t) - \widehat{\mathring{\phi}^I}(\kappa_1,t)\cosh(|\kappa_1|\Delta)\right)\widehat{h^B}(\kappa_2,t)\right]d_{12},$$

$$\gamma(\kappa,t)e^{-|\kappa|\Delta} = \widehat{\mathring{\phi}^B}(\kappa,t) - \frac{1}{\sqrt{2\pi}}\int_{-\infty}^{\infty}\int_{-\infty}^{\infty}|\kappa_1|\widehat{\mathring{\phi}^B}(\kappa_1,t)\widehat{h^B}(\kappa_2,t)\delta_{123}d_{12}. \tag{4.23}$$

The boundary conditions (4.8)-(4.12) require the knowledge of $\widehat{\frac{\partial\phi^{T,B}}{\partial y}}(x,h^{T,B}(x,t),t)$ (i.e., the Fourier transform of the derivative, not the derivative of the transform), $\widehat{\frac{\partial\mathring{\phi}^{T,I,B}}{\partial x}}(x,t)$, and $\widehat{\mathring{\psi}^T}(x,t)$:

$$\widehat{\frac{\partial\phi^T}{\partial y}}(x,h^T(x,t),t) = |\kappa|(\alpha(\kappa,t) - \beta(\kappa,t))$$
$$+\frac{1}{\sqrt{2\pi}}\int_{-\infty}^{\infty}\int_{-\infty}^{\infty}\kappa_1^2(\alpha(\kappa_1,t) + \beta(\kappa_1,t))\widehat{h^T}(\kappa_2,t)\delta_{123}d_{12},$$

$$\widehat{\frac{\partial\phi^T}{\partial y}}(x,h^B(x,t),t) = |\kappa|(\alpha(\kappa,t)e^{-|\kappa|\Delta} - \beta(\kappa,t)e^{|\kappa|\Delta})$$
$$+\frac{1}{\sqrt{2\pi}}\int_{-\infty}^{\infty}\int_{-\infty}^{\infty}\kappa_1^2(\alpha(\kappa_1,t)e^{-|\kappa_1|\Delta} + \beta(\kappa_1,t)e^{|\kappa_1|\Delta})\widehat{h^B}(\kappa_2,t)\delta_{123}d_{12},$$

$$\widehat{\frac{\partial\phi^B}{\partial y}}(x,h^B(x,t),t) = |\kappa|\gamma(\kappa,t)e^{-|\kappa|\Delta}$$
$$+\frac{1}{\sqrt{2\pi}}\int_{-\infty}^{\infty}\int_{-\infty}^{\infty}\kappa_1^2\gamma(\kappa_1,t)e^{-|\kappa_1|\Delta}\widehat{h^B}(\kappa_2,t)\delta_{123}d_{12},$$

$$\widehat{\frac{\partial \mathring{\phi}^T}{\partial x}}(x,t) = i\kappa(\alpha(\kappa,t)+\beta(\kappa,t))$$
$$+i\frac{1}{\sqrt{2\pi}}\int_{-\infty}^{\infty}\int_{-\infty}^{\infty}\kappa_1|\kappa_1|(\alpha(\kappa_1,t)-\beta(\kappa,t))\widehat{h^T}(\kappa_2,t)\delta_{123}d_{12}$$

$$\widehat{\frac{\partial \mathring{\phi}^I}{\partial x}}(x,t) = i\kappa(\alpha(\kappa,t)e^{-|\kappa|\Delta}+\beta(\kappa,t)e^{|\kappa|\Delta})$$
$$+i\frac{1}{\sqrt{2\pi}}\int_{-\infty}^{\infty}\int_{-\infty}^{\infty}\kappa_1|\kappa_1|(\alpha(\kappa_1,t)e^{-|\kappa_1|\Delta}-\beta(\kappa,t)e^{|\kappa_1|\Delta})\widehat{h^B}(\kappa_2,t)\delta_{123}d_{12},$$

$$\widehat{\frac{\partial \mathring{\phi}^B}{\partial x}}(x,t) = i\kappa\gamma(\kappa,t)e^{-|\kappa|\Delta}$$
$$+i\frac{1}{\sqrt{2\pi}}\int_{-\infty}^{\infty}\int_{-\infty}^{\infty}\kappa_1|\kappa_1|\gamma(\kappa_1,t)e^{-|\kappa_1|\Delta}\widehat{h^B}(\kappa_2,t)\delta_{123}d_{12},$$

$$\widehat{\mathring{\psi}^T}(x,t) = i\frac{|\kappa|}{\kappa}(\alpha(\kappa,t)-\beta(\kappa,t))$$
$$+i\frac{1}{\sqrt{2\pi}}\int_{-\infty}^{\infty}\int_{-\infty}^{\infty}\kappa_1(\alpha(\kappa_1,t)+\beta(\kappa_1,t))\widehat{h^T}(\kappa_2,t)\delta_{123}d_{12}.$$

The application of Fourier transform to the boundary conditions (4.8)-(4.12) and the subsequent use of the relationships above produce a system of five integral equations presented in appendix B.

Let us apply the method of two-timing (with the slow time τ given by (4.3)):

$$\widehat{h^T}(\kappa,t) = (\varepsilon\widehat{h_1^T}(\kappa,\tau)+\varepsilon^2\widehat{h_2^T}(\kappa,\tau))e^{-i\omega t},\ \widehat{h^B}(\kappa,t) = (\varepsilon\widehat{h_1^B}(\kappa,\tau)+\varepsilon^2\widehat{h_2^B}(\kappa,\tau))e^{-i\omega t},$$

$$\widehat{\mathring{\phi}^T}(\kappa,t) = (\varepsilon\widehat{\mathring{\phi}_1^T}(\kappa,\tau)+\varepsilon^2\widehat{\mathring{\phi}_2^T}(\kappa,\tau))e^{-i\omega t},\ \widehat{\mathring{\phi}^I}(\kappa,t) = (\varepsilon\widehat{\mathring{\phi}_1^I}(\kappa,\tau)+\varepsilon^2\widehat{\mathring{\phi}_2^I}(\kappa,\tau))e^{-i\omega t},$$

$$\widehat{\mathring{\phi}^B}(\kappa,t) = (\varepsilon\widehat{\mathring{\phi}_1^B}(\kappa,\tau)+\varepsilon^2\widehat{\mathring{\phi}_2^B}(\kappa,\tau))e^{-i\omega t},$$

where $\omega = \omega(\kappa)$.

We start by equating the $O(\varepsilon)$ terms in (B.1)–(B.5):

$$i(\omega+\Omega\Delta\kappa)\widehat{h_1^T}(\kappa,\tau)+|\kappa|\frac{\widehat{\mathring{\phi}_1^T}(\kappa,\tau)\cosh(|\kappa|\Delta)-\widehat{\mathring{\phi}_1^I}(\kappa,\tau)}{\sinh(|\kappa|\Delta)} = 0,$$

$$
\begin{aligned}
i\omega\widehat{h_1^B}(\kappa,\tau)+|\kappa|\frac{\widehat{\mathring{\phi}_1^T}(\kappa,\tau)-\widehat{\mathring{\phi}_1^I}(\kappa,\tau)\cosh(|\kappa|\Delta)}{\sinh(|\kappa|\Delta)} &= 0,\\
-i(\omega+\Omega\Delta\kappa)\widehat{\mathring{\phi}_1^T}(\kappa,\tau)&\\
+i\Omega\frac{|\kappa|}{\kappa}\frac{\widehat{\mathring{\phi}_1^T}(\kappa,\tau)\cosh(|\kappa|\Delta)-\widehat{\mathring{\phi}_1^I}(\kappa,\tau)}{\sinh(|\kappa|\Delta)}+g\widehat{h_1^T}(\kappa,\tau) &= 0,\\
i\kappa(\widehat{\mathring{\phi}_1^I}(\kappa,\tau)-\widehat{\mathring{\phi}_1^B}(\kappa,\tau))-\Omega\widehat{h_1^B}(\kappa,\tau) &= 0,\\
\frac{\widehat{\mathring{\phi}_1^T}(\kappa,\tau)-\widehat{\mathring{\phi}_1^I}(\kappa,\tau)\cosh(|\kappa|\Delta)}{\sinh(|\kappa|\Delta)}-\widehat{\mathring{\phi}_1^B}(\kappa,\tau) &= 0.
\end{aligned}
$$

These equations allow us to express $\widehat{h_1^B}$, $\widehat{\mathring{\phi}_1^T}$, $\widehat{\mathring{\phi}_1^I}$, and $\widehat{\mathring{\phi}_1^B}$ in terms of $\widehat{h_1^T}$ and obtain the dispersion relation (4.4).

Equating the $O(\varepsilon^2)$ terms and using the results for the $O(\varepsilon)$ terms to simplify the expressions, we obtain

$$
\begin{aligned}
\frac{\partial\widehat{h_1^T}}{\partial\tau}(\kappa,\tau)-i(\omega+\Omega\Delta\kappa)\widehat{h_2^T}(\kappa,\tau)-|\kappa|\frac{\widehat{\mathring{\phi}_2^T}(\kappa,\tau)\cosh(|\kappa|\Delta)-\widehat{\mathring{\phi}_2^I}(\kappa,\tau)}{\sinh(|\kappa|\Delta)}&\\
+\frac{1}{\sqrt{2\pi}}\int_{-\infty}^{\infty}\int_{-\infty}^{\infty}iV_1(\kappa,\kappa_1,\kappa_2)\delta_{123}e^{-i(\omega_1+\omega_2-\omega)t}d_{12} &= 0,\\
\frac{\partial\widehat{h_1^B}}{\partial\tau}(\kappa,\tau)-i\omega\widehat{h_2^B}(\kappa,\tau)-|\kappa|\frac{\widehat{\mathring{\phi}_2^T}(\kappa,\tau)-\widehat{\mathring{\phi}_2^I}(\kappa,\tau)\cosh(|\kappa|\Delta)}{\sinh(|\kappa|\Delta)}&\\
+\frac{1}{\sqrt{2\pi}}\int_{-\infty}^{\infty}\int_{-\infty}^{\infty}iV_2(\kappa,\kappa_1,\kappa_2)\delta_{123}e^{-i(\omega_1+\omega_2-\omega)t}d_{12} &= 0,\\
\frac{\partial\widehat{\mathring{\phi}_1^T}}{\partial\tau}(\kappa,\tau)-i(\omega+\Omega\Delta\kappa)\widehat{\mathring{\phi}_2^T}(\kappa,\tau)+i\Omega\frac{|\kappa|}{\kappa}\frac{\widehat{\mathring{\phi}_2^T}(\kappa,\tau)\cosh(|\kappa|\Delta)-\widehat{\mathring{\phi}_2^I}(\kappa,\tau)}{\sinh(|\kappa|\Delta)}&\\
+g\widehat{h_2^T}(\kappa,\tau)+\frac{1}{\sqrt{2\pi}}\int_{-\infty}^{\infty}\int_{-\infty}^{\infty}V_3(\kappa,\kappa_1,\kappa_2)\delta_{123}e^{-i(\omega_1+\omega_2-\omega)t}d_{12} &= 0\\
i\kappa(\widehat{\mathring{\phi}_2^I}(\kappa,\tau)-\widehat{\mathring{\phi}_2^B}(\kappa,\tau))-\Omega\widehat{h_2^B}(\kappa,\tau) &= 0,\\
\frac{\widehat{\mathring{\phi}_2^T}(\kappa,\tau)-\widehat{\mathring{\phi}_2^I}(\kappa,\tau)\cosh(|\kappa|\Delta)}{\sinh(|\kappa|\Delta)}-\widehat{\mathring{\phi}_2^B}(\kappa,\tau)&\\
+\frac{1}{\sqrt{2\pi}}\int_{-\infty}^{\infty}\int_{-\infty}^{\infty}iV_5(\kappa,\kappa_1,\kappa_2)\delta_{123}e^{-i(\omega_1+\omega_2-\omega)t}d_{12} &= 0,
\end{aligned}
$$

where

$$
\begin{aligned}
V_1(\kappa,\kappa_1,\kappa_2) &= -\frac{|\kappa|}{\sinh(|\kappa|\Delta)}\Big[\cosh(|\kappa|\Delta)(\omega_1+\Omega\Delta\kappa_1)\widehat{h_1^T}(\kappa_1,\tau)\widehat{h_1^T}(\kappa_2,\tau)\\
&\quad -\omega_1\widehat{h_1^B}(\kappa_1,\tau)\widehat{h_1^B}(\kappa_2,\tau)\Big]\\
&\quad -\kappa\kappa_1\widehat{\mathring{\phi}_1^T}(\kappa_1,\tau)\widehat{h_1^T}(\kappa_2,\tau)-i\Omega\kappa_1\widehat{h_1^T}(\kappa_1,\tau)\widehat{h^T}(\kappa_2,\tau),\\
V_2(\kappa,\kappa_1,\kappa_2) &= -\frac{|\kappa|}{\sinh(|\kappa|\Delta)}\Big[(\omega_1+\Omega\Delta\kappa_1)\widehat{h_1^T}(\kappa_1,\tau)\widehat{h_1^T}(\kappa_2,\tau)\\
&\quad -\cosh(|\kappa|\Delta)\omega_1\widehat{h_1^B}(\kappa_1,\tau)\widehat{h_1^B}(\kappa_2,\tau)\Big]\\
&\quad -\kappa\kappa_1\widehat{\mathring{\phi}^I}(\kappa_1,\tau)\widehat{h_1^B}(\kappa_2,\tau)-i\Omega\kappa_1\widehat{h_1^B}(\kappa_1,\tau)\widehat{h_1^B}(\kappa_2,\tau),\\
V_3(\kappa,\kappa_1,\kappa_2) &= -\frac{1}{2}\kappa_1\kappa_2\widehat{\mathring{\phi}_1^T}(\kappa_1,\tau)\widehat{\mathring{\phi}_1^T}(\kappa_2,\tau)\\
&\quad +\frac{1}{2}(\omega_1+\Omega\Delta\kappa_1)(\omega_2+\Omega\Delta\kappa_2)\widehat{h_1^T}(\kappa_1,\tau)\widehat{h_1^T}(\kappa_2,\tau)\\
&\quad -\Omega\frac{|\kappa|}{\kappa\sinh(|\kappa|\Delta)}\Big[\cosh(|\kappa|\Delta)(\omega_1+\Omega\Delta\kappa_1)\widehat{h_1^T}(\kappa_1,\tau)\widehat{h_1^T}(\kappa_2,\tau)\\
&\quad -\omega_1\widehat{h_1^B}(\kappa_1,\tau)\widehat{h_1^B}(\kappa_2,\tau)\Big],\\
V_5(\kappa,\kappa_1,\kappa_2) &= \frac{|\kappa|}{\sinh(|\kappa|\Delta)}\Big[(\omega_1+\Omega\Delta\kappa_1)\widehat{h_1^T}(\kappa_1,\tau)\widehat{h_1^T}(\kappa_2,\tau)\\
&\quad -\cosh(|\kappa|\Delta)\omega_1\widehat{h_1^B}(\kappa_1,\tau)\widehat{h_1^B}(\kappa_2,\tau)\Big]\\
&\quad +|\kappa\kappa_1|\widehat{\mathring{\phi}_1^B}(\kappa_1,\tau)\widehat{h_1^B}(\kappa_2,\tau)-i\Omega\kappa_1\widehat{h_1^B}(\kappa_1,\tau)\widehat{h_1^B}(\kappa_2,\tau).
\end{aligned}
$$

Upon combining the above five equations and using the dispersion relation (4.4), we obtain the following (Zakharov) integral equation:

$$
\begin{aligned}
P(\kappa)\frac{\partial\widehat{h_1^T}}{\partial\tau}(\kappa,\tau) &= \frac{1}{\sqrt{2\pi}}\int_{-\infty}^{\infty}\int_{-\infty}^{\infty} iV(\kappa,\kappa_1,\kappa_2)\widehat{h_1^T}(\kappa_1,\tau)\widehat{h_1^T}(\kappa_2,\tau)\\
&\quad \times e^{i(\omega(\kappa)-\omega(\kappa_1)-\omega(\kappa_2))t}\delta_{123}d_{12},
\end{aligned}
\tag{4.24}
$$

where the function V is given by

$$
\begin{aligned}
V(\kappa,\kappa_1,\kappa_2) &= (-\Omega^2\kappa(-1+e^{2\Delta|\kappa|})+2\kappa e^{2\Delta|\kappa|}\omega(\omega+\Omega\Delta\kappa)\\
&\quad +\Omega|\kappa|(\Omega\Delta\kappa-e^{2\Delta|\kappa|}(\omega-\Omega\Delta\kappa)+\omega))\frac{V_1(\kappa,\kappa_1,\kappa_2)}{|\kappa|(\Omega|\kappa|(-1+e^{2\Delta|\kappa|})+2\kappa e^{2\Delta|\kappa|}\omega)}
\end{aligned}
$$

$$-\frac{2\Omega e^{\Delta\kappa}(\omega+\Omega\Delta\kappa)}{\Omega|\kappa|(-1+e^{2\Delta|\kappa|})+2\kappa e^{2\Delta|\kappa|}\omega}V_2(\kappa,\kappa_1,\kappa_2)+iV_3(\kappa,\kappa_1,\kappa_2) \tag{4.25}$$
$$+\frac{2\kappa e^{\Delta\kappa}\omega(\omega+\Omega\Delta\kappa)}{|\kappa|(\Omega|\kappa|(-1+e^{2\Delta|\kappa|})+2\kappa e^{2\Delta|\kappa|}\omega)}V_5(\kappa,\kappa_1,\kappa_2).$$

Substituting

$$\widehat{h_1^T}(\kappa,\tau)=\sqrt{2\pi}\sum_{n=-3}^{3}h_{1,n}^T(\kappa,\tau)\delta(\kappa-k_n)$$

into (4.24), we recover the interaction equations:

$$P_1\frac{\partial h_{1,1}^T}{\partial\tau} = iH\left(h_{1,2}^T\right)^* h_{1,3}^T e^{-i\omega_{123}\tau}, \tag{4.26}$$
$$P_2\frac{\partial h_{1,2}^T}{\partial\tau} = iH\left(h_{1,1}^T\right)^* h_{1,3}^T e^{-i\omega_{123}\tau}, \tag{4.27}$$
$$P_3\frac{\partial h_{1,3}^T}{\partial\tau} = iHh_{1,1}^T h_{1,2}^T e^{i\omega_{123}\tau}, \tag{4.28}$$

where $\omega_{123}=(\omega_3-\omega_1-\omega_2)/\varepsilon$ is a "detuning" parameter (obviously, $\omega_{123}=0$ corresponds to resonant interactions); H is the interaction coefficient, which can be expressed in terms of the structure functions V in the following way:

$$\begin{aligned}H(k_1,k_2,k_3) &= V(k_1,-k_2,k_3)+V(k_1,k_3,-k_2)\\ &= V(k_2,-k_1,k_3)+V(k_2,k_3,-k_1)\\ &= V(k_3,k_1,k_2)+V(k_3,k_2,k_1).\end{aligned} \tag{4.29}$$

In the course of the stability calculations (section 4.3), (4.29) allowed us to check the correctness of our results by making sure that all three expressions above yielded the same answer for H, when V was substituted from (4.25).

4.3 Stability analysis

One possible approach to analyzing the stability is to use the "pump-wave" approximation. That is, assume that $|h_{1,2}^T|, |h_{1,3}^T| \ll |h_{1,1}^T|$, i.e., the waves with the wavenumbers k_2 and k_3 are considered to be infinitesimal in comparison with the wave corre-

sponding to the wavenumber k_1. Then the interaction equations (4.26)-(4.28) become (to leading order):

$$P_1 \frac{\partial h_{1,1}^T}{\partial \tau} = 0, \tag{4.30}$$

$$P_2 \frac{\partial h_{1,2}^T}{\partial \tau} = iH \left(h_{1,1}^T\right)^* h_{1,3}^T e^{-i\omega_{123}\tau}, \tag{4.31}$$

$$e^{-i\omega_{123}\tau} P_3 \frac{\partial h_{1,3}^T}{\partial \tau} = iH h_{1,1}^T h_{1,2}^T. \tag{4.32}$$

We deduce from (4.30) that $h_{1,1}^T = \text{const}$. Differentiating (4.32) with respect to τ and substituting for $\frac{\partial}{\partial \tau} h_{1,2}^T$ from (4.31), we get

$$\frac{\partial^2 h_{1,3}^T}{\partial \tau^2} - i\omega_{123} \frac{\partial h_{1,3}^T}{\partial \tau} = -\frac{|H h_{1,1}^T|^2}{P_2 P_3} h_{1,3}^T.$$

Hence $h_{1,3}^T \sim e^{i\lambda\tau}$, where

$$\lambda = \frac{1}{2} |h_{1,1}^T| \left(\frac{\omega_{123}}{|h_{1,1}^T|} \pm \sqrt{\left(\frac{\omega_{123}}{|h_{1,1}^T|}\right)^2 + \frac{4H^2}{P_2 P_3}} \right).$$

A wave is unstable with respect to the infinitesimal perturbations if λ has a non-zero imaginary part, i.e., if

$$P_2 P_3 < 0 \text{ and } \left(\frac{\omega_{123}}{|h_{1,1}^T|}\right)^2 + \frac{4H^2}{P_2 P_3} < 0.$$

A normalized dimensionless growth rate γ can be defined as

$$\gamma_{123} = \frac{|\text{Im}\lambda|}{c_0 k_1},$$

but a more convenient quantity to consider is

$$\widehat{\gamma}_{123} = \frac{\gamma_{123}}{\left|h_{1,1}^T\right|},$$

which is independent of the amplitude $h^T_{1,1}$ in the resonant case ($\omega_{123} = 0$), although no longer a dimensionless parameter. It is immediately obvious that the growth rates are smaller for the near-resonant interactions, provided that the quantity $h^2_{cr} = \left|\frac{H^2}{P_2 P_3}\right|$ does not increase (we introduced the symbol h_{cr} in order to emphasize that the quantity in question is proportional to the inverse of the critical amplitude, at which the instability first appears). Thus, we need to investigate h_{cr} for both the resonant and near-resonant cases.

Let "f" ("forward mode") denote the co-flowing wave, "b" ("backward mode") denote the counter-flowing wave, and "i" denote the third root, which lies between the other two. Using this notation we can write, for example, f-b-b, which would mean an interaction between a forward mode (k_1) and two backward modes (k_2 and k_3).

All the graphs in this section were obtained by fixing $k_1 = 1$ and letting Δ and Ω vary, so that the whole region of instability in fig. 2.4 ($0 < \Delta k_1 < 3$, $0 < V/c_0 < 10$) could be covered. The values of k_2 and k_3 were limited so that $0.1 < \frac{k_1}{k_2}, \frac{k_1}{k_3} < 10$.

Figs. 4.1–4.7 below show the regions of instability in the "pump-wave" approximation. Circles represent the region of instability due to the resonant ($\omega_{123} = 0$) three-wave interactions. The radius of the circles is proportional to the growth rate $\widehat{\gamma}_{123} \equiv h_{cr}$. Thus, circles of larger radius correspond to more unstable regions. These regions may also appear as darker areas in the plots.

It is interesting to note that more than one resonant triad can exist for given values of Ω, Δ, and $k_1 = 1$. If this is the case, the interactions with shorter waves ($k_2, k_3 > k_1$) result in the growth rates that can be several orders of magnitude larger than the growth rates in the case of approximately equal wavenumbers (k_2 or $k_3 \approx k_1$). This fact is illustrated especially well in fig. 4.2. The area with large circles is the one where the long and the short waves interact with each other. Due to the cut-off that we introduced ($k_2/k_1 < 10$), the nearby points correspond to the long-long three-wave interactions and therefore result in much smaller growth rates (represented by smaller circles). Thus, the energy can be transferred very efficiently between the long (counter-flowing, in this particular case) finite amplitude waves and the infinitesimal

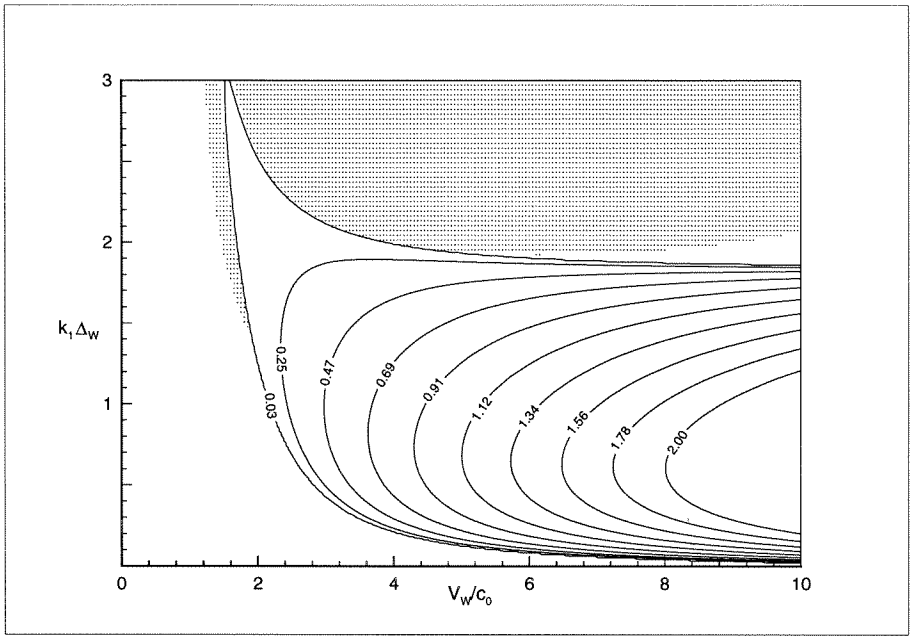

Figure 4.1: Growth rates for the b-b-b interactions. Solid lines, linear growth rates; circles, $\widehat{\gamma}_{123}$. $\omega_{123} = 0$.

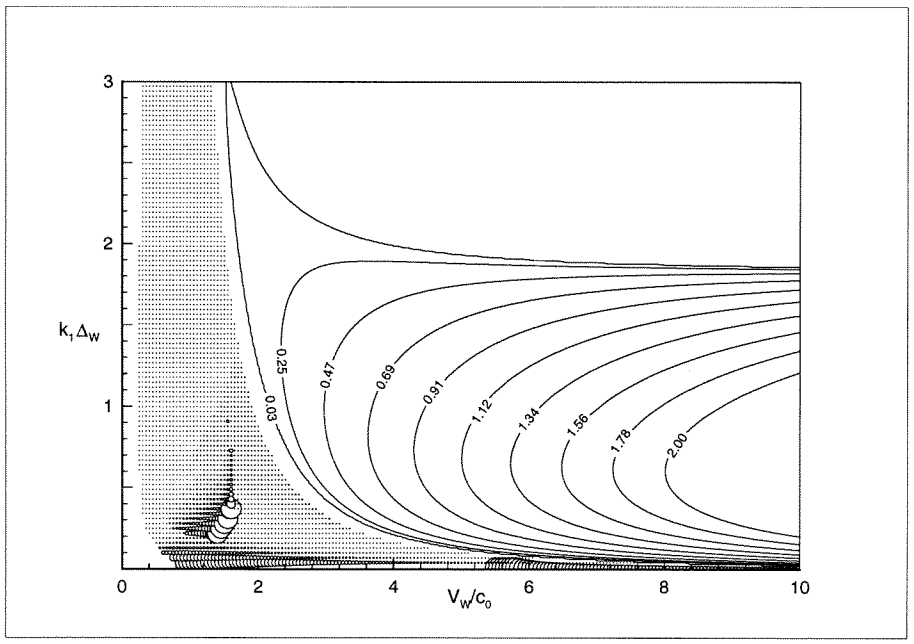

Figure 4.2: Growth rates for the b-i-b interactions. Solid lines, linear growth rates; circles, $\widehat{\gamma}_{123}$. $\omega_{123} = 0$.

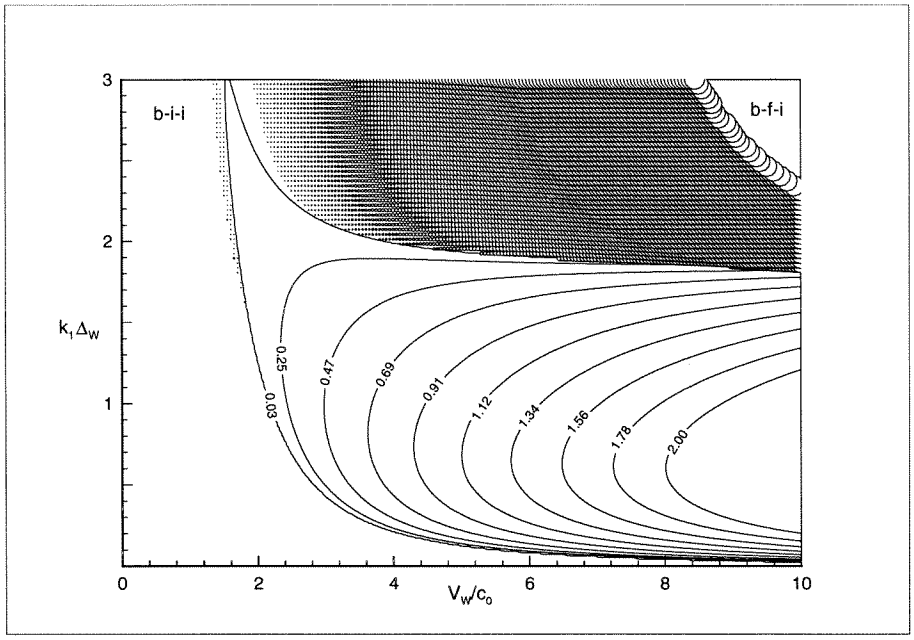

Figure 4.3: Growth rates for the b-i-i and b-f-i interactions. Solid lines, linear growth rates; circles, $\widehat{\gamma}_{123}$. $\omega_{123} = 0$.

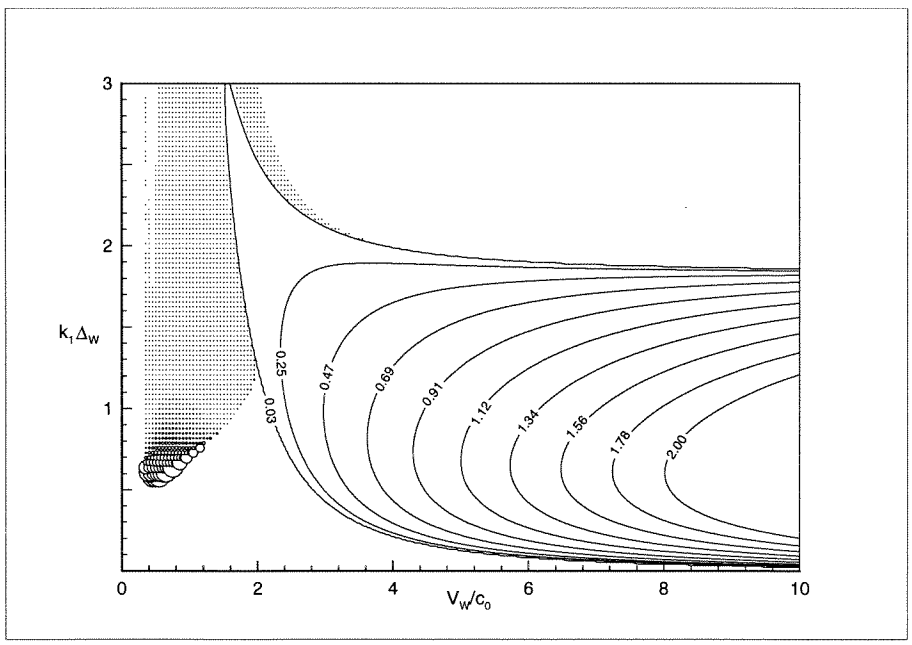

Figure 4.4: Growth rates for the i-b-b interactions. Solid lines, linear growth rates; circles, $\widehat{\gamma}_{123}$. $\omega_{123} = 0$.

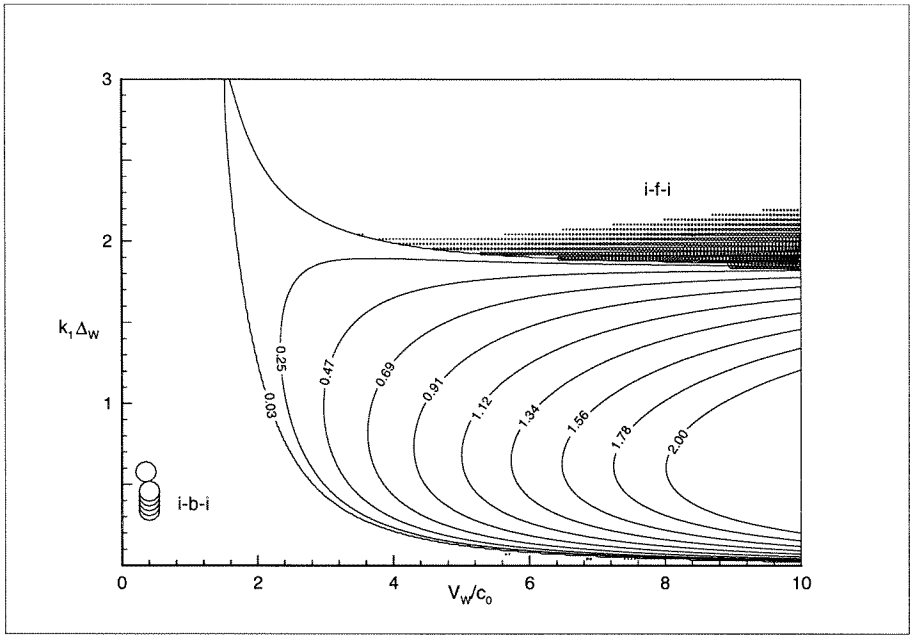

Figure 4.5: Growth rates for the i-b-i and i-f-i interactions. Solid lines, linear growth rates; circles, $\widehat{\gamma}_{123}$. $\omega_{123} = 0$.

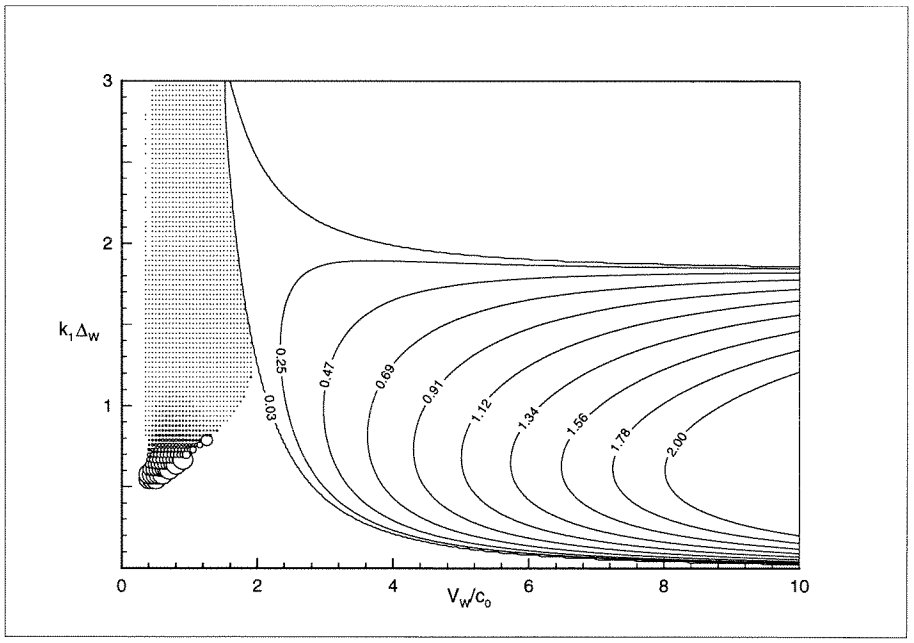

Figure 4.6: Growth rates for the i-i-i interactions. Solid lines, linear growth rates; circles, $\widehat{\gamma}_{123}$. $\omega_{123} = 0$.

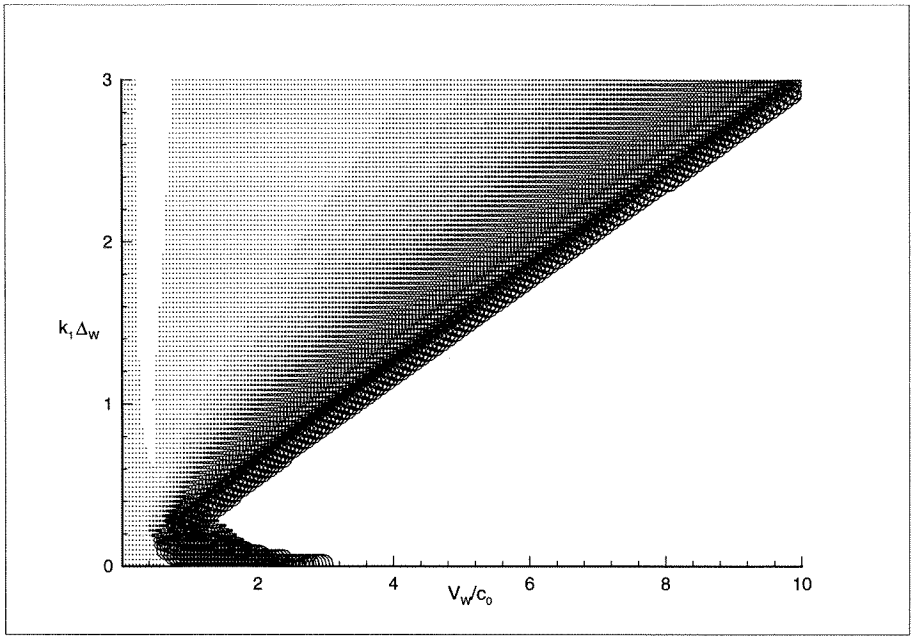

Figure 4.7: Growth rates for the f-b-i interactions. Solid lines, linear growth rates; circles, $\widehat{\gamma}_{123}$. $\omega_{123} = 0$.

short wind-generated waves.

Now let us consider the near-resonant interactions with $\varepsilon\omega_{123} = 0.01$ and choose the b-b-b interactions as an example. We still require that the wavenumbers satisfy the resonant conditions exactly:

$$k_1 + k_2 = k_3.$$

The main question that we have to answer is whether the parameter h_{cr} increases. If it does, the near-resonant interactions can turn out to be more unstable than the resonant ones. Direct comparison is complicated by the change in the wavenumbers k_2 and k_3 ($k_1 = 1$ is still held fixed), which is associated with the non-zero value of ω_{123}. In order to make our comparison meaningful, we restrict our attention to those points in the stability diagram that correspond to less than 10% change in the wavenumber k_2. Fig. 4.8 shows the points where h_{cr} increases. The radius of the

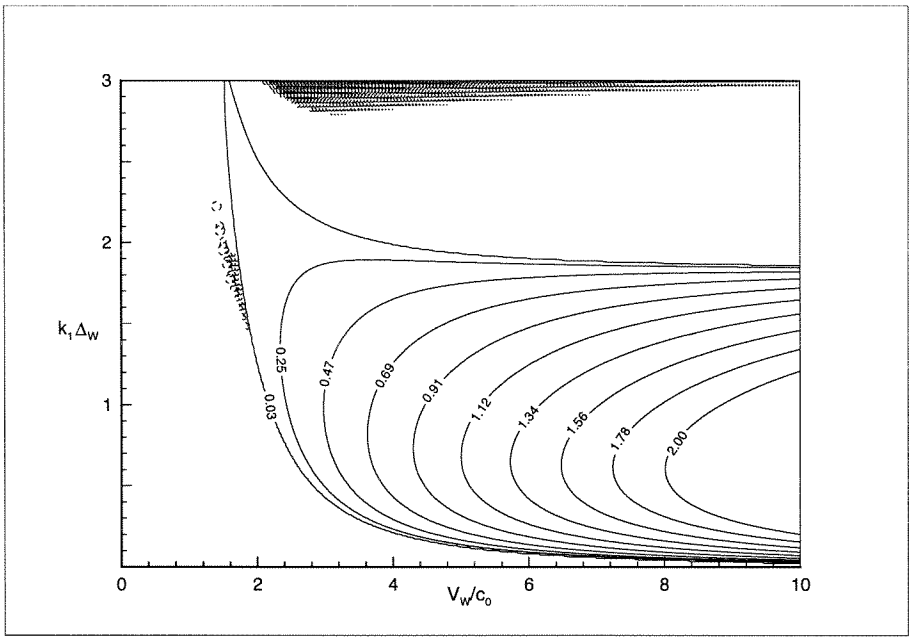

Figure 4.8: Critical amplitudes differences between the resonant and near-resonant b-b-b interactions. Solid lines, linear growth rates; circles, Δh_{cr}. $\varepsilon\omega_{123} = 0.01$.

circles is proportional to the relative increase of h_{cr}:

$$\Delta h_{cr} = \frac{h_{cr}^{near-resonant} - h_{cr}^{resonant}}{h_{cr}^{near-resonant}}.$$

Another possible type of instability is the explosive instability. It is well-known that under certain conditions amplitudes of the interacting waves can become infinite in finite time. Any solution of the system (4.5)-(4.7) exhibits this behavior regardless of the initial conditions, if the sign of the energy of the wave with the greatest frequency (in absolute value) is opposite to the sign of the energies of the other two waves, where the energy of a wave is given by $\frac{1}{2}\omega_j P_j |h_{1,j}^T|^2$. For example, if k_1 corresponds to the wave with the maximum frequency, the following condition should be satisfied:

$$P_1\omega_1 P_2\omega_2 < 0 \text{ and } P_1\omega_1 P_3\omega_3 < 0. \tag{4.33}$$

Since the above condition (4.33) does not involve the interaction coefficient H, the analysis of the regions where the explosive instability is possible can be carried out

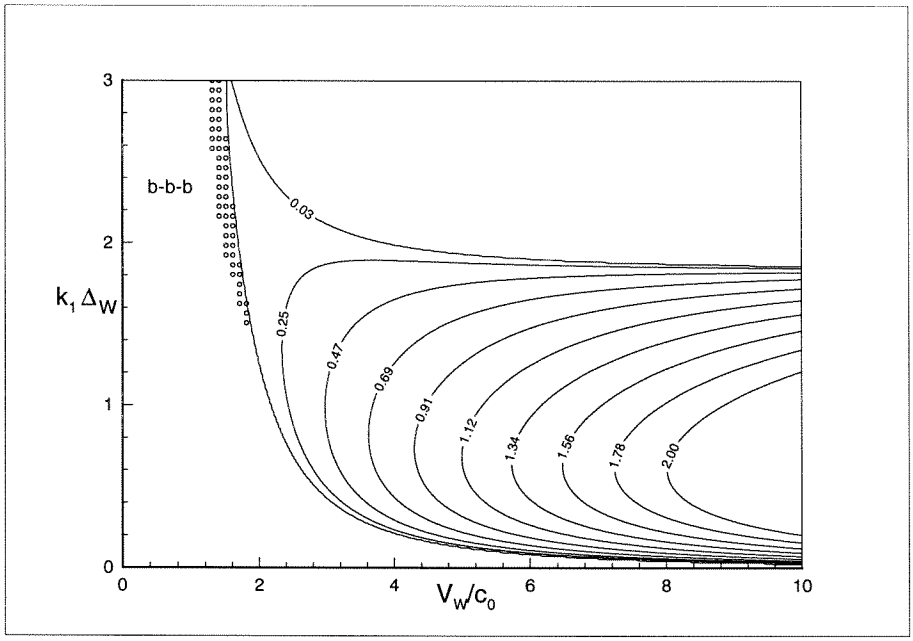

Figure 4.9: The region of explosive instability, corresponding to the b-b-b interactions.

entirely in the framework of the linear approximation. Specifically, all we need to know is the linear dispersion relation.

The following resonant interactions were found to result in the explosive instability (within the restrictions on k_1 and k_2 specified above): b-b-b, b-i-b, b-f-i, i-b-b, i-i-i, f-b-i. The regions of explosive instability are presented in figs. 4.9–4.12 and are marked by circles.

4.4 Conclusion

We have demonstrated that the resonant and near-resonant three-wave interactions lead to a significant expansion of the instability region. Even if the participating waves were originally stable in the whole physical domain (the f-b-i case), the nonlinear interaction can lead to the onset of instability. If the instability is of the explosive type, the amplitudes can become infinite in finite time. It is known, however, that if higher-order four-wave interactions are taken into account, the amplitudes need not become infinite. We have also shown that the near-resonant interactions can potentially be

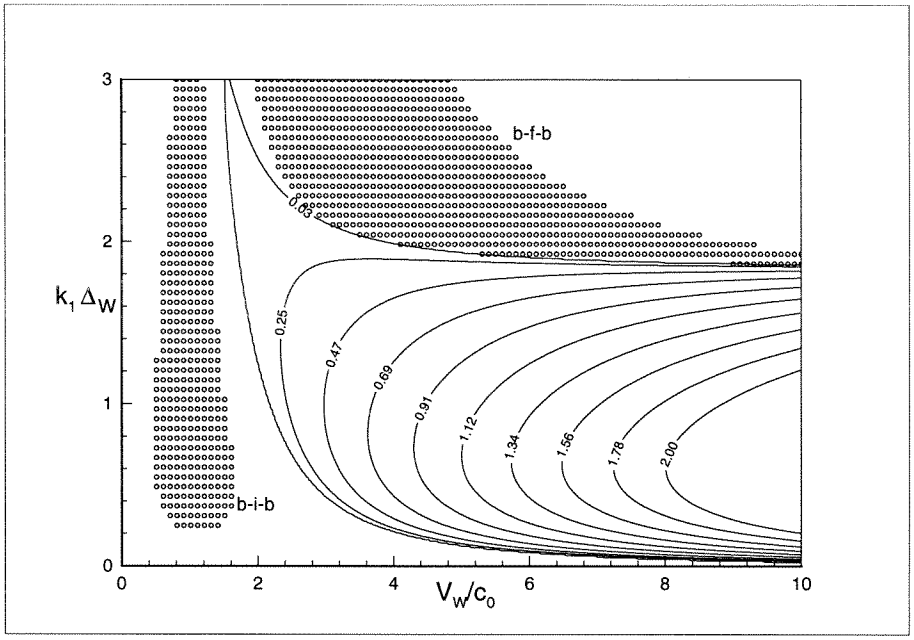

Figure 4.10: The region of explosive instability, corresponding to the b-i-b and b-f-i interactions.

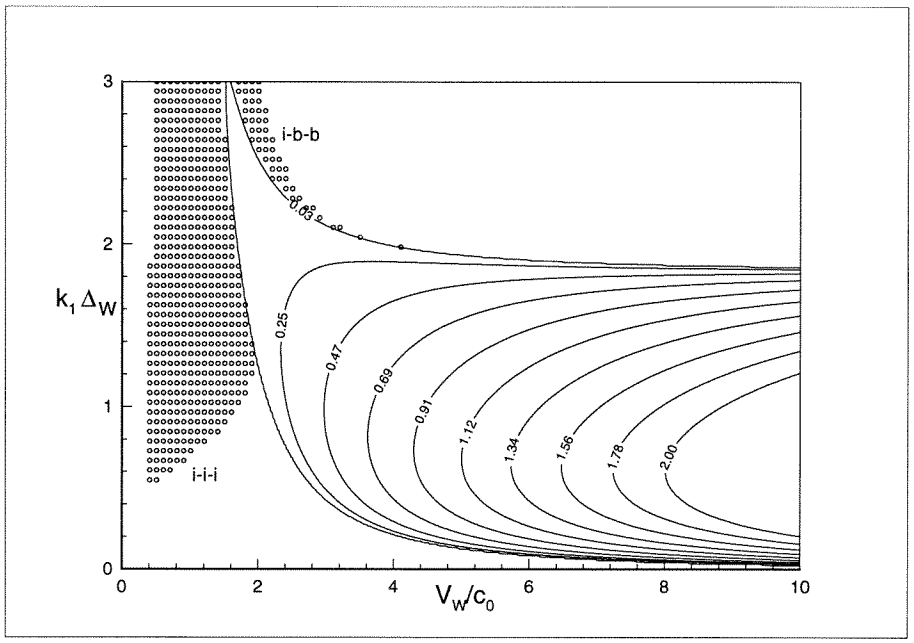

Figure 4.11: The region of explosive instability, corresponding to the i-b-b and i-i-i interactions.

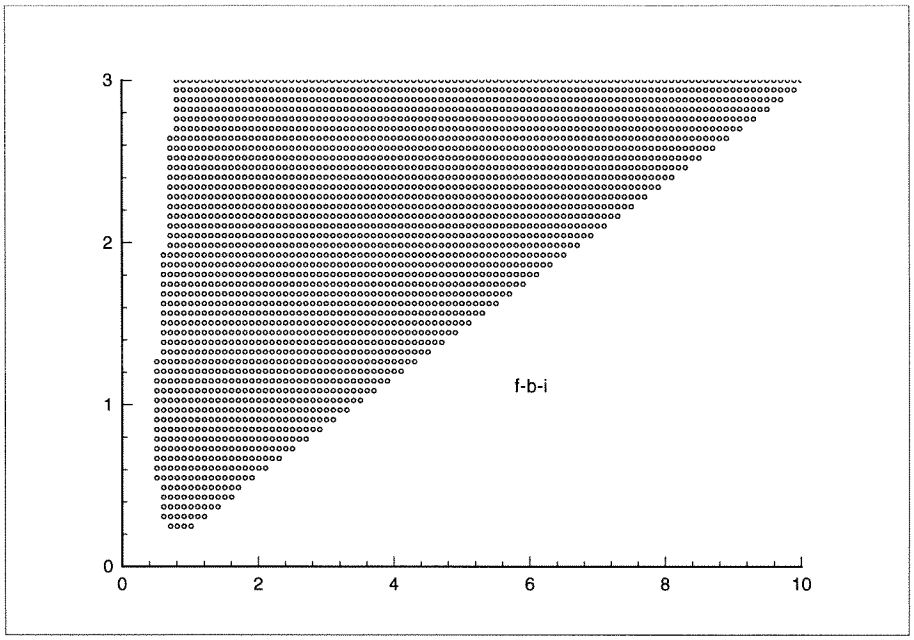

Figure 4.12: The region of explosive instability, corresponding to the f-b-i interactions.

more unstable than the resonant ones, depending on the wave amplitude and the parameters of the shear.

Chapter 5 Asymmetric waves

5.1 Introduction

In this chapter we investigate different shapes of steady two-dimensional inviscid gravity waves with shear in the water. It has been known for a long time that "... the shape of waves in the open sea can sometimes indicate the presence and direction of a current" ([13], p. 110). Therefore, we attempt to find free surface profiles which unlike "regular" waves are not symmetric about any trough or crest.

Solutions of this type were first presented by Zufiria [23], who investigated irrotational deep water gravity waves. He found a symmetry breaking bifurcation for the waves which were very close to the wave of greatest height. We reproduce this result in section 5.4.1.

One may expect that the presence of shear introduces a preferred direction and result in wave profiles with considerable asymmetry at low amplitudes. Indeed, it is possible to find bifurcations leading to a one-parameter family of low amplitude non-symmetric solutions. These bifurcations are associated with the existence of a slowly propagating wave, which is not present in the irrotational case. Unfortunately, in the absence of a good theoretical understanding or an analytical approach, the search for asymmetric profiles has to be carried out on a trial-and-error basis.

5.2 Mathematical formulation

As mentioned in the introduction, some of the effects that we are looking for occur at high wave amplitudes. The Fourier series formulation used in the three previous chapters fails for sufficiently large amplitudes (see [16]). We therefore adopt a boundary-integral method ([8]) which enables us to compute steep waves. In order to make our notation more suitable for use with this new formulation, we replace the

superscripts T, B, which we used previously, with the subscripts $1, 2$ and change the notation for the interfaces from $h^{T,B}$ to $y_{1,2}$.

Let $W_{1,2} = W_{1,2}(x, y) = \phi_{1,2}(x, y) + i\psi_{1,2}(x, y)$ denote the complex potential of the irrotational contribution to the flow, so that the total flow in the region with shear (between the two interfaces $y_1(x)$ and $y_2(x)$) is described by the following streamfunction

$$\Psi_1(x, y) = -cy + \Omega\Delta y + \frac{1}{2}\Omega y^2 + \psi_1(x, y) \text{ for } y_2(x) \leq y \leq y_1(x), \tag{5.1}$$

and the flow in the irrotational region (below the lower interface $y_2(x)$) is described by

$$\Psi_2(x, y) = -cy + \psi_2(x, y) \text{ for } -\infty < y \leq y_2(x). \tag{5.2}$$

Note that the signs of c and Ω are opposite to those used in the previous chapters.

Consider the following mapping of the infinite surface of the fluid:

$$\omega = e^{-iz} = e^{-i(x+iy)} = \omega(x, y).$$

This mapping transforms two infinite interfaces $y_{1,2}(x)$ into two closed contours $\omega_{1,2}(x)$ (see fig. 5.1), where

$$\omega_1(x) = \omega(x, y_1(x)), \ \omega_2(x) = \omega(x, y_2(x)).$$

Denote

$$\phi_{11}(x) = \phi_1(x, y_1(x)), \ \psi_{11}(x) = \psi_1(x, y_1(x)), \ W_{11}(x) = \phi_{11}(x) + i\psi_{11}(x), \tag{5.3}$$

i.e., ϕ_{11}, ψ_{11}, and W_{11} are the velocity potential, the streamfunction, and the complex potential evaluated at the free surface. Similarly, for the lower interface we have

$$\phi_{12}(x) = \phi_1(x, y_2(x)), \ \psi_{12}(x) = \psi_1(x, y_2(x)), \ W_{12}(x) = \phi_{12}(x) + i\psi_{12}(x),$$

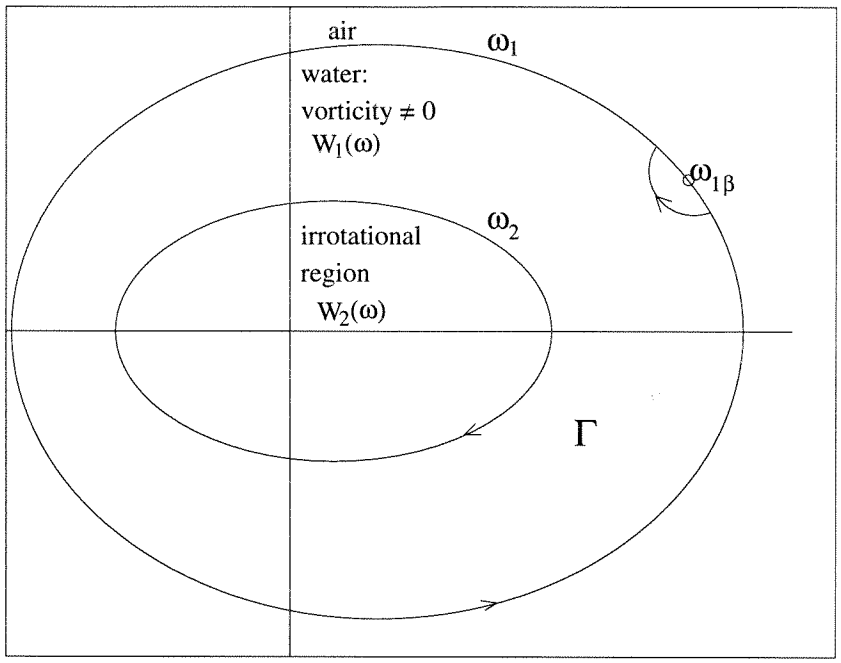

Figure 5.1: The two closed contours $\omega_1(x) = \omega(x, y_1(x))$ and $\omega_2(x) = \omega(x, y_2(x))$, comprising the contour Γ.

$$\phi_{22}(x) = \phi_2(x, y_2(x)),\ \psi_{22}(x) = \psi_2(x, y_2(x)),\ W_{22}(x) = \phi_{22}(x) + i\psi_{22}(x),$$

$$\omega_{\alpha\beta} \equiv \omega_\alpha(x_\beta) \equiv \omega(x_\beta, y_\alpha(x_\beta)) \text{ for } \alpha = 1, 2,$$

where x_β is an arbitrary point on either interface.

Since the function $W_1(z)$ is analytic, we can apply Cauchy's theorem to the contour Γ (see fig. 5.1):

$$\oint_\Gamma \frac{dW_1}{d\omega}(\omega)\ \frac{d\omega}{\omega - \omega_{\alpha\beta}} = 0. \tag{5.4}$$

Now we can use the Plemelj formulas to get an integral equation

$$\pi i \frac{dW_1}{d\omega}(\omega_{\alpha\beta}) + (P.V.) \int_\Gamma \frac{dW_1}{d\omega}(\omega)\ \frac{d\omega}{\omega - \omega_{\alpha\beta}} = 0, \tag{5.5}$$

where $(P.V.)$ denotes the principal value of an integral. First suppose that $\omega_{\alpha\beta}$ lies

on the outer contour, i.e., $\alpha = 1$. Multiplying both sides by $\frac{d\omega_1}{dx}(x_\beta)$, we obtain

$$\pi i \frac{dW_{11}}{dx}(x_\beta) + \frac{d\omega}{dx}(x_\beta) \left((P.V.) \int_0^{2\pi} \frac{dW_{11}}{dx}(x) \frac{dx}{\omega_1(x) - \omega_1(x_\beta)} - \int_0^{2\pi} \frac{dW_{12}}{dx}(x) \frac{dx}{\omega_2(x) - \omega_1(x_\beta)} \right) = 0. \quad (5.6)$$

Taking the imaginary part of this expression, we get

$$\pi \frac{d\phi_{11}}{dx}(x_\beta) + \mathrm{Im} \left[\frac{d\omega_1}{dx}(x_\beta) \left((P.V.) \int_0^{2\pi} \frac{dW_{11}}{dx}(x) \frac{dx}{\omega_1(x) - \omega_1(x_\beta)} - \int_0^{2\pi} \frac{dW_{12}}{dx} \frac{dx}{\omega_2(x) - \omega_1(x_\beta)} \right) \right] = 0. \quad (5.7)$$

Two additional equations come from placing $\omega_{\alpha\beta}$ on the lower interface:

$$-\pi \frac{d\phi_{12}}{dx}(x_\beta) + \mathrm{Im} \left[\frac{d\omega_2}{dx}(x_\beta) \left((P.V.) \int_0^{2\pi} \frac{dW_{12}}{dx}(x) \frac{dx}{\omega_2(x) - \omega_2(x_\beta)} - \int_0^{2\pi} \frac{dW_{11}}{dx}(x) \frac{dx}{\omega_1(x) - \omega_2(x_\beta)} \right) \right] = 0, \quad (5.8)$$

$$\pi \frac{d\phi_{22}}{dx}(x_\beta) + \mathrm{Im} \left[\frac{d\omega_2}{dx}(x_\beta) \left((P.V.) \int_0^{2\pi} \frac{dW_{22}}{dx}(x) \frac{dx}{\omega_2(x) - \omega_2(x_\beta)} \right) \right] = 0. \quad (5.9)$$

These integral equations have to be combined with the following boundary conditions applied at the interfaces:

1. The interfaces are streamlines:

$$\psi_{11}(x) = c y_1(x) - \Omega \Delta y_1(x) - \frac{1}{2} \Omega y_1^2(x), \quad (5.10)$$

$$\psi_{12}(x) = c y_2(x) - \Omega \Delta y_2(x) - \frac{1}{2} \Omega y_2^2(x), \quad (5.11)$$

$$\psi_{22}(x) = c y_2(x). \quad (5.12)$$

2. The tangential velocity is continuous at the bottom interface:

$$\frac{d\phi_{22}}{dx}(x) = \frac{d\phi_{12}}{dx}(x) + \Omega(\Delta + y_2(x)). \tag{5.13}$$

Note that this condition is equivalent to requiring that the pressure be continuous across the interface. In fact, it follows from (5.11) and (5.12) that the tangential derivatives of the streamfunctions $\Psi_1(x, y)$ and $\Psi_2(x, y)$ are zero at $y = y_2(x)$, i.e., normal velocities are zero at the interface. Therefore, using the Bernoulli equation, we deduce that the continuity of tangential velocity implies the continuity of pressure.

3. The pressure is continuous at the free surface (the Bernoulli equation):

$$\frac{1}{2}q^2 + gy_1(x) = \text{const}, \tag{5.14}$$

where

$$q^2 = \left[\left(\frac{\partial\Psi_1(x,y)}{\partial x}\right)^2 + \left(\frac{\partial\Psi_1(x,y)}{\partial y}\right)^2\right]\Bigg|_{y=y_1(x)}.$$

Let $\bar{n}$ and $\bar{\tau}$ denote the unit normal and the unit tangent to the free surface respectively:

$$\bar{n} = \frac{1}{\left(1 + \left(\frac{dy_1}{dx}(x)\right)^2\right)^{\frac{1}{2}}}\left(-\frac{dy_1}{dx}(x), 1\right),$$

$$\bar{\tau} = \frac{1}{\left(1 + \left(\frac{dy_1}{dx}(x)\right)^2\right)^{\frac{1}{2}}}\left(1, \frac{dy_1}{dx}(x)\right).$$

Then

$$q^2 = \left[\left(\frac{\partial\Psi_1(x,y)}{\partial\bar{\tau}}\right)^2 + \left(\frac{\partial\Psi_1(x,y)}{\partial\bar{n}}\right)^2\right]\Bigg|_{y=y_1(x)}.$$

The normal component of the velocity is zero on the free surface, i.e.,

$$\frac{\partial\Psi_1(x,y)}{\partial\bar{\tau}} = 0.$$

Therefore,

$$q^2 = \left(\frac{\partial \Psi_1(x,y)}{\partial \bar{n}}\right)^2 = \frac{\left(-\dfrac{\partial \Psi_1}{\partial x}\dfrac{dy_1}{dx} + \dfrac{\partial \Psi_1}{\partial y}\right)^2}{1 + \left(\dfrac{dy_1}{dx}\right)^2}.$$

Recall that

$$\begin{aligned} -\frac{\partial \Psi_1}{\partial x}\frac{dy_1}{dx} + \frac{\partial \Psi_1}{\partial y} &= -\frac{\partial \psi_1}{\partial x}\frac{dy_1}{dx} + \frac{\partial \psi_1}{\partial y} - c + \Omega(\Delta + y_1) \\ &= \frac{\partial \phi_1}{\partial x} + \frac{\partial \phi_1}{\partial y}\frac{dy_1}{dx} - c + \Omega(\Delta + y_1) \\ &= \frac{d\phi_1}{dx} - c + \Omega(\Delta + y_1), \end{aligned}$$

where all quantities are evaluated on $y = y_1(x)$. Using the notation introduced in (5.3), we obtain

$$q^2 = \frac{\left(\dfrac{d\phi_{11}}{dx} - c + \Omega(\Delta + y_1)\right)^2}{1 + \left(\dfrac{dy_1}{dx}\right)^2}.$$

Let us choose the constant on the right-hand side of the Bernoulli equation (5.14) to be equal to $\frac{1}{2}(c - \Omega\Delta)^2(1 - b) + gy_1(0)$. It is easy to show that $b = 1$ corresponds to the wave of greatest height, while $b = 0$ corresponds to the case when the wave amplitude is zero. Consider the Bernoulli equation (5.14) at $x = 0$:

$$\frac{1}{2}q^2 \equiv \frac{1}{2}\left.\frac{\left(\dfrac{d\phi_{11}}{dx} - c + \Omega(\Delta + y_1)\right)^2}{1 + \left(\dfrac{dy_1}{dx}\right)^2}\right|_{x=0} = \frac{1}{2}(c - \Omega\Delta)^2(1 - b).$$

First take $b = 0$. Then the pair $y_1 \equiv 0$ and $\phi_{11} \equiv 0$ is a solution. Now let $b = 1$. Then $q^2 = 0$, i.e., we have a stagnation point. If we require that this stagnation point be at the crest of the wave (see (5.16)), then $b = 1$ will, in fact, correspond to the wave

of greatest height. So $0 \leq b \leq 1$ encompasses all possible wave amplitudes, which makes it convenient to use b as the natural parameter in the continuation process.

Note that all equations are invariant under horizontal translation. Therefore, we have to impose three additional conditions in order to fix the origin and the depth of the shear layer:

$$\frac{1}{2\pi}\int_0^{2\pi} y_1(x)dx = 0, \tag{5.15}$$

$$\frac{dy_1}{dx}(0) = 0, \tag{5.16}$$

$$\frac{1}{2\pi}\int_0^{2\pi} (y_1(x) - y_2(x))dx = \Delta. \tag{5.17}$$

Condition (5.15) implies that the average elevation of the free surface is zero; condition (5.16) requires that a crest or a trough of the wave be located at $x = 0$; and condition (5.17) fixes the average depth of the shear layer to be equal to Δ. The above conditions are not unique. Instead of (5.15) we could have required, for example, that

$$y_1(0) = 0,$$

which would have placed the origin on a crest (or a trough). However, the conditions chosen are the most convenient for the numerical method being used.

5.3 Numerical method

Suppose we divide the interval $[0, 2\pi]$ into N equal parts so that the grid size h is equal to $2\pi/N$ (N is chosen to be odd). Let us expand $y_{1,2}$ in Fourier series:

$$y_{1,2} = a_0^{1,2} + \sum_{m=1}^{(N-1)/2} (a_m^{1,2}\cos(mx) + b_m^{1,2}\sin(mx)).$$

Since we deal with $2\pi-$periodic functions $\psi_{1,2}(x, y(x))$ and $y_{1,2}(x)$, it is natural to use the trapezoidal rule to evaluate the integrals. First we need to evaluate the

contribution from the singular point. Note that

$$\frac{\frac{d\omega_1}{dx}(x_\beta)}{\omega_1(x)-\omega_1(x_\beta)} = \frac{1}{x-x_\beta} - \frac{\frac{d^2\omega_1}{dx^2}(x_\beta)}{2\frac{d\omega_1}{dx}(x_\beta)} + O(x-x_\beta),$$

$$\lim_{x\to x_\beta} \frac{\frac{dW}{dx}(x) - \frac{dW}{dx}(x_\beta)}{x-x_\beta} = \frac{d^2W}{dx^2}(x_\beta).$$

Therefore, our integral equations produce $3N$ nonlinear equations of the following form:

$$\pi\frac{d\phi_{11}}{dx}(x_k) + h\frac{d^2\psi_{11}}{dx^2}(x_k) + h\mathrm{Im}\left[\frac{d\omega_1}{dx}(x_k)\left(\sum_{l=0,l\neq k}^{N}\frac{\alpha_l}{\omega_1(x_l)-\omega_1(x_k)}\frac{dW_{11}}{dx}(x_l) - \sum_{l=0}^{N}\frac{\alpha_l}{\omega_2(x_l)-\omega_1(x_k)}\frac{dW_{12}}{dx}(x_l)\right) - \frac{\frac{d^2\omega_1}{dx^2}(x_k)}{2\frac{d\omega_1}{dx}(x_k)}\frac{dW_{11}}{dx}(x_k)\right] = 0, \quad (5.18)$$

$$-\pi\frac{d\phi_{12}}{dx}(x_k) + h\frac{d^2\psi_{12}}{dx^2}(x_k) + h\mathrm{Im}\left[\frac{d\omega_2}{dx}(x_k)\left(\sum_{l=0,l\neq k}^{N}\frac{\alpha_l}{\omega_2(x_l)-\omega_2(x_k)}\frac{dW_{12}}{dx}(x_l) - \sum_{l=0}^{N}\frac{\alpha_l}{\omega_1(x_l)-\omega_2(x_k)}\frac{dW_{11}}{dx}(x_l)\right) - \frac{\frac{d^2\omega_2}{dx^2}(x_k)}{2\frac{d\omega_2}{dx}(x_k)}\frac{dW_{12}}{dx}(x_k)\right] = 0, \quad (5.19)$$

$$\pi\frac{d\phi_{22}}{dx}(x_k) + h\frac{d^2\psi_{22}}{dx^2}(x_k) + h\mathrm{Im}\left[\frac{d\omega_2}{dx}(x_k)\sum_{l=0,l\neq k}^{N}\frac{\alpha_l}{\omega_2(x_l)-\omega_2(x_k)}\frac{dW_{22}}{dx}(x_l) - \frac{\frac{d^2\omega_2}{dx^2}(x_k)}{2\frac{d\omega_2}{dx}(x_k)}\frac{dW_{22}}{dx}(x_k)\right] = 0, \quad (5.20)$$

where $x_k = 2\pi k/N$, $k = 1,\ldots,N$; $\alpha_l = 1$, $l = 1,\ldots,N-1$, $\alpha_0 = \alpha_N = \frac{1}{2}$.

Our unknowns are ϕ_{11}, ϕ_{12} (total $2N$), the Fourier coefficients of $y_{1,2}$ (total $2N$) and c. Note that the boundary conditions (5.10)–(5.13) allow us to eliminate ψ_{11},

ψ_{12}, ψ_{22}, and $\frac{d\phi_{22}}{dx}$ from consideration. Thus, the total number of unknowns is $4N+1$, so that we need a further $N+1$ equations, which come from the Bernoulli equation (5.14) and condition (5.15). The two remaining conditions (5.16) and (5.17), fixing the origin and the depth of the shear layer, have to be incorporated with the help of Lagrange multipliers $f_j(x)$, $j = 1, 2$: we multiply (5.16) by $f_1(x)$, (5.17) by $f_2(x)$ and add these quantities to all of the equations (5.18)-(5.20). $f_{1,2}$ are chosen by trial-and-error so that the system has the greatest condition number possible.

We start the computation by a choosing a small value of $b > 0$ and using an analytically derived linear solution to the system (5.18)–(5.20) with the boundary conditions (5.14)–(5.17) as an initial approximation in Newton's method to arrive at a nonlinear solution. We then continue our solution by increasing b. The continuation is done using either the natural parameter or arclength continuation method [12], whichever is more appropriate. We look for a change in sign of the Jacobian of the system, which indicates non-uniqueness of the solution at the point where the Jacobian matrix is singular, and then pinpoint the exact location of the bifurcation point by bisection.

5.4 Results

Any symmetric wave can be represented in the form

$$y_{1,2} = d_0^{1,2} + \sum_{k=1}^{(N-1)/2} d_k^{1,2} \cos(k(x-\delta)),$$

with $x = \delta$ being the axis of symmetry. Then

$$a_k^{1,2} = d_k^{1,2} \cos(k\delta),\ b_k^{1,2} = d_k^{1,2} \sin(k\delta).$$

Therefore, in order to determine whether a 2π-periodic wave is asymmetric, it is sufficient to check that for some n

$$\tan(n\delta) \neq \frac{b_n^{1,2}}{a_n^{1,2}}, \tag{5.21}$$

where

$$\tan(\delta) = \frac{b_1^{1,2}}{a_1^{1,2}}.$$

In practice, $a_1^{1,2}$ can be zero (for example, we may have a wave of period π). If $a_2^{1,2} \neq 0$, then

$$\tan(2\delta) = \frac{b_2^{1,2}}{a_2^{1,2}}$$

and

$$\tan(\delta_\pm) = \frac{-1 \pm (1 + \tan^2(2\delta))^{\frac{1}{2}}}{\tan(2\delta)},$$

so that we can use

$$\tan(n\delta_\pm) \neq \frac{b_n^{1,2}}{a_n^{1,2}} \tag{5.22}$$

instead of (5.21). This condition is very easy to check, since

$$\tan(n\delta_\pm) = \frac{\tan(\delta_\pm) + \tan((n-1)\delta_\pm)}{1 - \tan(\delta_\pm)\tan((n-1)\delta_\pm)},$$

so that recursion can be employed. Of course, (5.22) is meaningful only if $a_n^{1,2} \neq 0$.

5.4.1 Asymmetric waves in the absence of shear (Zufiria)

It was discovered by Zufiria [23] that there are symmetry breaking bifurcations for the waves of wavelength $2\pi/6$. Since Zufiria used a formulation significantly different from the one presented in this chapter, it is important to verify the results from [23].

Because all the interesting irrotational phenomena occur at high amplitudes, a sufficient resolution must be used. We let $N = 551$, which corresponds to keeping approximately 40 Fourier coefficients for the original wave of wavelength $2\pi/6$. The equations were considered to be satisfied if the error was less than 10^{-12}. In all the

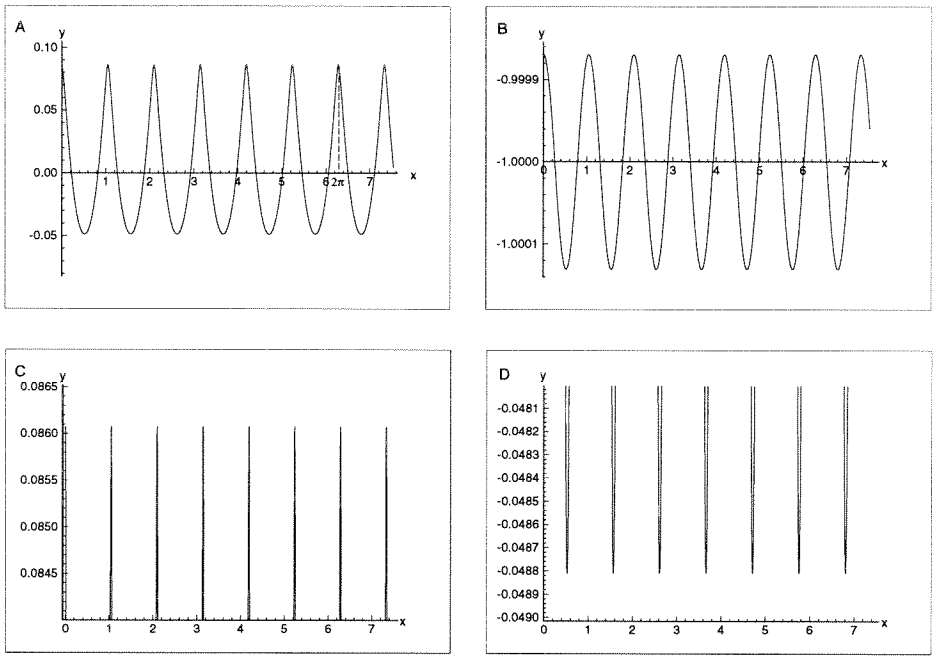

Figure 5.2: Main symmetric irrotational branch P-1, $b = 0.87900$, $c = 0.44255$. A: free surface; B: interface at $y = -0.5$; C: crests at the free surface; D: troughs at the free surface. The waves are symmetric with respect to any crest or trough.

calculations the time scale was normalized so that $g = 1$. Note that apart from normalizing the gravitational acceleration, we preserve the original dimensions of all quantities.

In accordance with [23], we denote the principal branch of the solution by P-1. We follow this branch from $b = 0$ to the neighborhood of the first bifurcation point (namely to $b = 0.87900$). Although in the absence of shear $\phi_{12}(x) \equiv \phi_{22}(x)$ and the lower interface $y_2(x)$ has no physical importance (since the flow is potential in both regions), we are going to compute both $\phi_{22}(x)$ and $y_2(x)$. These two quantities provide a useful check on the accuracy of the code and facilitate the comparison of the results obtained with and without vorticity. Fig. 5.2 shows corresponding profiles: graph A represents the free surface; graph B represents the lower interface at $y = -\Delta = -0.5$ (this is the same value of Δ as the one used below in section 5.4.2 for the computation with shear); graph C gives detailed picture of the crests at the free surface; and graph D shows the troughs at the free surface. After a period tripling

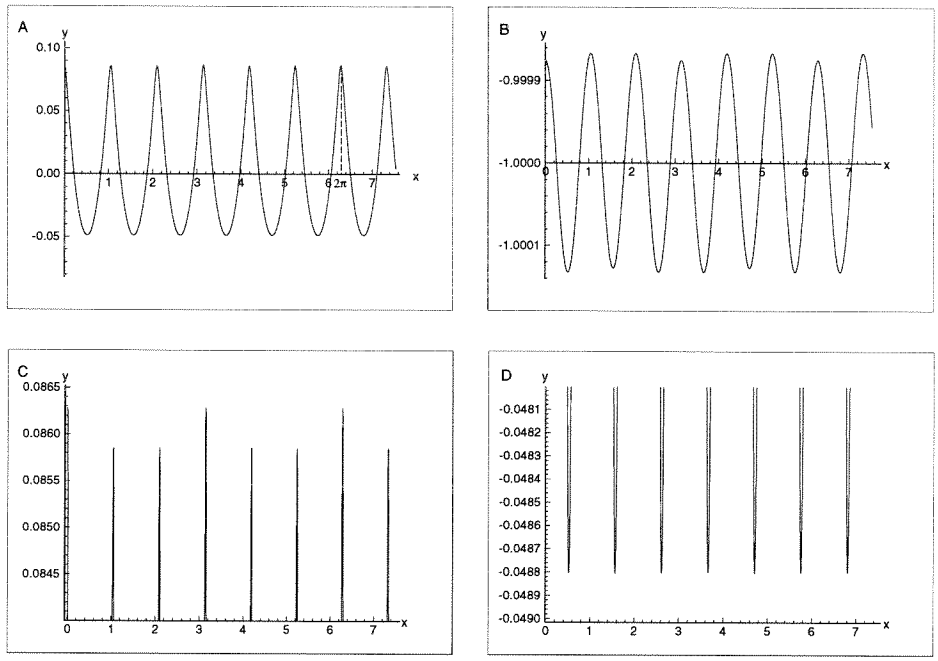

Figure 5.3: Symmetric irrotational branch P-3, $b = 0.88124$, $c = 0.44251$. Symmetry with respect to the three highest crests (in fig. C) and second and fifth troughs (counting from left to right in fig. D).

bifurcation, the wavelength becomes equal to π (see fig. 5.3). This branch is denoted by P-3. After another (period doubling) bifurcation, we switch to the branch which is denoted by P-6 (see fig. 5.4). Finally, we find a symmetry breaking bifurcation. The asymmetric branch is denoted by P-6a (fig. 5.5). An asymmetric profile far away from the bifurcation point is presented in fig. 5.6. The bifurcation diagram is presented in fig. 5.7. The locations of the bifurcation points agree very well with those found by Zufiria [23].

5.4.2 Asymmetric waves with shear

Let $\Delta = 0.5$ and consider two different symmetric waves with the wavenumbers $k = k_1 \equiv 2$ and $k = k_2 \equiv 15$, as an example. In this section we let $N = 251$, which corresponds to keeping approximately 60 Fourier coefficients for the original wave of wavelength $2\pi/k_1$ and 8 coefficients for the wave of wavelength $2\pi/k_2$.

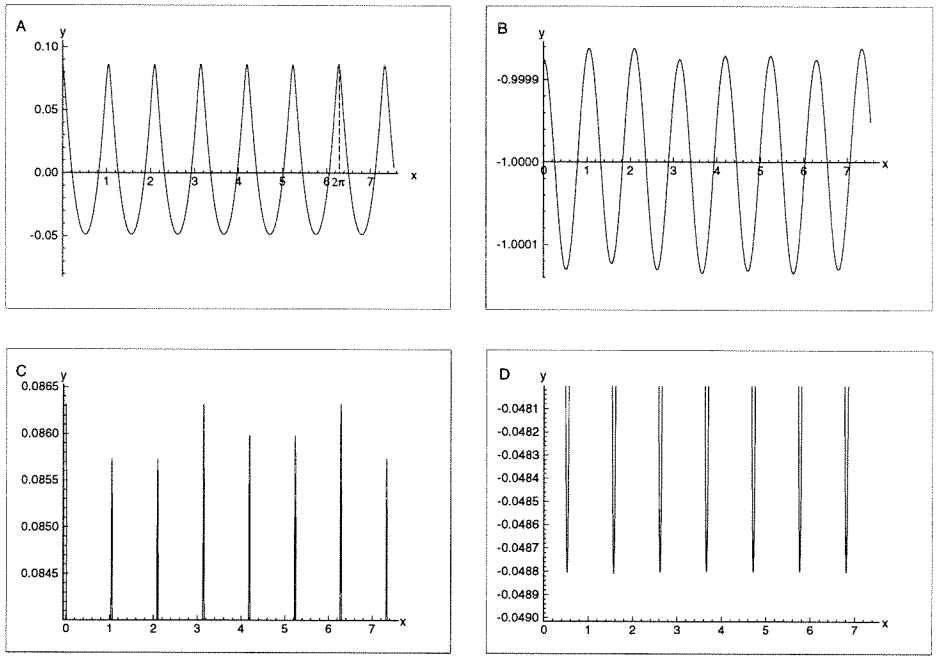

Figure 5.4: Symmetric irrotational branch P-6, $b = 0.88159$, $c = 0.44252$. Symmetry with respect to the fifth trough in fig. D.

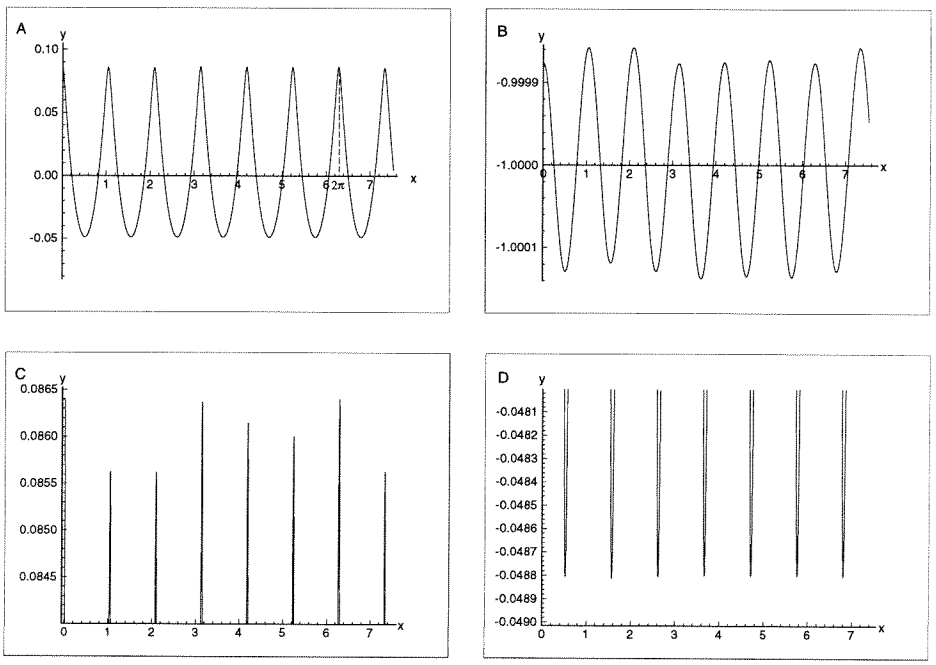

Figure 5.5: Asymmetric irrotational branch P-6a, $b = 0.88246$, $c = 0.44253$.

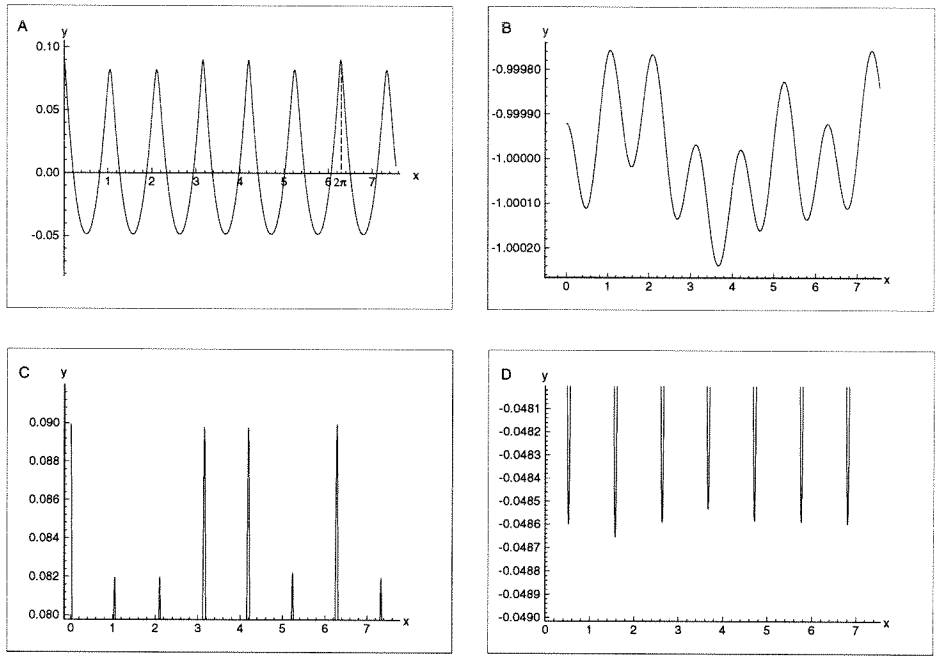

Figure 5.6: Asymmetric irrotational branch P-6a, $b = 0.91946$, $c = 0.44230$.

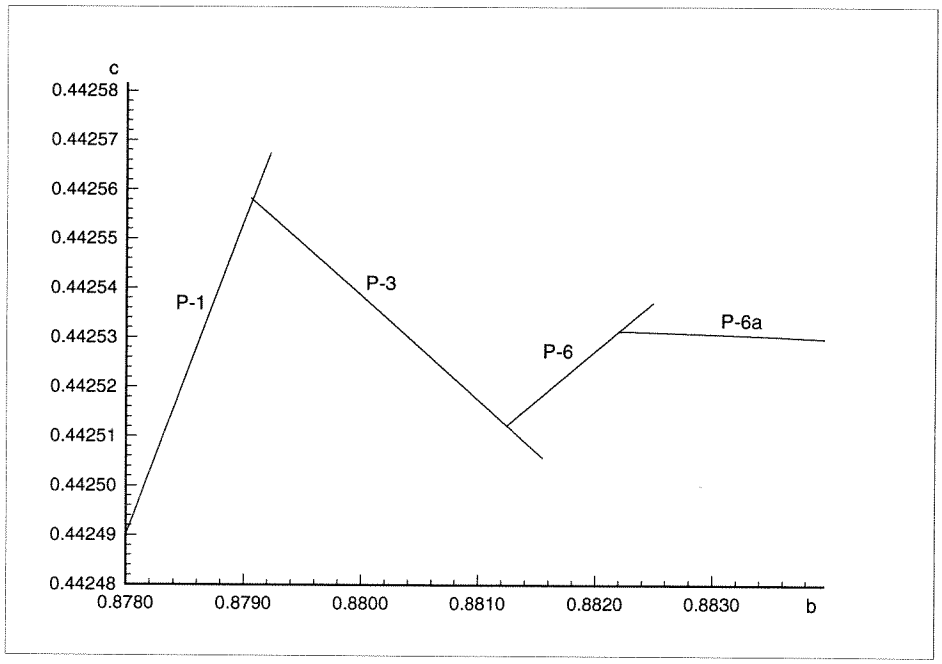

Figure 5.7: Bifurcation diagram. P-1, P-3, and P-6 are the symmetric irrotational branches. P-6a is the asymmetric irrotational branch.

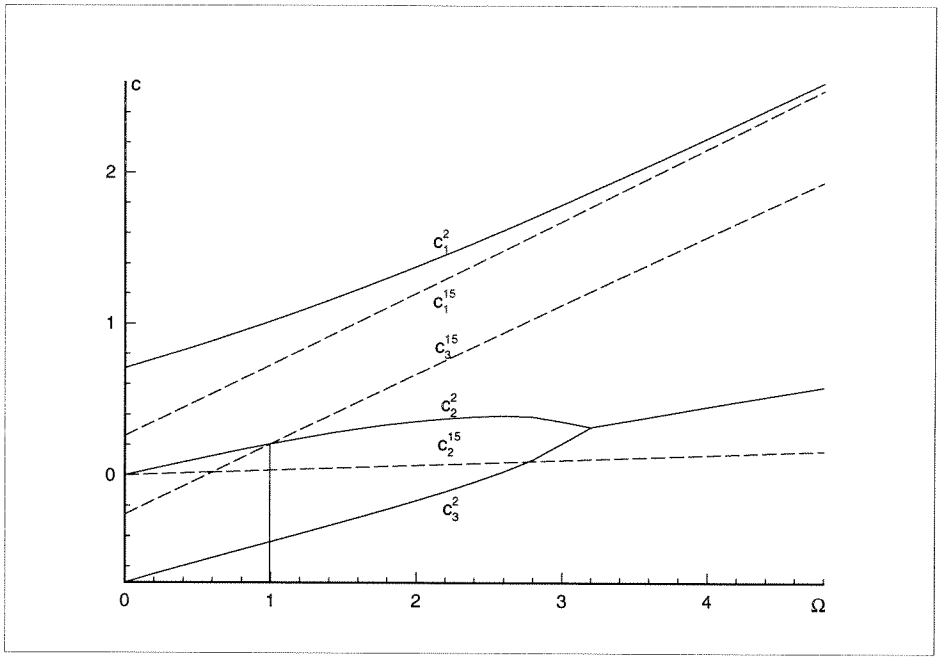

Figure 5.8: The wave speeds $c^2_{1,2,3}$ (solid lines) and $c^{15}_{1,2,3}$(dashed lines) as functions of Ω for infinitesimal waves (linear approximation).

Since the linear dispersion relation has the the form of a cubic equation, each pair (k, Ω) is associated with three possible wave speeds $c = c^k_j$, $k = 2, 15$, $j = 1, 2, 3$, namely c^k_1 (the co-flowing wave), c^k_3 (the counter-flowing wave), and c^k_2 (a wave which is propagating very slowly and is absent if $\Omega = 0$). The dependence of c^k_j on Ω in the linear approximation is plotted in fig. 5.8. We can see that the branches c^2_2 and c^{15}_3 intersect near $\Omega = 1$.

Moreover, c^2_2 increases with amplitude, while c^{15}_3 decreases, as illustrated in fig. 5.9 (solid lines). Therefore, if we start with $\Omega \geq 1$, these two branches intersect again for some $b > 0$. Let us check whether this behavior leads to any interesting bifurcation phenomena. We choose $\Omega = 1.0$.

Fig. 5.9 shows that there are, in fact, bifurcation points (B_1, B_2 and B_3) on both branches, where the Jacobian has two zero eigenvalues. Therefore, the Jacobian does not change its sign, which makes it very difficult to detect these bifurcation points. However, if the step size in the continuation process is small enough, a substantial

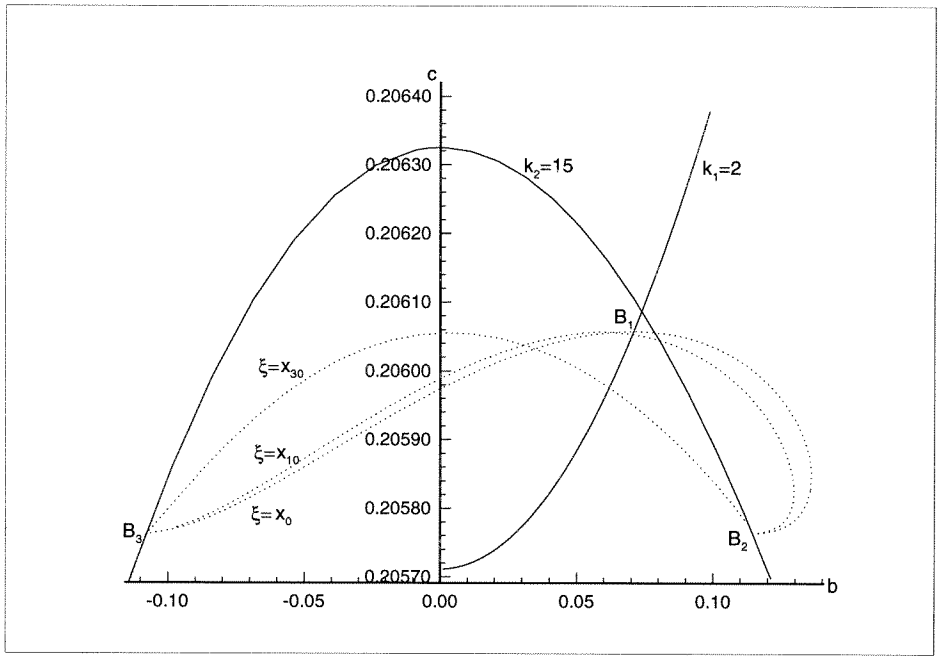

Figure 5.9: Bifurcation diagram for the waves in the presence of shear. Solid line, "main" branches; dotted line, bifurcated branches.

decrease in the magnitude of the Jacobian can be observed in the neighborhood of these points.

The bifurcated branches exhibit singular behavior, i.e., the Jacobian does not become nonsingular as we move away from the bifurcation points. This makes it virtually impossible to obtain any solutions along these branches. Such singular behavior is due to the fact that each point on the bifurcated branch is itself a bifurcation point. Therefore, the formulation of the problem has to be adjusted in order to allow further progress. A solution is provided by adding another auxiliary condition, namely

$$\frac{dy_2}{dx}(\xi) = 0. \tag{5.23}$$

This condition fixes the location of the lower interface crest (it is no longer required that this crest be exactly under the crest of the upper interface, so in general $\xi \neq 0$). We incorporate (5.23) in the same manner as (5.16) and (5.17) using another Lagrange multiplier $f_3(x)$. The Jacobian becomes nonsingular and we can follow the bifurcated

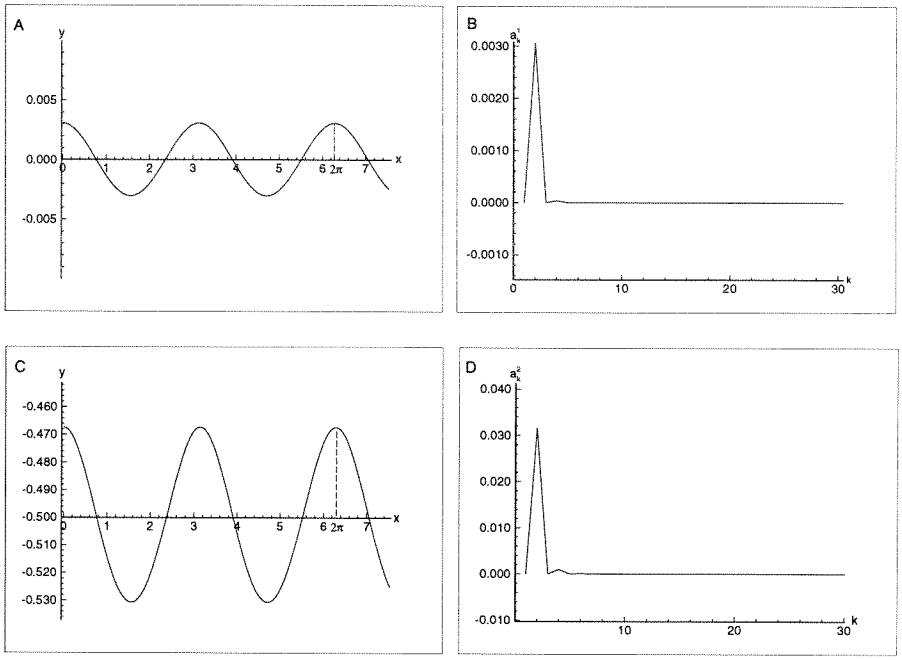

Figure 5.10: Main branch $k_1 = 2$, near the bifurcation point B_1, $b = 0.070911$. A: free surface; B: Fourier coefficients a_k^1 for the free surface; C: interface at $y = -\Delta$; D: Fourier coefficients a_k^2 for the interface.

branch using our usual methods. This technique can be also used to facilitate the pinpointing of the bifurcation points. For this purpose we set $\xi = 0$ while on the main branch. Then the bifurcation points are characterized by simple eigenvalues, so that the Jacobian changes sign, which in turn allows us to detect the bifurcation points very easily.

Let us start with the bifurcation point B_1. Near B_1 the main branch is just a wave of wavelength π, as shown in fig. 5.10 (graphs A and B represent the free surface and its Fourier coefficients, graphs C and D represent the interface at $y = -\Delta$ and its Fourier coefficients). Note that the amplitude of the lower interface is larger than the amplitude of the free surface. The bifurcated branch combines the modes close to $k_1 = 2$ and $k_2 = 15$, but as long as $\xi = 0$, symmetry is preserved. The profiles to the left and to the right of the bifurcation point B_1 are shown in figs. 5.11 and 5.12 respectively. As one can expect, the bifurcated branch eventually joins the solution branch corresponding to $k_2 = 15$. To the right, it first passes through a fold, and

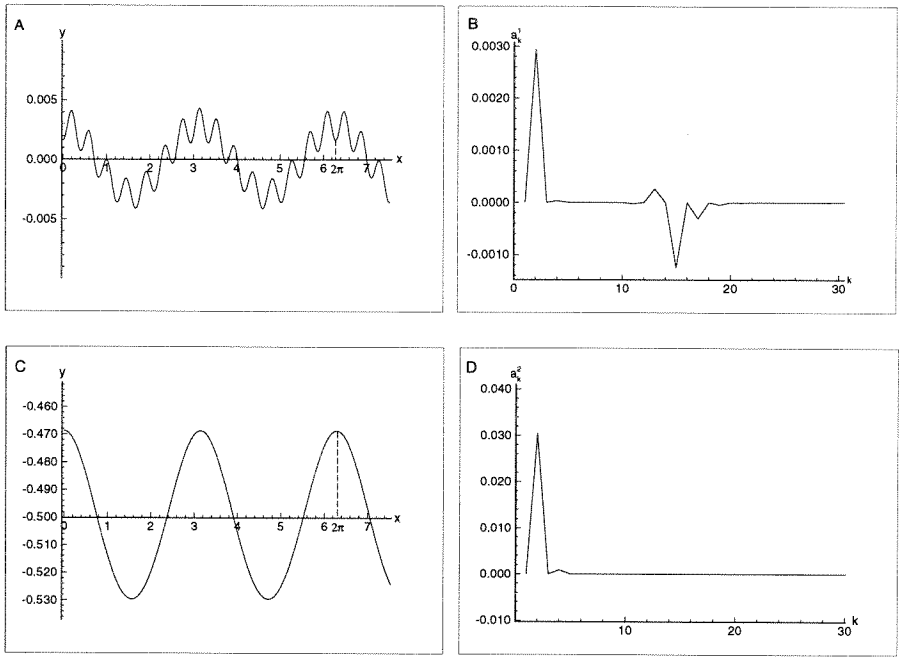

Figure 5.11: Symmetric bifurcated branch. $\xi = x_0 \equiv 0$, $b = 0.037021$.

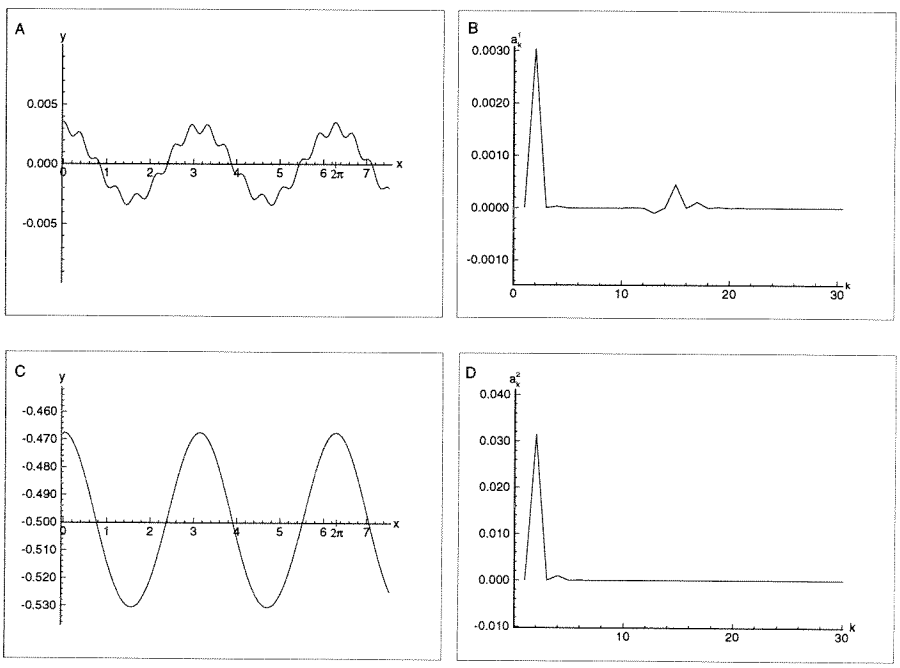

Figure 5.12: Symmetric bifurcated branch. $\xi = x_0 \equiv 0$, $b = 0.082021$.

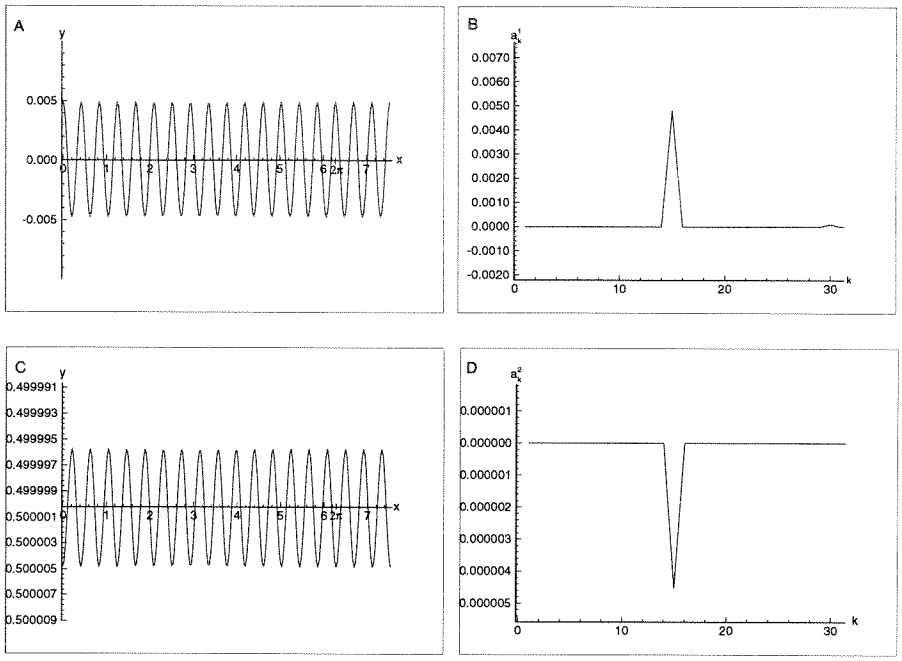

Figure 5.13: Main branch $k_2 = 15$ near the bifurcation point B_2, $b = 0.11450$.

then reaches B_2. To the left, it reaches B_3. Note that both branches corresponding to k_2 have a π/k_2 phase shift between the free surface and the lower interface and with respect to each other (compare figs. 5.13 and 5.14).

If we now set $\xi \neq 0$ on the bifurcated branch, we obtain non-symmetric wave profiles. Figs. 5.15, 5.16 and tables 5.1, 5.2 illustrate these profiles for two different values of ξ: $\xi = x_{10} \equiv 2\pi\frac{10}{N}$ and $\xi = x_{30} \equiv 2\pi\frac{30}{N}$. The asymmetry manifests itself in higher modes, associated with k_2, i.e., the underlying wave of wavelength π remains symmetric, but the ripples (of wavelength $2\pi/15$) introduce asymmetry. For example, we can see from table 5.1 that relationship (5.22) indicates asymmetry for $n \geq 7$ (only the modes for which $a_n^1 > 10^{-8}$ were taken into account).

This type of bifurcations is not limited to $k_1 = 2$, $k_2 = 15$, $\Omega = 1$, and $\Delta = 0.5$, and occurs in many other cases as well. However, unless the separation between k_1 and k_2 is large enough, no asymmetric waves are present.

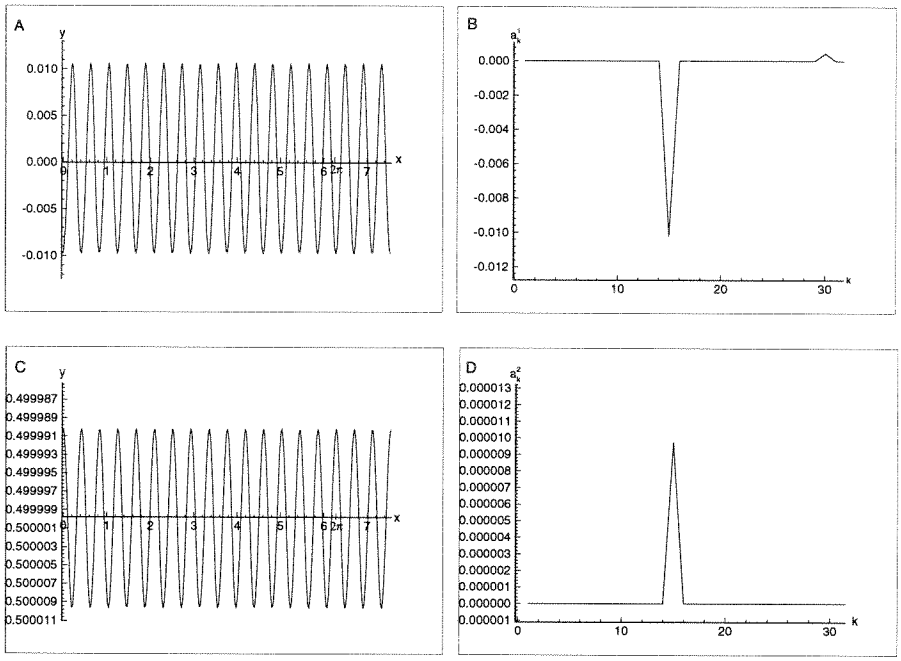

Figure 5.14: Main branch $k_2 = 15$ near the bifurcation point B_3, $b = -0.21798$.

k	b_k^1/a_k^1	b_k^2/a_k^2	$\tan(k\delta_+)$	$\tan(k\delta_-)$
2	0.54746	0.54746	0.54746	0.54746
4	1.56355	1.56355	1.56355	1.56355
6	14.65888	14.65888	14.65888	14.65888
7	1.00107	1.00107	-5.42350	0.18438
9	3.42634	3.42634	-1.22848	0.81402
11	-4.53733	-4.53733	-0.40717	2.45597
13	-1.14519	-1.14519	0.11472	-8.71675
15	-0.36739	-0.36739	0.70656	-1.41530
17	0.14992	0.14992	2.04511	-0.48897
19	0.75974	0.75974	-21.67202	0.04614
21	2.23811	2.23811	-1.64206	0.60899
23	-12.36454	-12.36454	-0.57642	1.73486
24	1.35424	1.35223	-0.27940	-0.27940
25	-1.52103	-1.52103	-0.02201	45.44144
26	7.35378	7.35432	0.23250	0.23250
28	-2.61117	-2.61118	0.89373	0.89373
30	-0.84943	-0.84943	2.82191	2.82191

Table 5.1: Fourier coefficients for an asymmetric profile with $\xi = x_{10}$. Test (5.22) indicates asymmetry for $n \geq 7$. $\xi = x_{10}$, $b = 0.092021$.

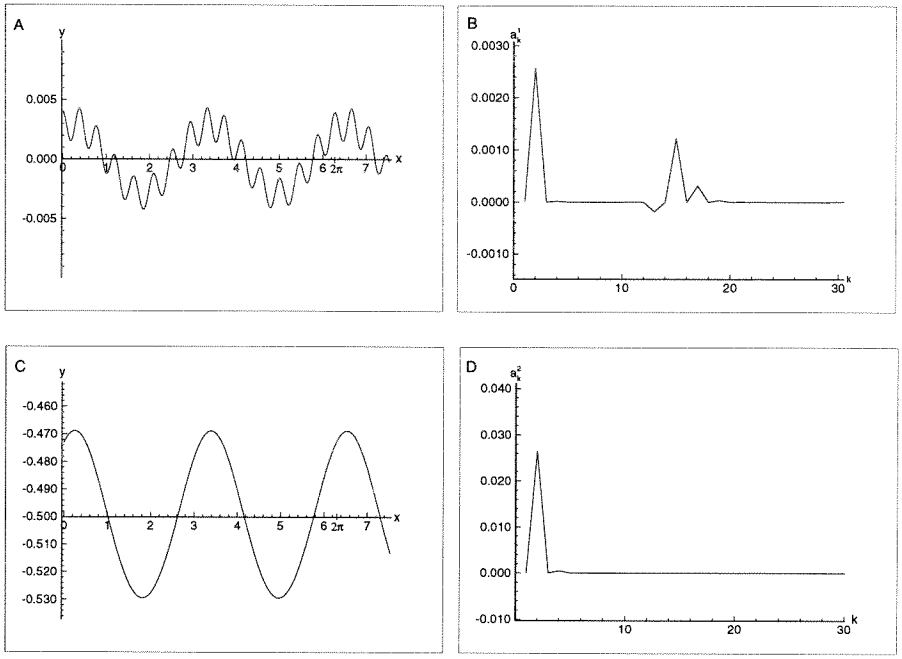

Figure 5.15: Asymmetric bifurcated branch. $\xi = x_{10}$, $b = 0.092021$.

k	b_k^1/a_k^1	b_k^2/a_k^2	$\tan(k\delta_+)$	$\tan(k\delta_-)$
2	14.73065	14.73065	14.73065	14.73065
4	-0.13640	-0.13640	-0.13640	-0.13640
6	4.84978	4.84978	4.84978	4.84978
9	6.74821	6.74821	0.52109	-1.91904
11	-0.21827	-0.21827	-2.28454	0.43772
13	3.44283	3.44283	0.35917	-2.78423
15	-0.36555	-0.36555	-3.51682	0.28435
17	2.24988	2.24988	0.21236	-4.70893
19	-0.52829	-0.52829	-7.02130	0.14242
21	1.61719	1.61719	0.07382	-13.54568
23	-0.71631	-0.71631	-169.23364	0.00591
24	1.84107	1.84107	-1.05759	-1.05759
26	-0.63444	-0.63444	0.82472	0.82472
28	1.36251	1.36251	-1.39526	-1.39526
30	-0.84387	-0.84387	0.61872	0.61872

Table 5.2: Fourier coefficients for an asymmetric profile with $\xi = x_{30}$. Test (5.22) indicates asymmetry for $n \geq 9$. $\xi = x_{30}$, $b = 0.092021$.

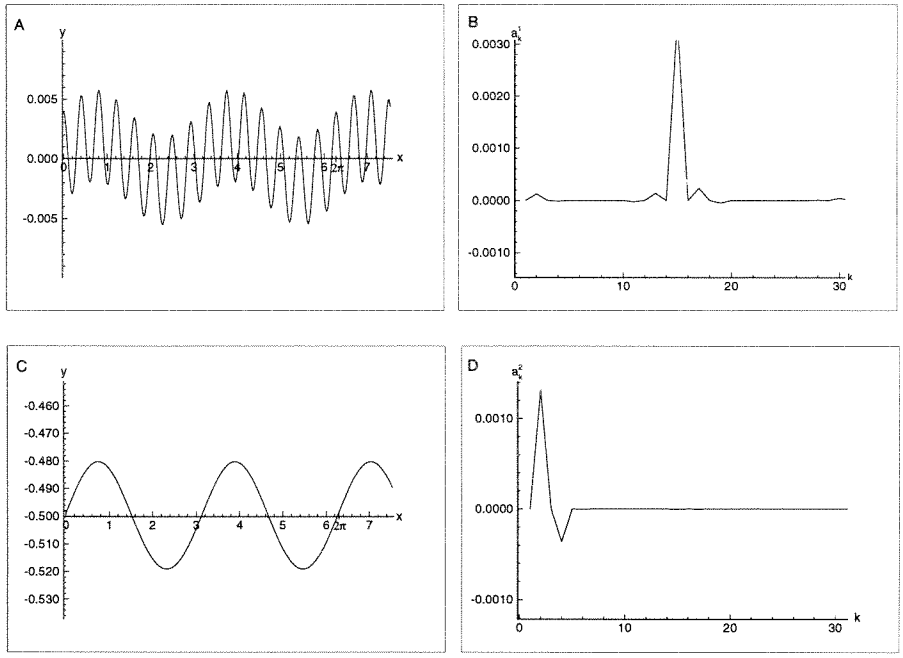

Figure 5.16: Asymmetric bifurcated branch. $\xi = x_{30}$, $b = 0.092021$.

5.5 Computational aspects

Although the numerical method being used is very efficient, the large number of Fourier coefficients, which is required to reproduce all the bifurcation phenomena at high amplitudes, leads to a large size of the Jacobian used in Newton's method. For example, $N = 551$ produces a Jacobian of order 2200×2200, i.e., approximately 35 Mb of memory is needed to store one copy. Moreover, computation of most elements of the Jacobian involves evaluation of an integral, and therefore takes a long time. However, all elements of the Jacobian can be computed completely independently of each other. Therefore, parallelization seems to be an attractive option. One can follow several different strategies, but the cheapest solution is provided by the use of PVM ([10]), since it allows the use of a local workstation network as a virtual parallel machine. Besides the opportunity to execute different parts of the code concurrently, PVM also allows us to use remote computers to store additional copies of the Jacobian and other data, if required by the algorithms being used.

We split the Jacobian into several blocks and compute them concurrently on different computers. The size and the number of the blocks have to be chosen so that the blocks are small enough to be computed on a standard workstation and provide uniform load of the participating computers, and at the same time big enough to make the overhead involved in setting up the parallel machine negligible. In other words, we have to make sure that the program is scalable. This task is complicated by the fact that the computers available on a local network are typically very different with regard to their memory and speed, and the number of computers can change. Therefore, the "master-and-slave" approach is used, so that the main routine can monitor the load on various machines across the network and assign appropriate number of tasks to each of them.

The result is then sent back to the main routine, which performs the LU decomposition of the Jacobian. It is possible to perform LU decomposition concurrently, using ScaLAPACK. As described in [7], the ScaLAPACK (or Scalable LAPACK) library includes a subset of LAPACK routines redesigned for distributed memory MIMD parallel computers. It is currently written in a Single-Program-Multiple-Data style using explicit message passing for interprocessor communication. It assumes matrices are laid out in a two-dimensional block cyclic decomposition. The ScaLAPACK routines are based on block-partitioned algorithms in order to minimize the frequency of data movement between different levels of the memory hierarchy (the memory hierarchy includes the off-processor memory of other processors, in addition to the hierarchy of registers, cache, and local memory on each processor).

In our computations, however, the above approach to performing LU factorization provided very little advantage over the conventional method. This was due to a considerable overhead, both in terms of storage and speed, caused by the exchange of data between the processes. Moreover, the number of computers necessary for an efficient implementation of the block cyclic decomposition was at least nine, which proved to be hard to achieve.

5.6 Final remarks

We have shown the existence of a new type of steady finite-amplitude non-symmetric gravity waves with shear in the water. These waves appear as a result of a "merger" between two waves with different wavenumbers, and a phase shift between them. One of the questions that remains to be answered is why such a shift becomes possible. It would be also interesting to explore the phenomena for a range of wavenumbers, as well as different Ω and Δ.

Another challenging task is to reproduce the results for a smooth velocity profile, when the "middle" branch c_2^k is not present. Recall that it was the collision of the two solution branches, c_2^2 and c_3^{15}, that resulted in non-symmetric profiles.

Appendix A Equations arising in the derivation of the NLS

Denote $\omega_d \equiv \omega + \Omega\Delta k$, $c_{gd} \equiv c_g + \Omega\Delta$.

- Boundary condition (3.7)
  - $E^1\epsilon^1$:
$$k(A_1^T - A_2^T) + i\omega_d h_{1,1}^T = 0;$$
  - $E^1\epsilon^2$:
$$-k(C_1^T - C_2^T) - i\omega_d h_{1,2}^T + i\frac{\partial(A_1^T - A_2^T)}{\partial\xi} - c_{gd}\frac{\partial h_{1,1}^T}{\partial\xi} = 0;$$
  - $E^2\epsilon^2$:
$$-2k(B_1^T - B_2^T) - 2k^2(A_1^T + A_2^T)h_{1,1}^T - ik\Omega(h_{1,1}^T)^2 - 2i\omega_d h_{2,2}^T = 0;$$
  - $E^1\epsilon^3$:
$$\begin{aligned} -2k^2(B_1^T + B_2^T)\bar{h}_{1,1} - k(D_1^T - D_2^T) - k^3(A_1^T - A_2^T)|h_{1,1}^T|^2 \\ +\frac{1}{2}k^3(\bar{A}_1 - \bar{A}_2)(h_{1,1})^2 - i\omega_d h_{1,3} + k^2(\bar{A}_1^T + \bar{A}_2^T)h_{2,2}^T \\ +\frac{\partial h_{1,1}^T}{\partial\tau} + i\frac{\partial(C_1^T - C_2)^T}{\partial\xi} - c_{gd}\frac{\partial h_{1,2}}{\partial\xi} - ik\Omega\bar{h}_{1,1}^T h_{2,2}^T &= 0. \end{aligned}$$
- Boundary condition (3.8)
  - $E^1\epsilon^1$:
$$-ikA_1^B + e^{k\Delta}\omega h_{1,1}^B = 0;$$

- $E^1\epsilon^2$:

$$ikC_1^B - e^{k\Delta}\omega h_{1,2}^B + \frac{\partial A_1^B}{\partial \xi} - k\Delta\frac{\partial A_1}{\partial \xi} + ic_g e^{k\Delta}\frac{\partial h_{1,1}^B}{\partial \xi} = 0;$$

- $E^2\epsilon^2$:

$$-ikB_1^B - ie^{k\Delta}k^2 A_1^B h_{1,1}^B + e^{2k\Delta}\omega h_{2,2}^B = 0;$$

- $E^1\epsilon^3$:

$$\begin{aligned} -2k^2 B_1^B \bar{h}_{1,1}^B - e^{k\Delta}kD_1^B - e^{\Delta k}k^3 A_1^B \left|h_{1,1}^B\right|^2 + \frac{1}{2}e^{\Delta k}k^3 \bar{A}_1^B (h_{1,1}^B)^2 - \\ ie^{2\Delta k}\omega h_{1,3}^B + e^{\Delta k}k^2 \bar{A}_1^B h_{2,2}^B + e^{2\Delta k}\frac{\partial h_{1,1}^B}{\partial \tau} + ie^{\Delta k}\frac{\partial C_1^B}{\partial \xi} \\ -i\Delta e^{\Delta k}k\frac{\partial C_1^B}{\partial \xi} - c_g e^{2\Delta k}\frac{\partial h_{1,2}^B}{\partial \xi} &= 0. \end{aligned}$$

- Boundary condition (3.9)

- $E^1\epsilon^1$:

$$-i\omega_d(A_1^T + A_2^T) + i\Omega(A_1^T - A_2^T) + gh_{1,1}^T = 0;$$

- $E^1\epsilon^2$:

$$-i\omega_d(C_1^T + C_2^T) + i\Omega(C_1^T - C_2^T) + gh_{1,2}^T - c_{gd}\frac{\partial(A_1^T + A_2^T)}{\partial \xi} = 0;$$

- $E^2\epsilon^2$:

$$\begin{aligned} -2k^2 A_1^T A_2^T - 2i\omega_d(B_1^T + B_2^T) + i\Omega(B_1^T - B_2^T) \\ -ik\omega_d(A_1^T - A_2^T)h_{1,1}^T + gh_{2,2}^T &= 0; \end{aligned}$$

- $E^1\epsilon^3$:

$$4k^2(B_1^T \bar{A}_1^T + B_2\bar{A}_2^T) - 4ik\omega_d(B_1^T - B_2^T)\bar{h}_{1,1}^T - i\omega_d(D_1^T + D_2^T)$$

$$
\begin{aligned}
+i\Omega(D_1^T - D_2^T) + 4k^3(|A_1^T|^2 - |A_2^T|^2)h_{1,1}^T - ik^2\omega_d(A_1^T + A_2^T)|h_{1,1}^T|^2 \\
-ik^2\Omega(A_1^T - A_2^T)|h_{1,1}^T|^2 + \frac{1}{2}ik^2\omega_d(\bar{A}_1^T + \bar{A}_2^T)(h_{1,1}^T)^2 \\
+\frac{1}{2}ik^2\Omega(\bar{A}_1^T - \bar{A}_2^T)(h_{1,1}^T)^2 + gh_{1,3}^T \\
+ik\omega_d(\bar{A}_1^T + \bar{A}_2^T)h_{2,2}^T + \frac{\partial(A_1^T + A_2^T)}{\partial\tau} - c_{gd}\frac{\partial(C_1^T + C_2^T)}{\partial\xi} &= 0.
\end{aligned}
$$

- Boundary condition (3.12)

  - $E^1\epsilon^1$:

$$\omega A_1^T - \Omega A_1^T + e^{2k\Delta}A_2^T(\omega + \Omega) - \omega A_1^B = 0;$$

  - $E^1\epsilon^2$:

$$
\begin{aligned}
i(-\omega + \Omega)C_1^T - ie^{2k\Delta}(\omega + \Omega)C_2^T - c_g\frac{\partial A_1^T}{\partial\xi} + \Delta\omega\frac{\partial A_1^T}{\partial\xi} \\
-\Omega\Delta\frac{\partial A_1^T}{\partial\xi} - c_g e^{2k\Delta}\frac{\partial A_2^T}{\partial\xi} - \Delta e^{2k\Delta}\omega\frac{\partial A_2^T}{\partial\xi} \\
-\Omega\Delta e^{2k\Delta}\frac{\partial A_2^T}{\partial\xi} + i\omega C_1^B + c_g\frac{\partial A_1^B}{\partial\xi} - \Delta\omega\frac{\partial A_1^B}{\partial\xi} &= 0;
\end{aligned}
$$

  - $E^2\epsilon^2$:

$$
\begin{aligned}
2ie^{2k\Delta}k^2A_1^TA_2^T - 2\omega B_1^T + \Omega B_1^T - 2e^{4k\Delta}\omega B_2^T - e^{4k\Delta}\Omega B_2^T \\
-e^{k\Delta}k\omega A_1^T h_{1,1} + e^{3k\Delta}k\omega A_2^T h_{1,1} + +2\omega B_1^B + e^{k\Delta}k\omega A_1^B h_{1,1}^B &= 0;
\end{aligned}
$$

  - $E^1\epsilon^3$:

$$
\begin{aligned}
4k^2B_1^T\bar{A}_1^T + 4e^{6k\Delta}k^2B_2^T\bar{A}_2^T - 4ie^{k\Delta}k\omega(B_1^T - B_2^Te^{4k\Delta})\bar{h}_{1,1}^B \\
-4k^2B_1^B\bar{A}_1^B - ie^{2k\Delta}\omega(D_1^T + e^{2k\Delta}D_2^T) + ie^{2k\Delta}\Omega(D_1^T - e^{2k\Delta}D_2^T) \\
+4e^{k\Delta}k^3(\left|A_1^T\right|^2 - e^{4k\Delta}\left|A_2^T\right|^2)h_{1,1}^B - ie^{2k\Delta}k^2\omega(A_1^T + e^{2k\Delta}A_2^T)\left|h_{1,1}^B\right|^2 \\
-ie^{2k\Delta}k^2\Omega(A_1^T - e^{2k\Delta}A_2^T)\left|h_{1,1}^B\right|^2 + \frac{1}{2}ie^{2k\Delta}k^2\Omega(\bar{A}_1^T - e^{2k\Delta}\bar{A}_2^T)(h_{1,1}^B)^2 \\
+\frac{1}{2}ie^{2k\Delta}k^2\omega(\bar{A}_1^T + e^{2k\Delta}\bar{A}_2^T)(h_{1,1}^B)^2 + ie^{2k\Delta}k\omega(\bar{A}_1^Th_{2,2}^B - e^{2k\Delta}\bar{A}_2^T)h_{2,2}^B
\end{aligned}
$$

$$
\begin{aligned}
&+e^{2k\Delta}\frac{\partial(A_1^T+e^{2k\Delta}A_2^T)}{\partial\tau}-c_ge^{2k\Delta}\frac{\partial C_1^T}{\partial\xi}-\Delta e^{2k\Delta}\Omega\frac{\partial C_1^T}{\partial\xi}\\
&-c_ge^{4k\Delta}\frac{\partial C_2^T}{\partial\xi}-\Delta e^{4k\Delta}\omega\frac{\partial C_2^T}{\partial\xi}-\Delta e^{4k\Delta}\Omega\frac{\partial C_2^T}{\partial\xi}-ic_g\Delta e^{2k\Delta}\frac{\partial^2A_1^T}{\partial\xi^2}\\
&+\frac{1}{2}i\Delta^2e^{2k\Delta}\omega\frac{\partial^2A_1^T}{\partial\xi^2}-\frac{1}{2}i\Delta^2e^{2k\Delta}\Omega\frac{\partial^2A_1^T}{\partial\xi^2}+ic_g\Delta e^{4k\Delta}\frac{\partial^2A_2^T}{\partial\xi^2}\\
&+\frac{1}{2}i\Delta^2e^{4k\Delta}\omega\frac{\partial^2A_2^T}{\partial\xi^2}+\frac{1}{2}i\Delta^2e^{4k\Delta}\Omega\frac{\partial^2A_2^T}{\partial\xi^2}+4ie^{k\Delta}k\omega B_1^B\bar{h}_{1,1}^B\\
&+ie^{2k\Delta}\omega D_1^B-4e^{k\Delta}k^3A_1^B\bar{A}_1^Bh_{1,1}^B+ie^{2k\Delta}k^2\omega A_1^B\bar{h}_{1,1}^Bh_{1,1}^B\\
&-\frac{1}{2}ie^{2k\Delta}k^2\omega\bar{A}_1^B(h_{1,1}^B)^2-ie^{2k\Delta}k\omega\bar{A}_1^Bh_{2,2}^B-e^{2k\Delta}\frac{\partial A_1^B}{\partial\tau}+c_ge^{2k\Delta}\frac{\partial C_1^B}{\partial\xi}\\
&+\Delta e^{2k\Delta}\omega\frac{\partial C_1^T}{\partial\xi}-\Delta e^{2k\Delta}\omega\frac{\partial C_1^B}{\partial\xi}+ic_g\Delta e^{2k\Delta}\frac{\partial^2A_1^B}{\partial\xi^2}\\
&-\frac{1}{2}i\Delta^2e^{2k\Delta}\omega\frac{\partial^2A_1^B}{\partial\xi^2} &= 0.
\end{aligned}
$$

- Boundary condition (3.13)

  - $E^1\epsilon^1$:

$$-A_1^T+e^{2k\Delta}A_2^T+A_1^B=0;$$

  - $E^1\epsilon^2$:

$$
\begin{aligned}
&-kC_1^T+e^{2k\Delta}kC_2^T+i\frac{\partial A_1^T}{\partial\xi}-i\Delta k\frac{\partial A_1^T}{\partial\xi}-ie^{2k\Delta}\frac{\partial A_2^T}{\partial\xi}\\
&-i\Delta e^{2k\Delta}k\frac{\partial A_2^T}{\partial\xi}+kC_1^B-i\frac{\partial A_1^B}{\partial\xi}+i\Delta k\frac{\partial A_1^B}{\partial\xi} &= 0;
\end{aligned}
$$

  - $E^2\epsilon^2$:

$$
\begin{aligned}
&-2B_1^T+2e^{4k\Delta}B_2^T-2e^{k\Delta}kA_1^Th_{1,1}^B-2E^{3k\Delta}A_2^Th_{1,1}^B-ie^{2k\Delta}\Omega h_{1,1}^2\\
&+2B_1^B+2e^{k\Delta}kA_1^Bh_{1,1}^B &= 0;
\end{aligned}
$$

  - $E^1\epsilon^3$:

$$-4k^2B_1^T\bar{h}_{1,1}^B-4e^{4k\Delta}k^2B_2^T\bar{h}_{1,1}^B-2e^{k\Delta}kD_1^T+2e^{3k\Delta}kD_2^T$$

$$
\begin{aligned}
&-2e^{k\Delta}k^3A_1^T\left|h_{1,1}^B\right|^2+2e^{3k\Delta}k^3A_2^T\bar{h}_{1,1}^Bh_{1,1}^B\\
&+e^{k\Delta}k^3\bar{A}_1^T(h_{1,1}^B)^2-e^{3k\Delta}k^3\bar{A}_2^T(h_{1,1}^B)^2+2e^{k\Delta}k^2\bar{A}_1^Th_{2,2}^B\\
&+2e^{3k\Delta}k^2\bar{A}_2^Th_{2,2}^B-2ie^{2k\Delta}k\Omega\bar{h}_{1,1}^Bh_{2,2}^B+2ie^{k\Delta}\frac{\partial C_1^T}{\partial\xi}-2i\Delta e^{k\Delta}k\frac{\partial C_1^T}{\partial\xi}\\
&-2ie^{3k\Delta}\frac{\partial C_2^T}{\partial\xi}-2i\Delta e^{3k\Delta}k\frac{\partial C_2^T}{\partial\xi}-2\Delta e^{k\Delta}\frac{\partial^2A_1^T}{\partial\xi^2}+\Delta^2e^{k\Delta}k\frac{\partial^2A_1^T}{\partial\xi^2}\\
&-2\Delta e^{3k\Delta}\frac{\partial^2A_2^T}{\partial\xi^2}-\Delta^2e^{3k\Delta}k\frac{\partial^2A_2^T}{\partial\xi^2}+4k^2B_1^B\bar{h}_{1,1}^B+2e^{k\Delta}kD_1^B\\
&+2e^{k\Delta}k^3A_1^B\left|h_{1,1}^B\right|^2-e^{k\Delta}k^3\bar{A}_1^B(h_{1,1}^B)^2-2e^{k\Delta}k^2\bar{A}_1^Bh_{2,2}^B-2ie^{k\Delta}\frac{\partial C_1^B}{\partial\xi}\\
&+2i\Delta e^{k\Delta}k\frac{\partial C_1^B}{\partial\xi}+2\Delta e^{k\Delta}\frac{\partial^2A_1^B}{\partial\xi^2}-\Delta^2e^{k\Delta}k\frac{\partial^2A_1^B}{\partial\xi^2} \quad = \quad 0.
\end{aligned}
$$

Appendix B Integral equations describing the three-wave interactions

Applying Fourier transfrom to the boundary conditions (4.8)-(4.12), we obtain:

$$\begin{aligned}
&\frac{\partial \widehat{h^T}}{\partial t}(\kappa,t) - |\kappa|\frac{\widehat{\phi^T}(\kappa,t)\cosh(|\kappa|\Delta) - \widehat{\phi^I}(\kappa,t)}{\sinh(|\kappa|\Delta)} - i\Omega\Delta\kappa\widehat{h^T}(\kappa,t) \\
&\qquad + \frac{1}{\sqrt{2\pi}}\int_{-\infty}^{\infty}\int_{-\infty}^{\infty}\left(\frac{|\kappa\kappa_1|}{\sinh(|\kappa|\Delta)\sinh(|\kappa_1|\Delta)}\right. \\
&\qquad \times\left[\cosh(|\kappa|\Delta)\left(\widehat{\phi^T}(\kappa_1,t)\cosh(|\kappa_1|\Delta) - \widehat{\phi^I}(\kappa_1,t)\right)\widehat{h^T}(\kappa_2,t)\right. \\
&\left.\left. - \left(\widehat{\phi^T}(\kappa_1,t) - \widehat{\phi^I}(\kappa_1,t)\cosh(|\kappa_1|\Delta)\right)\widehat{h^B}(\kappa_2,t)\right] - \kappa\kappa_1\widehat{\phi^T}(\kappa_1,t)\widehat{h^T}(\kappa_2,t)\right. \\
&\left.\qquad -i\Omega\kappa_1\widehat{h^T}(\kappa_1,t)\widehat{h^T}(\kappa_2,t)\right)\delta_{123}d_{12} \;=\; 0,
\end{aligned} \tag{B.1}$$

$$\begin{aligned}
&\frac{\partial \widehat{h^B}}{\partial t}(\kappa,t) - |\kappa|\frac{\widehat{\phi^T}(\kappa,t) - \widehat{\phi^I}(\kappa,t)\cosh(|\kappa|\Delta)}{\sinh(|\kappa|\Delta)} \\
&\qquad + \frac{1}{\sqrt{2\pi}}\int_{-\infty}^{\infty}\int_{-\infty}^{\infty}\left(\frac{|\kappa\kappa_1|}{\sinh(|\kappa|\Delta)\sinh(|\kappa_1|\Delta)}\right. \\
&\qquad \times\left[\left(\widehat{\phi^T}(\kappa_1,t)\cosh(|\kappa_1|\Delta) - \widehat{\phi^I}(\kappa_1,t)\right)\widehat{h^T}(\kappa_2,t)\right. \\
&\left.\left. - \cosh(|\kappa|\Delta)\left(\widehat{\phi^T}(\kappa_1,t) - \widehat{\phi^I}(\kappa_1,t)\cosh(|\kappa_1|\Delta)\right)\widehat{h^B}(\kappa_2,t)\right]\right. \\
&\left.\qquad -\kappa\kappa_1\widehat{\phi^I}(\kappa_1)\widehat{h^B}(\kappa_2) - i\Omega\kappa_1\widehat{h^B}(\kappa_1)\widehat{h^B}(\kappa_2)\right)\delta_{123}d_{12} \;=\; 0,
\end{aligned} \tag{B.2}$$

$$\begin{aligned}
&\frac{\partial \widehat{\phi^T}}{\partial t}(\kappa,t) - i\Omega\Delta\kappa\widehat{\phi^T}(\kappa,t) + i\Omega\frac{|\kappa|}{\kappa}\frac{\widehat{\phi^T}(\kappa,t)\cosh(|\kappa|\Delta) - \widehat{\phi^I}(\kappa,t)}{\sinh(|\kappa|\Delta)} + g\widehat{h^T}(\kappa,t) \\
&\qquad -\frac{1}{\sqrt{2\pi}}\int_{-\infty}^{\infty}\int_{-\infty}^{\infty}\left(\frac{1}{2}\kappa_1\kappa_2\widehat{\phi^T}(\kappa_1,t)\widehat{\phi^T}(\kappa_2,t)\right. \\
&\left.+\frac{1}{2}|\kappa_1\kappa_2|\frac{\widehat{\phi^T}(\kappa_1,t)\cosh(|\kappa_1|\Delta) - \widehat{\phi^I}(\kappa_1,t)}{\sinh(|\kappa_1|\Delta)}\frac{\widehat{\phi^T}(\kappa_2,t)\cosh\kappa_2\Delta - \widehat{\phi^I}(\kappa_2,t)}{\sinh\kappa_2\Delta}\right.
\end{aligned}$$

$$-i\Omega\frac{|\kappa\kappa_1|}{\kappa\sinh(|\kappa|\Delta)\sinh(|\kappa_1|\Delta)}\Big[\cosh(|\kappa|\Delta)\left(\widehat{\mathring{\phi}^T}(\kappa_1,t)\cosh(|\kappa_1|\Delta)-\widehat{\mathring{\phi}^I}(\kappa_1,t)\right)$$
$$\times\widehat{h^T}(\kappa_2,t)-\left(\widehat{\mathring{\phi}^T}(\kappa_1,t)-\widehat{\mathring{\phi}^I}(\kappa_1,t)\cosh(|\kappa_1|\Delta)\right)\widehat{h^B}(\kappa_2,t)\Big]\Big)\,\delta_{123}d_{12} = 0, \tag{B.3}$$

$$i\kappa(\widehat{\mathring{\phi}^I}-\widehat{\mathring{\phi}^B})-\Omega\widehat{h^B}(\kappa,t)$$
$$-i\frac{1}{\sqrt{2\pi}}\int_{-\infty}^{\infty}\int_{-\infty}^{\infty}|\kappa_1|\kappa_2\left(\frac{\widehat{\mathring{\phi}^T}(\kappa_1,t)-\widehat{\mathring{\phi}^I}(\kappa_1,t)\cosh(|\kappa_1|\Delta)}{\sinh(|\kappa_1|\Delta)}-\widehat{\mathring{\phi}^B}(\kappa_1,t)\right)$$
$$\times\widehat{h^B}(\kappa_2,t)\delta_{123}d_{12} = 0, \tag{B.4}$$

$$|\kappa|\left(\frac{\widehat{\mathring{\phi}^T}(\kappa,t)-\widehat{\mathring{\phi}^I}(\kappa,t)\cosh(|\kappa|\Delta)}{\sinh(|\kappa|\Delta)}-\widehat{\mathring{\phi}^B}(\kappa,t)\right)$$
$$-\frac{1}{\sqrt{2\pi}}\int_{-\infty}^{\infty}\int_{-\infty}^{\infty}\left(\frac{|\kappa\kappa_1|}{\sinh(|\kappa|\Delta)\sinh(|\kappa_1|\Delta)}\Big[\left(\widehat{\mathring{\phi}^T}(\kappa_1,t)\cosh(|\kappa_1|\Delta)-\widehat{\mathring{\phi}^I}(\kappa_1,t)\right)\right.$$
$$\times\widehat{h^T}(\kappa_2,t)-\cosh(|\kappa|\Delta)\left(\widehat{\mathring{\phi}^T}(\kappa_1,t)-\widehat{\mathring{\phi}^I}(\kappa_1,t)\cosh(|\kappa_1|\Delta)\right)\widehat{h^B}(\kappa_2,t)\Big]$$
$$\left.-|\kappa\kappa_1|\widehat{\mathring{\phi}^B}(\kappa_1,t)\widehat{h^B}(\kappa_2,t)-\kappa_1^2(\widehat{\mathring{\phi}^I}(\kappa_1,t)-\widehat{\mathring{\phi}^B}(\kappa_1,t))\widehat{h^B}(\kappa_2)\right)\delta_{123}d_{12} = 0. \tag{B.5}$$

Bibliography

[1] J.M. Becker and R.H.J. Grimshaw. Explosive resonant triads in a continuously stratified flow. *J. Fluid Mech.*, 257:219–228, 1993.

[2] E.A. Caponi, M.Z. Caponi, P.G. Saffman, and H.C. Yuen. A simple model for the effect of water shear on the generation of waves by wind. *Proc. R. Soc. Lond. A*, 438:95–101, 1992.

[3] E.A. Caponi, H.C. Yuen, F.A. Milinazzo, and P.G. Saffman. Water-wave instability induced by a drift layer. *J. Fluid Mech.*, 222:207–213, 1991.

[4] M. Z. Caponi, P. G. Saffman, and H. Yuen. Effects of long waves on the stability of wind generated waves. In M.A. Donelan, W.H. Hui, and W.J. Plant, editors, *The Air-Sea Interface.* The University of Toronto Press, 1994.

[5] M.Z. Caponi and P.G. Saffman. Effect of wind and shear on surface waves. *Naval Research Reviews*, XLVIII(3):63–72, 1996.

[6] Z. Cheng and H. Mitsuyasu. Laboratory studies on the surface drift current induced by wind and swell. *J. Fluid Mech.*, 243:247–259, 1992.

[7] J. Choi, J. Demmel, I. Dhillon, J. Dongarra, S. Ostrouchov, A. Petitet, K. Stanley, D. Walker, and R.C. Whaley. Lapack working note 95. ScaLAPACK: A portable linear algebra library for distributed memory computers - design issues and performance. Technical report, Oak Ridge National Laboratory, 1995.

[8] J.W. Dold and D.H. Peregrine. An efficient boundary-integral method for steep unsteady water waves. In K.W. Morton and M.J. Baines, editors, *Numerical methods for fluid dynamics II*, pages 671–679. Claredon, 1986.

[9] J.R.D. Francis. Of shoes... and ships... and sealing wax... Inaugural Lecture, Imperial College, London, March 1967.

[10] A. Geist, A. Beguelin, J. Dongara, W. Jiang, R. Manchek, and V. Sunderam. *PVM: Parallel Virtual Machine. A Users' Guide and tutorial for networked parallel computing.* MIT Press, 1995.

[11] H. Hasimoto and H. Ono. Nonliner modulation of gravity waves. *J. Phys. Soc. Japan*, 33(3), September 1972.

[12] H.B. Keller. *Lectures on numerical methods in bifurcation problems.* Springer Verlag, 1987.

[13] D. Lewis. *We, the Navigators.* University of Hawaii Press, 1975.

[14] J.C. Li, W.H. Hui, and M.A. Donelan. Effects of velocity shear on the stability of surface deep water wave trains. In K. Horikawa and H. Maruo, editors, *Nonlinear Water Waves.* Springer-Verlag, 1988.

[15] M.S. Longuet-Higgins. The instabilities of gravity waves of finite amplitude in deep water. II. Subharmonics. *Proc. R. Soc. Lond. A*, 360:489–505, 1978.

[16] F.A. Milinazzo and P.G. Saffman. Effect of a surface shear layer on gravity and gravity-capillary waves of permanent form. *J. Fluid Mech.*, 216:93–101, 1990.

[17] H. Mitsuyasu. Interactions between water waves and wind. *Rep. Res. Inst. Appl. Mech., Kyushu University*, 14(48):67–89, 1966.

[18] N.N. Romanova and V.I. Shrira. Explosive generation of surface waves by wind. *Izvestiya, Atmospheric and Oceanic Physics*, 24(7):528–535, 1988.

[19] P.G. Saffman. *Vortex Dynamics.* Cambridge University Press, 1992.

[20] J. Vanneste and F. Vial. On the nonlinear interactions of geophysical waves in shear flows. *Geophys. Astrophys. Fluid Dynamics*, 78:115–141, 1994.

[21] H.C. Yuen and B.M. Lake. Nonlinear dynamics of deep-water gravity-waves. *Advances in Applied Mechanics*, 22:67–229, 1982.

[22] Q.P. Zhou. Nonlinear instability of wavetrain under influences of shear with varying vorticity and air pressure. *Acta Mecanica Sinica*, 12(1):24–38, Feb. 1996.

[23] J.A. Zufiria. Non-symmetric gravity waves on water of infinite depth. *J. Fluid Mech.*, 181:17–39, 1987.